Hydrogen-Driven Hydrocarbon Oxidation by Cytochrome P450 enzymes

Kouji Urata

A thesis submitted to the Board of the Faculty of Physical Sciences,

for the degree of Doctor of Philosophy, University of Oxford

University College

Trinity 2016

Inorganic Chemistry Laboratory

Oxford University

Hydrogen-Driven Hydrocarbon Oxidation by Cytochrome P450 Enzymes

Kouji Urata D Phil. Thesis abstract
University College Trinity, 2016

$P450_{BM3}$ (CYP102A1) from *Bacillus megaterium* is a 119 kDa, 1,046-residue polypeptide with the FAD/FMN reductase domain fused to the C-terminus of the haem domain and, as such it is catalytically self-sufficient; only NADPH and oxygen are required for monooxygenase activity. $P450_{BM3}$ is a sub-terminal fatty acid hydroxylase, but generations of CYP102A1 engineering allowed them to be used in, e.g. drug metabolism and alkane oxidation. This thesis describes protein engineering of $P450_{BM3}$ and altering reaction conditions to enhance $C_1 – C_8$ alkane oxidation activities, with the long-term goal of oxidising methane, and using the hydrogen-driven cofactor regeneration system to drive these reactions. Catalytic hydrocarbon oxidation under mild conditions is highly desirable in fuel synthesis and energy applications. Methane is a greenhouse gas and its effect can be minimised if methane is selectively oxidised to methanol, which can be used as a liquid fuel or feedstock. The R47L/Y51F, KT2, I401P and A330P mutants, which previously showed higher activities for a wide range of substrates, were used as templates to build a library of mutants. The R47L/Y51F/KT2/A330P mutant (RT2/AP) showed total turnover number (TTN) of 680 ± 10 under atmospheric pressure at ambient temperature for propane oxidation, and the TTN improved by 16-fold under 5 bar propane pressure (TTN is defined as the maximum number of moles of substrate converted per mole of $P450_{BM3}$). TTN values of 14,250 ± 1,370 (KU4/AP) and 920 ± 50 (KU3/AP) were observed under 5 bar propane and 8 bar ethane, respectively, at ambient temperature. The effect of adding an inert perfluorocarboxylic acid (PFC), which resembles the structures of natural substrates and constrains small alkanes to bind closer to the haem, was investigated. The R47L/Y51F/N70S/M237L/A328V mutant (RL/YF/NMA) with PFC11 gave a TTN of 13,590 ± 30 under 5 bar propane at ambient temperature. Higher TTNs of 26,320 ± 1,010 for propane and 1,440 ± 70 for ethane oxidation were observed for the RL/YF/NMA mutant at 4 °C due to improved aqueous alkane solubility. Octane and propane oxidations were performed using a hydrogen-driven $NADP^+$ recycling system without changing the selectivity of products, although the observed propane oxidation activity was 15% of the glucose/GDH cofactor recycling system.

Acknowledgements

I would like to thank University College and University of Oxford for the past eight years, and many thanks to Johnson-Matthey and EPSRC for funding this work. I am grateful to my industrial supervisors, Dr. James Cookson and Dr. Laura Ashfield for their support.

I am extremely grateful for all the advice I have received over the years from Xinkun Ren (Tony), Yang Cao, Matthew Fisher, and Dr. Alize Pennec. They were extremely helpful in designing new mutations and keeping me calm during those stressful days. I had great times talking to Tony about golf during lunch breaks, talking to Alize about South Africa, talking to Yang about which takeaways are good, and talking to Matt about the history of wine!

I am very appreciative of all the Part II's I have worked with (Elizabeth Macfarlane, James Skinner and Jake Jacobs), and other members of our group. I could not have asked for a better group of people. I am also thankful for Lawrence Knight, whose work I have taken over.

Dr. Holly Reeve offered me a huge amount of help in understanding the hydrogenase side of chemistry, and I am extremely thankful for her.

Thank you very much to Dr. Jake Yorke, Dr. Eachan Johnson and Dr. Christopher Whitehouse in the early stages of my DPhil degree for teaching my how to use some of the equipments in the lab.

I have to thank my family, friends, housemates and Marieke for their continuous support. I could not have done this without them.

My two supervisors – Professor. Kylie Vincent and Professor. Luet Wong. I cannot thank them enough for all the support they have given me over the last four years. Discussing new ideas/strategies have always been exciting, and I thoroughly enjoying the last few years working in their groups.

Table of Contents

List of Figures

List of Tables

Abbreviations

AU: absorbance unit

Bpy: 2,2′-bipyridine

BROD: benzyloxyresorufin O-dealkylation

CAST: combinational active-site saturation test

CPO: chloroperoxidase

CPR: cytochrome P450 reductase

CRAM: challenge response authentication mechanism

CSSM: combinatorial site-saturation mutagenesis

CYP: cytochrome P450

DME: dimethyl ether

EDA: ethyl diazoacetate

ee: enantiomeric excess

EET: 14,15-*cis*-epoxyeicosatrienoic acid

EETA: 17,18-*cis*-epoxyeicosatetraenoic acid

EROD: ethoxyresorufin-O-dealkylation

FAD: flavin adenine dinucleotide

FID: flame ionisation detector

FMN: flavin mononucleotide

GC: gas chromatography

GDH: glucose dehydrogenase

HME: hexyl methyl ether

IA-phen: 5-iodoacetamido-1,10-phenanthroline

IPTG: isopropyl-β-D-1-thiogalactopyranoside

IS: internal standard

Kan: kanamycin

LB: lysogeny broth

MD: molecular dynamics

MDMA: 3,4-methylenedioxymethylamphetamine

MMO: methane monooxygenase

MROD: methoxyresorufin-O-dealkylation

NAD(P)(H): nicotine adenine dinucleotide (phosphate) (H = reduced form)

NOS: nitric oxide synthase

NPG: *N*-palmitoyl glycine

OH-AA: hydroxyicosatetraenoic acid

PAH: polycyclic aromatic hydrocarbon

PCR: polymerase chain reaction

PFC: perfluorocarboxylic acid

PFR: product formation rate

PhenA: 5-acetamido-1,10-phenanthroline

PROD: pentoxyresorufin-O-dealkylation

TAE: tris-acetate EDTA buffer

TOF: turnover frequency

TTN: total turnover number

SH: soluble hydrogenase

WT: wild-type

Chapter 1

Introduction

1.1 Overview

Selective catalytic hydrocarbon oxidation under mild conditions is a highly desirable reaction in synthesis and energy applications.[1] No viable process for one-step alkane oxidation to an alcohol is currently available in industry. Biofuels from fermentation have the potential to provide cost-effective fuels. In Brazil, most biofuels are produced from sugarcane (Figure 1-1).[2] Corn starch is the main source for bioethanol in the United States,[3] with up to 472 L of ethanol is predicted per ton (2,000 lbs, 900 kg) of dry corn grain. Other common biodiesel feedstocks include soy, palm and rapeseed,[4] but fermentation from these raw materials are also not yet cost competitive as main sources of fuel, mainly due to a rapid increase in food market prices.[5] The conversion of Cassava starch from TMS 30572 *Idileru* using α-amylase and amyloglycosidase by two strains of *Saccharomyces cerevisiae* led to ethanol concentration of 5.3% at 10% initial sugar concentration with a sugar conversion efficiency of 37.3%.[6] The production of 61.8 g of ethanol per litre (86.5% yield) using *Saccharomyces cerevisiae* with *Rhizopus oryzae* glucoamylase and *Streptococcus bovis* α-amylase has also been reported.[7] The renewables target in transport of 10% has been set by 2020 for the EU, and 20% by 2022 for the US. The production of ethanol from cellulosic biomass is an alternative, as this method does not reduce the food source. The high capital cost and expensive feedstock costs, however, mean that the unsubsidised product is not yet viable on a commercial scale.

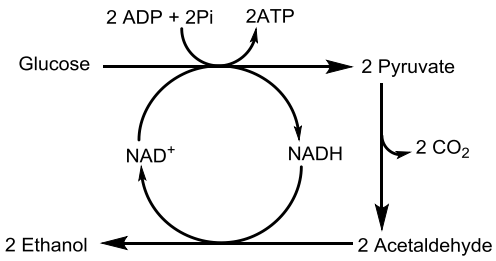

Figure 1-1: The Ethanol fermentation mechanism. CO_2 is produced as a by-product.

Hydrogen as a source of fuel may be another alternative.[8–10] Hydrogen is one of the cleanest, most efficient fuels and the lightest.[11,12] There are problems associated with preparation and storage.[13] Capital costs may also be a problem, as hydrogen is not naturally found[14] and needs to be produced from primary energy sources, such as natural gas steam reforming[15] and electrolysis of water.[16]

Thousands of barrels of fuels are mass produced by indirect conversion processes, and more plants operating on coal-to-liquid (CTL) or gas-to-liquid (GTL) processes are being built (Figure 1-2).[17] Syngas is formed via the gasification of coal and biomass,[18] or steam reformation of natural gas and shale gas,[19] and converted to hydrocarbons via Fisher-Tropsch conversion[20] or to gasoline from methanol via the Mobil process.[21] The Mobil processes require the use of the zeolite ZSM-5; this is an attractive catalyst, due to high stability even at 500 °C,[22] and high surface area with, e.g. the external surface area of 12 $m^2 g^{-1}$ and 404 $m^2 g^{-1}$ surface area for "L20".[23] The overall process can be made more cost efficient and environmentally friendly, if volatile side products (C_5 – C_9 alkanes) can be selectively oxidised to alcohols. Most oxidation reactions using metal catalysts lead to unwanted further products such as aldehydes and CO_2, and require high pressures and temperatures.[24,25] Recent work using a Pd/Fe_2O_3 catalyst with hydrogen converted ethylene glycol to methanol with *ca.* 50% selectivity, but the reaction mixture was pressurised to 20 bars of hydrogen and heated to 195 °C.[26] The oxidation of n-hexane using H_2O_2 with $Tp^{Br3}Cu(MeCN)$ led to 8.5% yield at 60 °C, with 2- and 3-hexanone being the main products.[27]

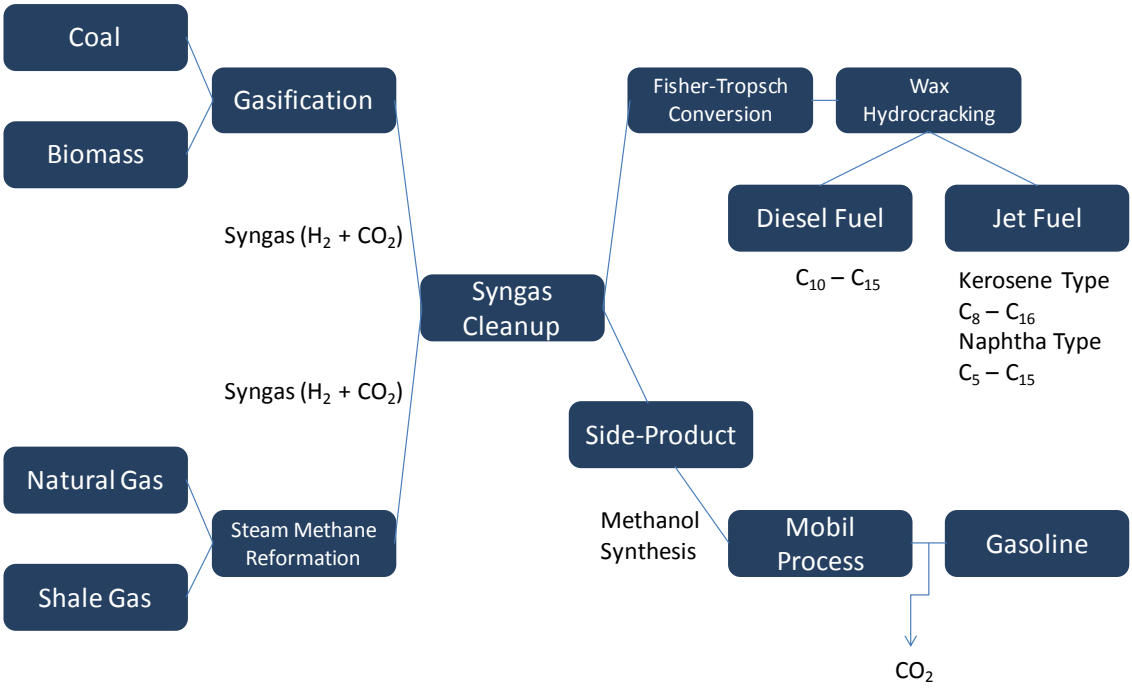

Figure 1-2: Indirect Conversion processes. Syngas can be produced by gasification of coal or biomass, and steam methane reformation. Hydrocarbons are formed via the Fisher-Tropsh conversion, and gasoline is converted from methanol using the Mobil process.

Natural gas is being used as a substitute source of fuel for coal and oil. Less CO_2 is emitted per unit energy than coal or oil,[28] but natural gas is mainly composed of methane.[29] Methane is a greenhouse gas and toxic in the air. Atmospheric methane levels have increased over the last 300 years, and it is 26 times more effective as a greenhouse gas than CO_2.[30] As observed in Figure 1-3, the reduction in hydroxyl ($^{\cdot}OH$) radical concentration leads to a further increase in methane levels in the atmosphere.[31] The decrease in hydroxyl radical formation is caused by the reduced emission of NO_x, which amplifies the formation of hydroxyl radical indirectly via the photolysis of O_3.[32] This environmental damage can be reduced if methane is selectively oxidised under mild conditions to methanol, which can be used as a liquid fuel or feedstock. This technology is currently available, but only economically practical on a large scale up to 250,000 tonnes per annum per plant.

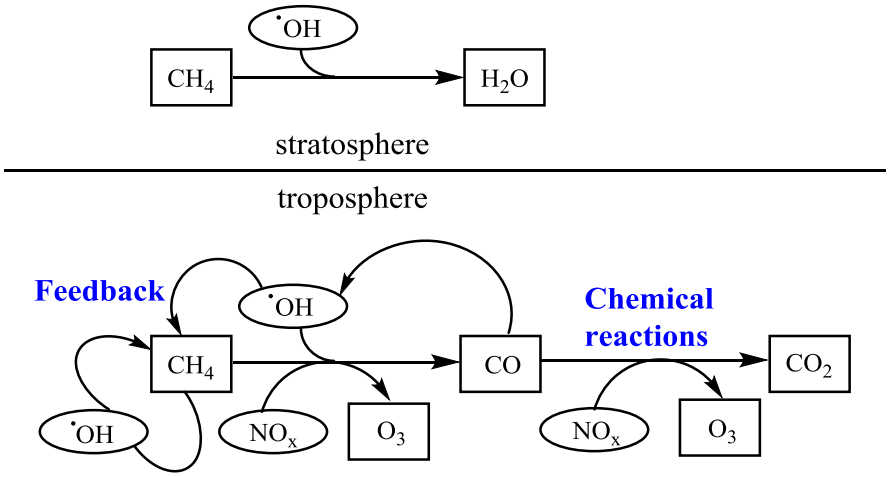

Figure 1-3: Indirect effect of methane oxidation in the atmosphere.[33] Methane levels are increased, if less NO_x is released in the air and the hydroxyl radical concentration is reduced.

Other short-chain alcohols are also in high demand. Ethanol can be blended with gasoline to produce an excellent source of fuel due to its clean burning properties.[34] The product distribution of octane oxidation, especially those favouring oxidation at the terminal position, is of great interest,[35,36] as 1-octanol possesses diesel-like characteristics and is a highly attractive fuel.[37] In addition, it is useful for controlling essential tremor up to 64 mg kg^{-1}.[38] 2-Octanol can be used as solvent and defoaming agent.[39,40]

1.1.1 Chemical catalysts

Chemical oxidation processes of alkanes are known. Fenton chemistry involves Fe^{2+} and H_2O_2,[41] and its mechanism is shown in Figure 1-4. Formation of hydroxyl ($^{\cdot}OH$) radical initiates the reaction, with an alkyl radical as intermediate.[42] This binds to O_2, leading to the formation of alcohol. It is known that Cu, Cr, Co, V and Ni can also catalyse this reaction.[43] The drawbacks are low turnover numbers and large amount of metal waste.[44] The use of Fe(bpmen)OTf_2 catalyst (Figure 1-5) led to the oxidation of cyclohexane to cyclohexanol and cyclohexanone, with a yield of 65% based on the H_2O_2 added.[45] Selective oxidation by Fenton-type systems is unusual.[46]

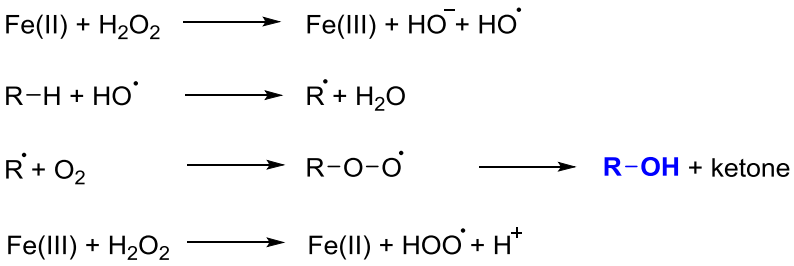

Figure 1-4: The mechanism of the Fenton reaction. H_2O_2 is required to initiate the reaction and the alcohol product is produced via the alkyl intermediate.

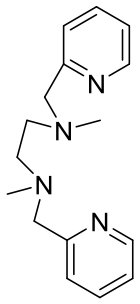

Figure 1-5: The bpmen structure.[45]

The Gif system described in Figure 1-6 involves using acetic acid, zinc, oxygen, an iron salt as catalyst and pyridine as the solvent. The formation of unwanted zinc acetate is an issue,[47] and another process uses an electrode to provide electrons.[48] This system gives better selectivity control than the Fenton reaction, with the main product being the ketone and disfavouring the aldehyde.[49] The ketone products are typically in 3 – 26% yield and alcohols are between 0.5 – 2.5%.[50]

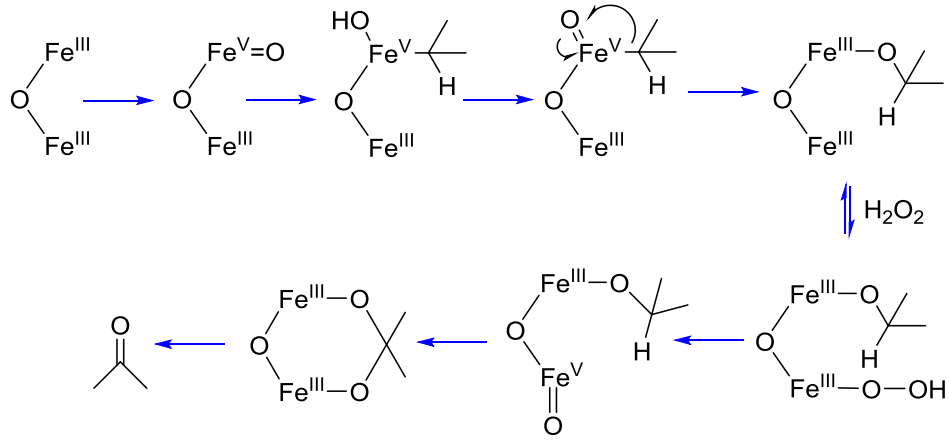

Figure 1-6: Proposed mechanism for Gif systems, which requires an iron salt catalyst.[51]

Shilov *et al.* discovered the oxidation of hydrocarbons to alcohols using a Pt catalyst.[52] This system can offer an attractive alkane oxidation pathway, as the reaction condition is mild (100 – 120 °C). The initial step involves the cleavage of R–H bond, followed by the oxidation of the Pt^{II} centre. The product R–OH is formed by reductive elimination (Figure 1-7).[53] The Shilov reaction, however, leads to low product yield, with just 3% for methane, and the platinum catalyst is short-lived.[25,54]

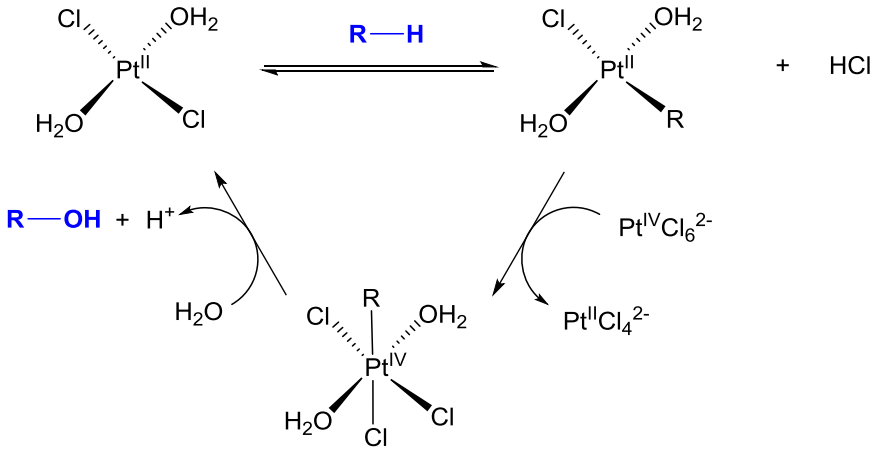

Figure 1-7: Mechanism of the Shilov reaction.[55] The catalytic cycle involves C – H bond activation, followed by the oxidation of Pt^{II} centre, and the alcohol product is produced by reduction elimination.

1.1.2 Biological catalysts

Enzymatic systems such as terminal (ω) alkane hydroxylases and cytochrome P450 (CYP) monooxygenases, which oxidise alkanes with the use of oxygen as the oxidant, offer attractive C–H activation systems.[56] The enzymatic approach is more suitable for localised applications and is attractive due to the mild conditions and potential product selectivity.[57]

1.1.2.1 Terminal alkane hydroxylase

Alkane hydroxylase is a membrane-bound three-component system expressed in *Pseudomonas oleovorans* and *E. coli*.[58–60] The hydroxylase protein consists of ferrous ion prosthetic group, rather than haem,[61] and requires phospholipids for activation in vitro.[62] The three components consist of *AlkT*, *AlkG* and *AlkB*;[63] rubredoxin reductase is encoded by *AlkT*,

rubredoxin by *AlkG*, and the monooxygenase component is *AlkB*.[64] The AlkB enzyme from *Pseudomonas putida* GPo1 has been extensively studied for medium-chain alkane oxidation, and its natural substrates are C_{10} or longer alkanes.[65,66] The expression of AlkB can be regulated up to 1.5 – 2% of the total cell protein in *E. coli* and *P. putida*.[58] AlkB contains six α-helices creating a hydrophobic region.[67] Amino acids 1 – 20 forms a short N-terminus peptide, 70 – 87 and 138 – 226 form two hydrophilic loops, and 271 – 401 forms a large C-terminus domain.[67] The *AlkB* gene is responsible for coding the polypeptide with the molecular weight of 27 kDa.[68] The enzyme is also active towards a broad range of substrates,[69] including both aliphatic and aromatic compounds, and C–H bond activation is believed to occur via a radical mechanism.[70] The turnover rate of 210 min^{-1} has been reported for octane.[71,72] Oxidations of both propane and n-butane have been observed using the AlkB hydroxylase.[73]

1.1.2.2 Methane monooxygenase

Soluble methane monooxygenases (sMMOs) are multicomponent systems which require NADH as an electron donor to catalyse the initial oxidation of methane by oxygen.[74,75] These components include a dimeric hydroxylase protein (three subunits of $\alpha_2\beta_2\gamma_2$), an NADH oxidoreductase, a small regulatory protein,[76] and some contain a Rieske-type ferredoxin. The hydroxylase protein, which interacts with methane, has a relative molecular mass of 210 kDa, and the 20 kDa regulatory protein contains no prosthetic groups. The NADH ferredoxin contains one FAD and one Fe_2S_2 centre per molecule within a single 42 kDa polypeptide chain.[77] sMMOs are found in *Methylococcus capsulatus* (Bath)[78] and *Methylosinus trichosporium* OB3b,[79] but are difficult to express in a suitable host organism such as *E. coli*, which makes them impractical.[80] The mechanism of sMMO is likely to be concerted, as the oxidation of chiral (*S*)- or (*R*)-[1-$^3H_1$,$^2H_1$]ethane led to 68% retention and 32% inversion of configuration ethanol products (Figure 1-8).[81]

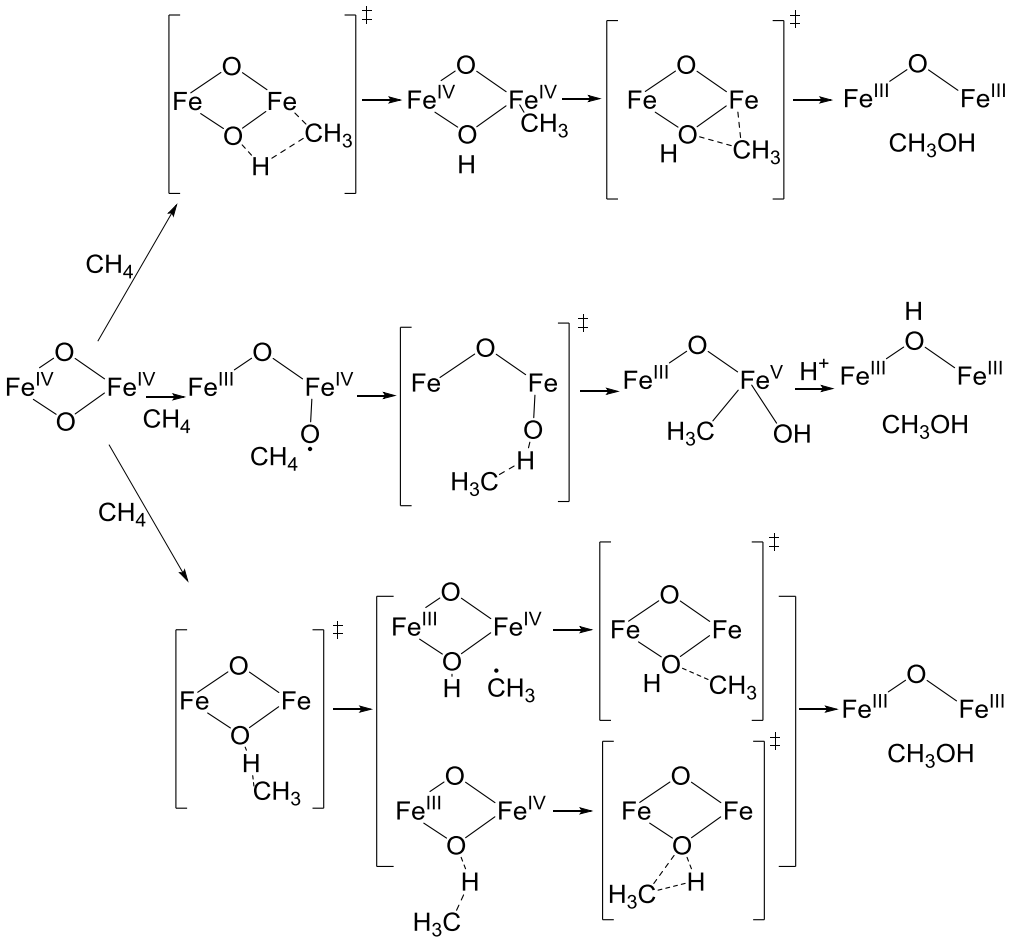

Figure 1-8: Possible mechanisms of sMMO.[82] Three possible pathways are non-radical, radical and concerted mechanisms.

sMMO is expressed at less than 0.8 μM copper concentration, but at *ca.* 4 μM, particulate methane monooxygenase (pMMO) is expressed.[83] pMMO is a trimer ($\alpha_3\beta_3\gamma_3$ polypeptide), with three metal centres.[84] Three subunits are pmoB corresponding to α of *ca.* 47 kDa, pmoA corresponding to β of *ca.* 24 kDa, and pmoC corresponding to γ of *ca.* 22 kDa.[85,86] Mononuclear copper and dinuclear copper metal centres are found in the N-terminus of each pmoB subunit, and the third metal centre is found inside the membrane, but the metal content is unclear.[87,88] The role played by methane monooxygenase is illustrated in Figure 1-9.

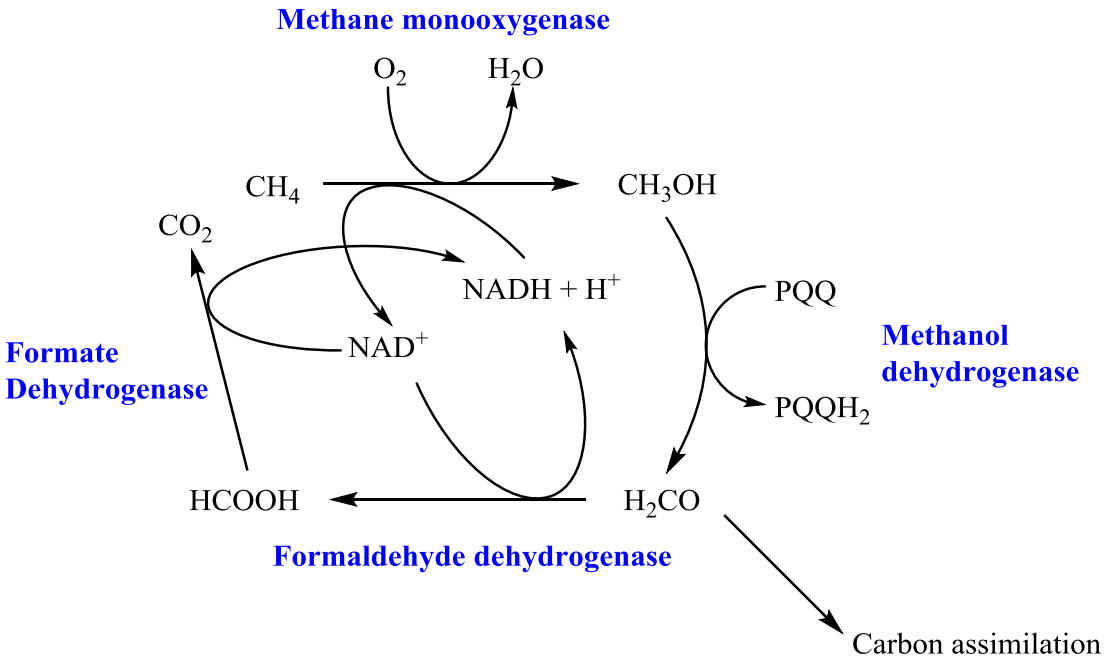

Figure 1-9: Methane oxidation and assimilation pathway in microorganisms.

1.2 Cytochromes P450

1.2.1 Background

P450 (CYP) enzymes contain a haem *b* moiety,[89] linked to the polypeptide by a thiolate ligand of the conserved cysteine residue (Figure 1-10).[90] The name P450 is given from the unique Soret band seen at 450 nm for the ferrous-CO form of the enzyme found by Omura and Sato in 1964.[91] It is believed that cytochrome P450 was involved in oxygen detoxification in early stages on Earth.[92] Cytochrome P450 monooxygenases are found in virtually every organism,[93] with the notable exception of *Escherichia coli* and *Salmonella typhimurium*.[94] $P450_{cam}$, which is found in the soil bacterium *Pseudomonas putida*, is the first P450 to be isolated[95] and expressed in *E. coli*.[95–97] Bacterial enzymes are soluble, but eukaryotic P450 enzymes are membrane bound.[98]

$$R–H + O_2 + NAD(P)H + H^+ \rightarrow R–OH + H_2O + NAD(P)^+$$

CYP monooxygenase activity requires two electrons, most commonly provided by NAD(P)H.[99] The electrons are transferred sequentially and there are different ways in which electrons are delivered (see section **1.2.3**).

All P450 enzymes and genes are currently labelled with the CYP prefix.[100,101] A numeral representing the family, a letter representing the subfamily, and a number representing the individual gene follow.[102] It has been proposed that >40% and >55% identity in amino acid sequence are shared within members of a family and members of a subfamily, respectively.[103] $P450_{BM3}$ for example, is given the notation CYP102A1, where 102 denotes the family, A denotes the subfamily and 1 denotes the individual gene.

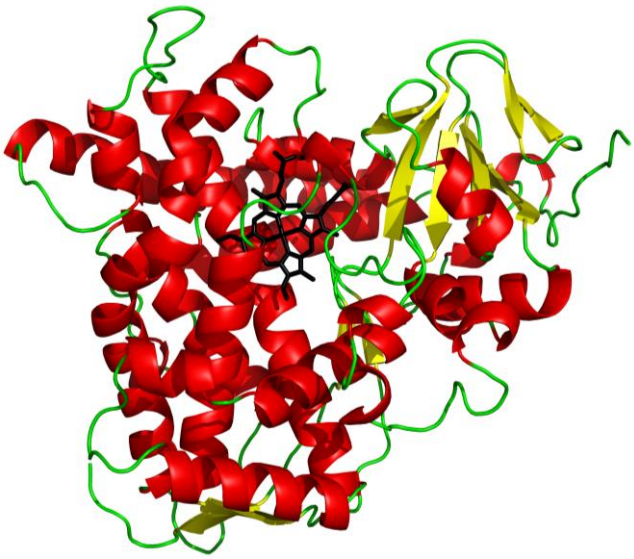

Figure 1-10: Schematic representation of the $P450_{BM3}$ fold. The haem is in black, α-helices are in red, and β-sheets are in yellow.

The first P450 enzyme to have its crystal structure solved was $P450_{cam}$.[104] X-ray diffraction indicates that the structures of P450 resemble trigonal prisms 40 – 60 Å in size.[105] The P450 fold contains 11 α-helices and 4 or 5 β-strands. For easy identification, helices are labelled according to their location in the peptide sequence. The haem is located on the base of the binding site for substrates with the I-helix along the side.[106] More than 350,000 CYP genes are in databases (http://drnelson.utmem.edu/CytochromeP450.html),[107] but the proximal

cysteine ligand that provides the thiolate ligand to the haem iron is conserved,[98] due to its important role in O–O bond heterolysis.[108] In almost all microsomal P450s, the motif PPGPXPXPXXGN (found in between Pro-30 and Asn-41, and lies in the left-handed polyproline II-like sequence in the case of CYP2C5) is generally conserved and considered important.[109]

Cytochrome P450 monooxygenases are capable of accepting a broad range of substrates.[110] The versatility of P450 enzymes allows them to be used in drug metabolism,[111] and biosynthesis of steroid hormones[112] and antibiotics.[113] P450 can synthesise secondary metabolites, such as alkaloids and terpenoids, and taxol functionalisation has been reported by CYP725A4.[114] The metabolism of artemisinin by P450 is possible, and camphor can be oxidised by $P450_{cam}$.[115,116] CYP3A enzymes in the liver metabolise a broad range of drugs.[117] There are four *CYP3A* genes found in humans, but CYP3A4 and CYPA5 are the most common.[118] Substrate specificities are similar, but substrates such as quinine and erythromycin can be oxidised by only CYP3A4.[119,120] CYP703, typically found in plants, is capable of catalysing the oxidation of lauric acid to aid sporopollenin formation in pollen.[121] Other biological roles include metabolism of vitamins,[122] cholesterol,[123] and bile acids.[124] 57 human P450 genes are present[125] and *ca.* 95% of the P450 drug oxidations are performed by five P450 enzymes (CYP1A2, CYP2C9, CYP2C19, CYP2D6 and CYP3A4).[126,127]

1.2.2 The P450 catalytic cycle

The consensus P450 catalytic cycle shown in Figure 1-11, has been intensely studied for over 30 years. The resting state (**A**) has a six-coordinate low-spin Fe^{III}, and the water ligand is found in the axial position *trans* to the thiolato ligand. The dissociation of water ligand is caused by the arrival of the substrate in the active site. The 5-coordinate iron (**B**) is high-spin, where the haem is shifted to a more oxidising potential. The addition of an electron will lead to the ferrous form (**C**) and this binds oxygen rapidly to form the oxy complex (**D**). The

second reduction step leads to the formation of the peroxo form (**E**), which is immediately protonated to form the ferric-hydroperoxy complex (**F**). A water molecule is released with the protonation of this complex at the terminal oxygen, and a hydrogen atom from the substrate is abstracted by the ferryl intermediate (**G**).[128,129] The ferryl intermediate can oxidise C–H bonds with the rate constant of 1×10^7 M^{-1} s^{-1}.[130] This leads to the formation of Fe^{IV}–OH(Por) species (**H**), and the substrate radical immediately recombine with the iron-bound OH to form the alcohol product, which then leaves the active site.

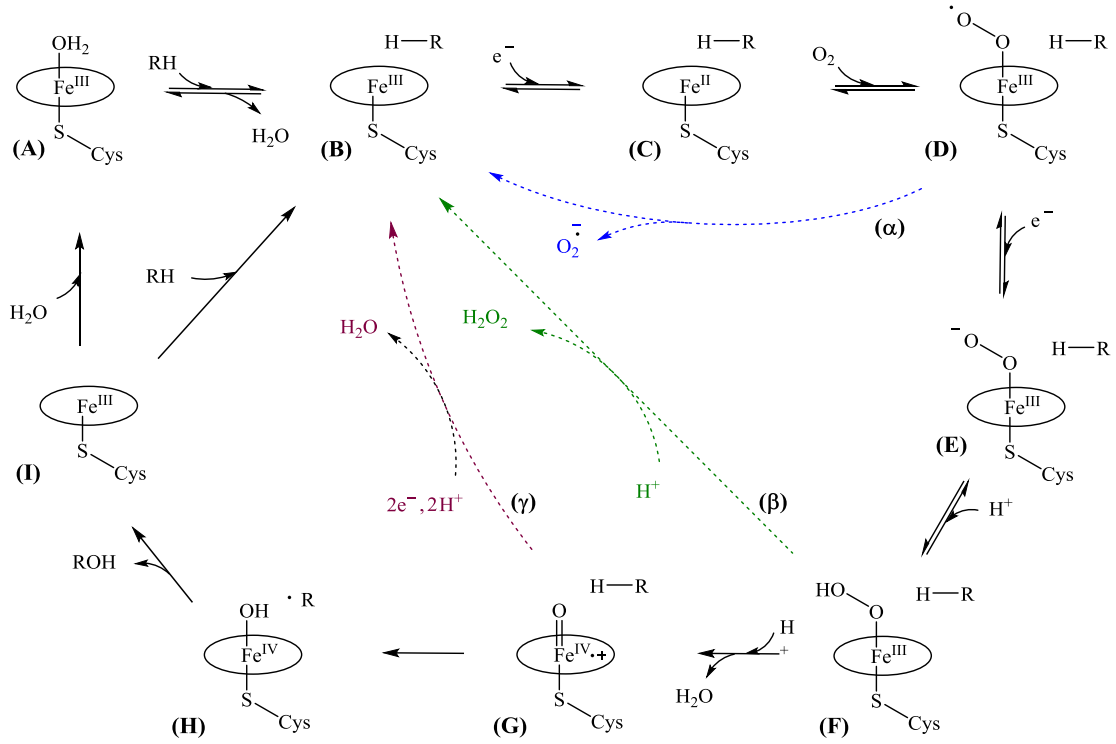

Figure 1-11: The P450 catalytic cycle.[131] The ferric iron atom is six-coordinate in the resting state (A) and the water ligand is found *trans* to the thiolato ligand. The reaction takes place via a ferryl intermidate (G). Uncoupling pathways are labelled α, β and γ.

Uncoupling pathways occur when oxidation of substrates cannot take place. The main pathways (Figure 1-11) are superoxide uncoupling (α), peroxide uncoupling (β), and oxidase uncoupling (γ).[132,133] Superoxide uncoupling happens when the second electron transfer to **D** is too slow or weak binding to dioxygen, and leads to auto-oxidation and loss of superoxide. The second uncoupling pathway is the loss of peroxide when the substrate cannot bind

strongly to the haem iron centre and the protonation at the iron-bound oxygen atom takes place. The last uncoupling pathway arises if the substrate binds tightly, but no abstraction of hydrogen atom is possible, leading to the reduction of oxygen to H_2O.

1.2.3 Electron transfer chains

There are four broad classes of electron transfer chains by which cytochrome P450 enzymes receive two electrons required for oxygen activation.[134]

Class I systems: Common in bacteria and mitochondria they comprise of three-component systems as shown in Figure 1-12.[135] The electrons are donated from NAD(P)H to flavin (FAD or FMN)-dependent reductases, and redoxins (most commonly a [2Fe–2S] ferredoxin) are subsequently reduced. The haem centre is ultimately reduced by these electrons from a redoxin.[136]

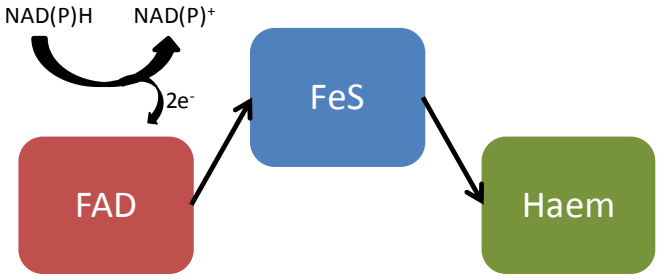

Figure 1-12: The class I system. Electrons supplied from NAD(P)H travel from the flavin to the haem via redoxins.

Class II systems: The majority of eukaryotic P450s belongs to this class. This consists of two membrane-bound proteins, the P450 and the NADPH-cytochrome P450 oxidoreductase (CPR) that contain separate FAD and FMN domains (Figure 1-13).[137]

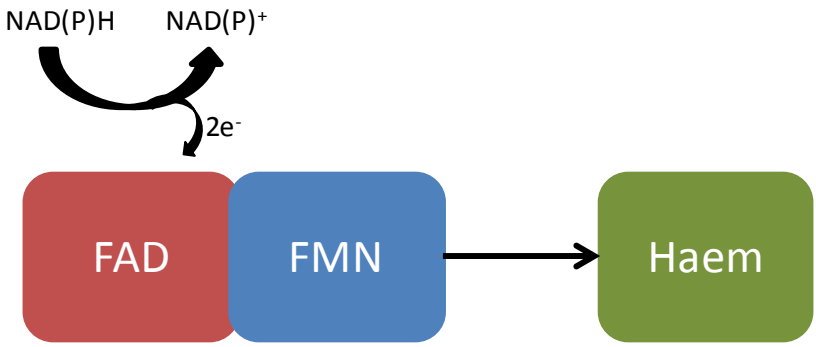

Figure 1-13: The class II system. This system contains both FAD and FMN.

Class III systems: No electron-transfer cofactors are required and the substrate peroxide group is used as the oxygen source.[138] Prostacyclin synthase (PGIS) is the known example of class III.[139]

Class IV systems: Electrons are directly received from reduced pyridine nucleotides.[140,141] Examples of class IV P450s include CYP119 from *Sulfolobus solfataricus*. This 43 kDa enzyme can be active even in harsh conditions (up to 91°C).[142]

All these systems contain an iron-protoporphyrin IX group[143] with a proximal cysteine thiolate ligand.[144] The overall molecular oxygen reduction mechanism is believed to be in common between these systems. $P450_{BM3}$, the subject of this thesis, belongs to the 'fused' Class II systems.[145]

1.3 Peroxygenases

Peroxygenases are similar to P450 monooxygenases, as both form the oxyferryl intermediate (see **1.2.2**); slow decomposition rate of *Aae*APO peroxygenase intermediate ($1.4 \pm 0.03\ s^{-1}$) enabled activities of this peroxygenase to be determined for various substrates, and spectral characterisation studies showed the formation of the same oxoiron (IV) porphyrin radical cation intermediate as P450 enzymes.[146] Peroxidases contain a proximal histidine-ligand, but

the proximal ligand in peroxygenases is a cysteine ligand. Peroxygenases do not require electron-transport chains, as they use H_2O_2 in place of oxygen, two electrons and two protons required for P450 enzymes (Figure 1-14).[147]

The major problem with these systems is that H_2O_2 can also act as an inhibitor and therefore careful control of peroxide supply is necessary.[148] Chloroperoxidase (CPO) from *Caldariomyces fumago* has been extensively studied, but the 45 kDa unspecific peroxygenase (UPO) from *Agrocybe aegerita* has reportedly oxidised cyclohexane, with a total turnover number (TTN) of 4,500 and 92% coupling. Linear alkanes were also oxidised at the ω–1 and ω–2 positions for C_5 – C_8 (octane oxidation led to 55% 2-octanol and 45% 3-octanol products) and only at the ω–1 position for propane and butane, with 729 µM and 918 µM products being produced (TTN values of 960 and 1,210), respectively.[149] Directed evolution was performed on UPO, and the introduction of 9 mutations led to as much as 3,000-fold increase in activity towards substrates such as benzyl alcohol and pNCA without destabilising the enzyme.[150] Aromatic peroxygenase (APO), also from *Agrocybe aegerita*, can catalyse the oxidation of benzene, and it is known to form phenol via a benzene oxide intermediate, as well as further oxidation products.[151] The TTN of 110,000 was achieved with *ee* >99% in the case of (1*R*,2*S*)-*cis*-β-methylstyrene oxide formation.[152] Oxidation of other polycyclic aromatic hydrocarbons (PAHs), such as methylnaphthalenes and dibenzofuran were reported; 2-methylnaphthalene was oxidised to up to 14 products by AaP and CrP peroxygenases.[153]

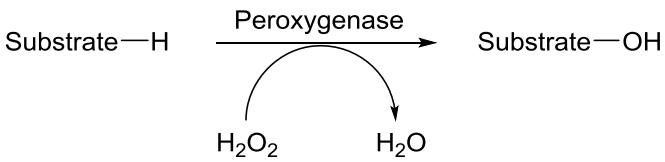

Figure 1-14: Oxidation reactions catalysed by peroxygenase.[154] H_2O_2 is required to initiate the reaction, but a careful control of peroxide supply is necessary, as high concentrations of H_2O_2 are inhibitory.

1.4 Photobiocatalysis reactions

NADH or NADPH cofactors are expensive, and the cofactor recycling systems, such as the use of glucose and glucose dehydrogenase, have several drawbacks (see **1.9**), and thus the photobiocatalysis method may be an attractive alternative. Various reactions were performed using the photosensitive approach, including Baeyer-Villiger (BV) reactions (Figure 1-15), alkene reductions, C–H bond hydroxylations and epoxidations.

The use of EDTA, light and the phenylacetone monooxygenase variant (PAMO-P3) performed conversion of 2-phenylcyclohexan-1-one to (*R*)-7-phenyloxepan-2-one (48% conversion), with high enantioselectivity of 97% *ee*.[155] PAMO was reported to be relatively tolerant to H_2O_2, with 20% of the relative residual activity being observed at 64 mM H_2O_2 concentration. Disadvantages of using EDTA are that at least 0.6 equivalents are required for full conversion, and formations of undesired side products (formaldehyde and amines) are environmentally unfriendly.

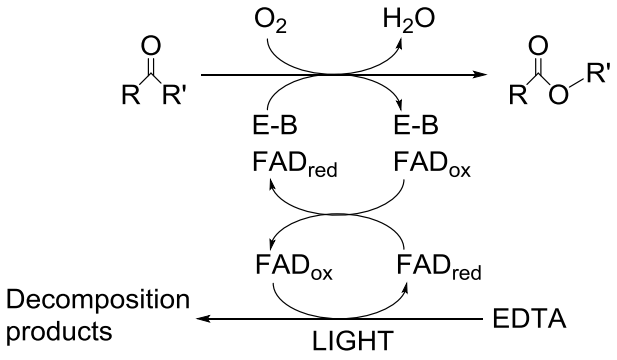

Figure 1-15: A light-driven Baeyer-Villiger reaction using EDTA and a flavin. E-B = enzyme bound. Formation of side products is, however, unfavourable.

A light-driven alkene reduction was performed using enoate reductases (old yellow enzymes – OYEs), with the rate of up to 65% of the standard NADH-driven reaction.[156] This approach allowed direct Flavin prosthetic group regeneration, and thus prevented the formation of unwanted carbonyl reduction products. The photocatalysed citral reduction by YqjM (OYE)

led to 100% citronellal product and no citronnellol, geraniol or nerol products (Figure 1-16). The change of the light bulb from 40 W to 250 W led to >50% increase in activity with FMN as the catalyst towards ketoisophrone (Figure 1-17). The use of different photocatalyst (FMN and riboflavin) led to different rates and enantioselectivity, with FAD giving slightly higher rate, but lower enantioselectivity (from *ca.* 70% to 45% *ee*). Anaerobic condition was required to minimise the production of oxidised flavins and H_2O_2.

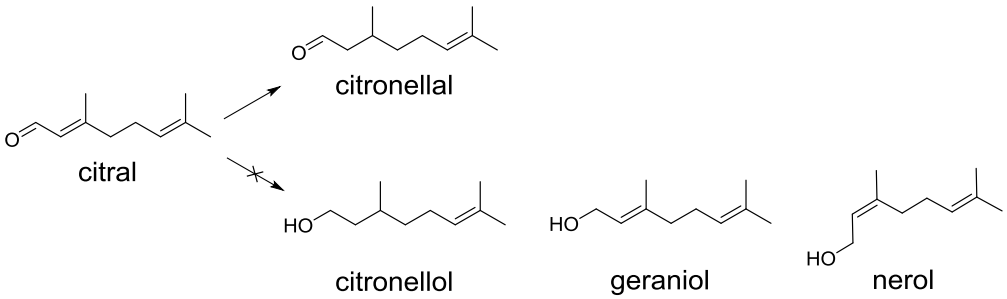

Figure 1-16: The photocatalysed reduction of citral by YqjM. The only product formed was citronellal.

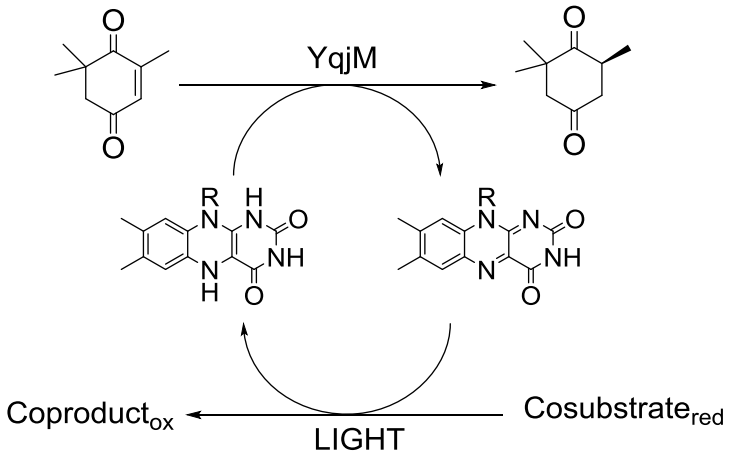

Figure 1-17: A direct regeneration of flavin prosthetic group in YqjM using light.

Previous work on attaching $[Ru(bpy)_3]^{2+}$ (bpy: 2,2′-bipyridine) to horseradish peroxidase allowed the formation of ferryl and ferryl porphyrin radical cation (**G** and **H** in Figure 1-11) by laser flash-quench oxidation. Site-directed mutagenesis was performed on Cys62 and Cys156 residues to alanine and serine, respectively, and the K97C mutation was added to $P450_{BM3}$ haem domain, to enable linking of $[Ru(bpy)_2(IA\text{-}phen)]^{2+}$

(IA-phen: 5-iodoacetamido-1,10-phenanthroline) to the $P450_{BM3}$ via the Cys97 residue. The flash-quench oxidation of the resulting Ru^{II}_{K97C}-Fe^{III}_{P450} conjugate led to the formation of ferryl porphyrin radical cation (**H**), with the reverse of catalytic cycle in Figure 1-11 observed (the first step involved dissociation of H_2O).[157] Similarly, the $\{Ru[(OMe)bpy]_2PhenA\}^{2+}$ complex (phenA: 5-acetamido-1,10-phenanthroline) was added to the $P450_{BM3}$ haem domain with the L407C mutation, and light-driven lauric acid hydroxylation was performed using this conjugate, with a TTN of 940.[158]

Hydroxylation of C–H bond and epoxidation reactions were performed using *Aae*APO mentioned in **1.3**. H_2O_2 required by *Aae*APO was regenerated using light and FMN (Figure 1-18).[159] Various alkylbenzene oxidations were performed with high enantioselectivity, where the ethyl benzene oxidation reached turnover number of 11,470 and >97% *ee*. Cyclohexane and octane oxidation reactions were also performed, with the turnover number of the former being 17,900. The rate of photochemical H_2O_2 generation was reduced to *ca.* 30% of the stoichiometric amounts of H_2O_2, but the *Aae*APO enzyme was active for longer period using this approach, and thus the turnover number reportedly reached >200,000 for some substrates. The increase in the light intensity and FMN concentration led to higher enzymatic activities. The activity and selectivity of epoxidation reactions were dependent on the substitution pattern of the double bond. Hydroxylation to 2-phenyloxirane led to relatively high turnover number of 10,390, though enantioselectivity was low with 4% *ee*. *cis*-β-Methyl styrene was oxidised to >99% *ee*, but *trans*-β-methyl styrene was oxidised 100-fold slower than the *cis* isomer and enantioselectivity was low with 4% *ee*.

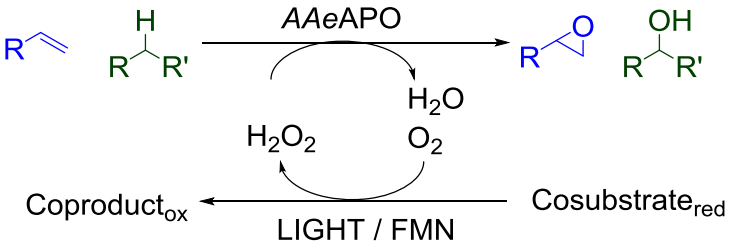

Figure 1-18: Hydroxylation and epoxidation reactions using *AAe*APO and a light source.

1.5 CYP102A1 ($P450_{BM3}$)

$P450_{BM3}$ (CYP102A1) was discovered by Fulco in the early 1970s, and is a 119 kDa, 1,046-residue single polypeptide from *Bacillus megaterium*.[160] $P450_{BM3}$ is often called the "fused Class II" enzyme as the *ca.* 55 kDa P450 (haem domain) is fused at its C-terminus with a *ca.* 65 kDa FAD/FMN reductase domain (Figure 1-19).[161] Electron transfer between the two domains is efficient.[162,163] In $P450_{BM3}$, the electron transfer from the FMN to the haem is proposed to pass through the peptide backbone from Gln387 to Cys400.[164] This was tested by attaching the photoactive Ru(II) to the mutated Cys residues found in the haem domain. The rate of haem reduction was found to be 4.6×10^5 s^{-1} when Ru(II) was attached to Cys387, using the photoexcitation of Ru(II). The rate of reduction was, however, zero when attached to Cys62, which is at the same distance from the haem, indicating the preferred electron transfer path is from Gln387 to Cys400.[165] $P450_{BM3}$ functions as a dimer. The sedimentation velocity experiments suggested the enzyme was dimeric with molecular weight of *ca.* 236 kDa, when the enzyme was incubated with DTT.[166] Either or both of the FAD → FMN and FMN → P450 electron transfers take place across the dimer interface.[167,168]

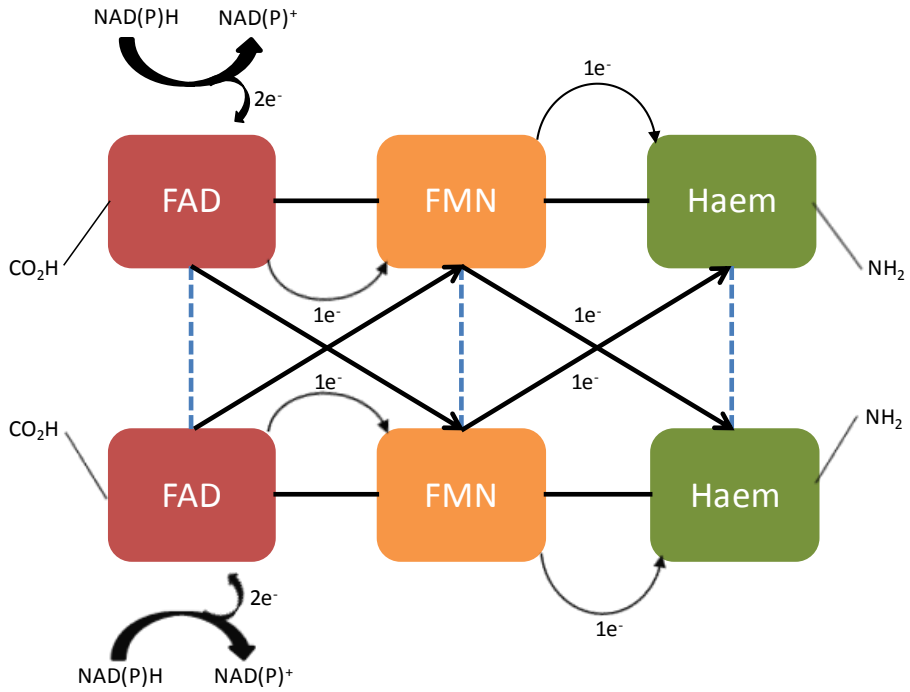

Figure 1-19: The fused class II system $P450_{BM3}$. Electron transfers take place across the dimer surface.

CYP102A1 is catalytically self-sufficient[169] and co-factor proteins are not required for its activity.[170] Only NADPH and oxygen are required for monooxygenase activity. $P450_{BM3}$ is a sub-terminal fatty acid hydroxylase, and early studies showed that the hydroxylation of a range of fatty acids mostly occurred at the ω–2 position (Figure 1-20).[171] Palmitic acid (C_{16}) oxidation by WT $P450_{BM3}$ led to 31% ω–1, 48% ω–2 and 21% ω–3.[131] The oxidation of myristic acid (C_{14}), however, favoured terminal oxidation, with 44% ω–1 product.[131] The highest activity (k_{cat} = 122 ± 5.9 s^{-1} with palmitic acid) is seen with medium chain (C_{12} – C_{16}) linear and branched fatty acids for the wild type (WT) enzyme.[172] A k_{cat} of *ca.* 17,000 min^{-1} has been reported with arachidonate.[173] Rowlatt and Wong[174] reported that both the ionic strength and chain length affect the cooperativity of fatty acid oxidation, leading to the hypothesis that $P450_{BM3}$ may regulate membrane fluidity according to the external phosphate concentration.[172]

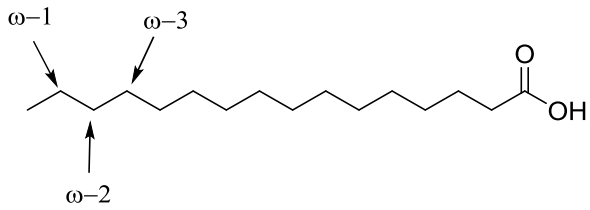

Figure 1-20: Palmitic acid oxidation selectivity of $P450_{BM3}$. Omega labelling system is illustrated.

The enzyme is soluble and stable,[175] with high expression levels up to 1.5 g L^{-1} (12.6 μmoles L^{-1}) in *E. coli* fed-batch cultures have been reported,[176] making $P450_{BM3}$ an excellent target for protein engineering for the oxidation of non-natural substrates. The activity of WT towards non-natural substrates is normally minimal, with the exception of, for example, propylbenzene oxidation (894 min^{-1}),[177] and therefore the engineering of the enzymes is important for increased activity and product selectivity. Different approaches have been used previously, such as site-directed and site-saturated mutagenesis, random mutagenesis, and both small focused libraries and high-throughput screening of site-saturation libraries at two or three residues.[131,178]

The FAD/FMN-reductase domain resembles mammalian cytochrome P450 reductase (CPR) with 33% identity,[179,180] and both CPR and $P450_{BM3}$ have a lower binding affinity for FMN than for FAD. The haem domain shows 25 – 30% sequence homology with fatty acid ω-hydroxylases from eukaryotes.[181] The first enzymes reported to be both structurally and mechanistically similar to $P450_{BM3}$ were eukaryotic nitric oxide synthases (NOS).[182] $P450_{BM3}$ also has similar characteristics to eukaryotic members of the CYP4A fatty acid hydroxylases,[183] which are found in the liver, kidney and other vital organs in various mammals.[184]

1.6 The engineering of P450

The first report of oxidation of non-natural substrates by $P450_{BM3}$ was by Munro *et al.*, with the NADPH consumption rate of 66 min^{-1} and 24 min^{-1} reported for hexane and octane after the leak rate was taken into account, although product formation rates were not reported.[185]

The Arg47 residue, found at the entrance of this access channel, was replaced by Glu using site-directed mutagenesis, as this was the only charged residue in the substrate-binding site. The activity of the R47E mutant was compared with the WT using C_{12} – C_{16} fatty acids and trimethylammonium compounds as test substrates. R47E was still active towards fatty acids with no selectivity changes, but k_{cat}/K_M values dropped up to 20-fold. The WT showed no significant activity towards C_{12} – C_{16} trimethylammonium compounds, but the R47E variant produced ω–1, ω–2, ω–3 oxidation products with k_{cat} of up to 19 s^{-1}.[186]

The amino acid residues located near the substrate access channel are important in controlling the regio- and stereoselectivity of oxidation reactions by $P450_{BM3}$,[181] and further work on Arg47, and nearby 'sterically gating' Phe87 residues, were not unexpected, as the aromatic ring of phenylalanine lies close to the haem and considered important for controlling the regioselectivity of the products (Figure 1-21). The R47E mutation led to inactivation of the enzyme, but the introduction of the hydrophobic alanine residue led to a preference towards 14,15-*cis*-epoxyeicosatrienoic acid (EET) from arachidonic acid oxidation (154% of the WT), with (14*S*,15*R*)-EET being the major enantiomer (99%), and towards 17,18-*cis*-epoxyeicosatetraenoic acid (EETA) from eicosapentaenoic acid oxidation (137% of the WT), with (17*S*,18*R*)-EETA being the major enantiomer (96%). The F87V mutant formed two-fold more 14,15-EETA product than the WT and with 99% optical purity, and no 18-hydroxyicosatetraenoic acid (OH-AA) product, which was produced from the oxidation by

the WT. The formation of 14,15-EETA was detected for the first time with the F87V mutant, as well as 17,18-EETA, which led to 94% (14*S*,15*R*)-EETA and 96% (17*S*,18*R*)-EETA.[187]

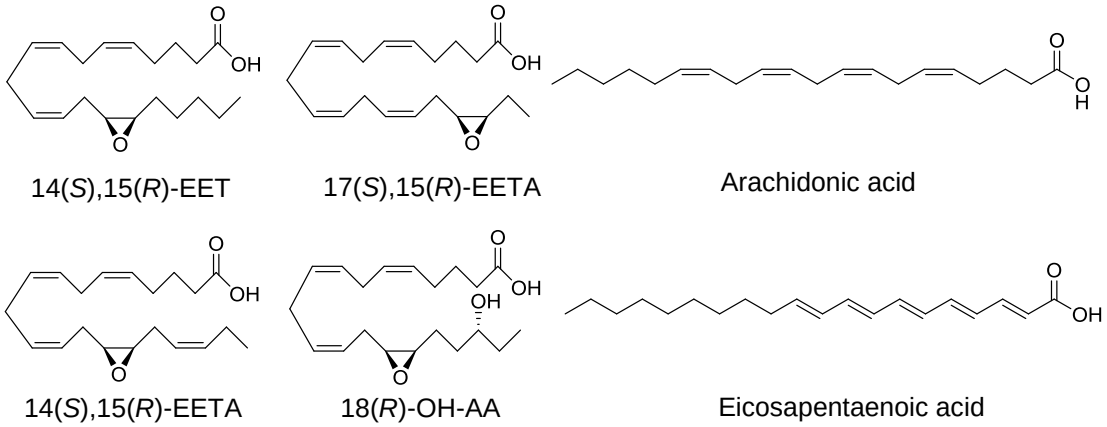

Figure 1-21: Substrates and main products of F87V $P450_{BM3}$ oxidation reactions. Arachidonic acid and eicosapentaenoic acid are selected for test substrates.

Roberts *et al.* introduced the F87A mutation, and NMR paramagnetic relation measurements indicated that this induced a change in the substrate-bound position when the haem centre was in the reduced form (see Figure 1-11).[188]

Schmid *et al.* reported an alternative method of detecting $P450_{BM3}$ activity, using a colorimetric system. This technique was used instead of using NADPH/O_2 or ^{14}C-carboxylic acids, as it was time-saving and cost-effective. The ω oxidation of *p*-nitrophenoxycarboxylate (pNCA) led to the formation of yellow *p*-nitrophenolate (Figure 1-22), and its concentration was assayed at 410 nm (ε = 13,200 M^{-1} cm^{-1}). WT and the F87A mutant were screened with pNCA of different chain length. The use of 96-well plate allowed multiple screening at the same time. For 10- to 15-pNCA the F87A mutant showed higher activities than the WT for longer chain pNCA, with k_{cat} towards 12- and 15-pNCA oxidation improving from 114 min^{-1} to 508 min^{-1} and 246 min^{-1} to 680 min^{-1}, respectively. Interestingly, the hydroxylated ω-product increased to 100% from 33% for 12-pNCA.[189]

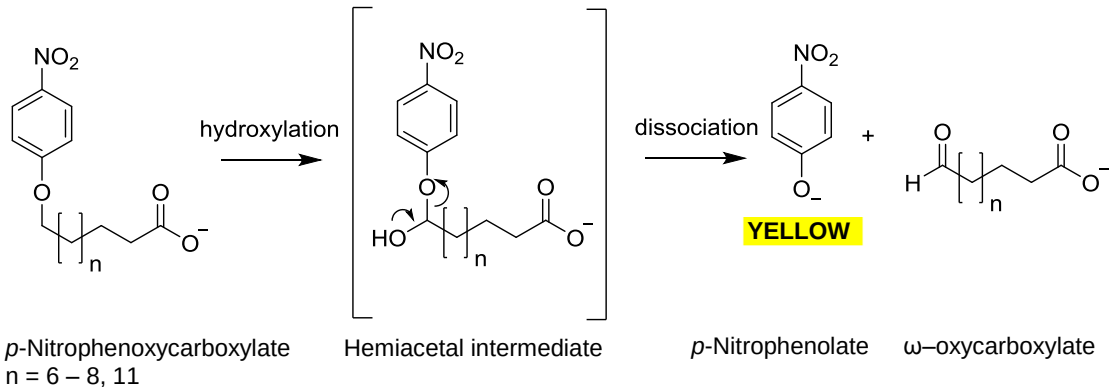

Figure 1-22: The fast colorimetric system to detect high enzymatic activities. The formation of *p*-nitrophenolate from *p*-NCA caused yellow colour to be visible.

Whilst mutants were engineered to target high activity towards shorter-chain fatty acids by Schmid *et al.*, some colonies formed blue pigments after a few hours induction, which were later identified as indigo and indirubin from oxidation of indole in the growth medium (Figure 1-23). Blue pigments were also previously observed during several P450/hNPR expressions.[190] No blue pigments were formed by WT $P450_{BM3}$, and it was concluded that the indigo formation was due to those $P450_{BM3}$ mutants that showed high enzymatic activities, and therefore directed evolution of $P450_{BM3}$ was performed to make variants with more efficient indole hydroxylating abilities. All $P450_{BM3}$ variants that formed blue pigments contained one mutations at Phe87, Leu188 and Ala74 residues, and therefore saturation mutagenesis was performed at these positions. Phe87 was targeted first, and it was found that F87V showed highest formation of the blue pigment. The F87V mutant was previously found to oxidise arachidonic acid with high regio- and stereoselectivity.[187] Subsequently, Leu188 and Ala74 were targeted, and the resulting A74G/F87V/L188Q (GVQ) mutant gave the highest amount of blue pigment. The hydroxylation of indole was performed with the GVQ mutant, and k_{cat} was found to be 2.73 s^{-1}.[191] The GVQ mutant has been used as a basis for various screening work, and will be discusses later.

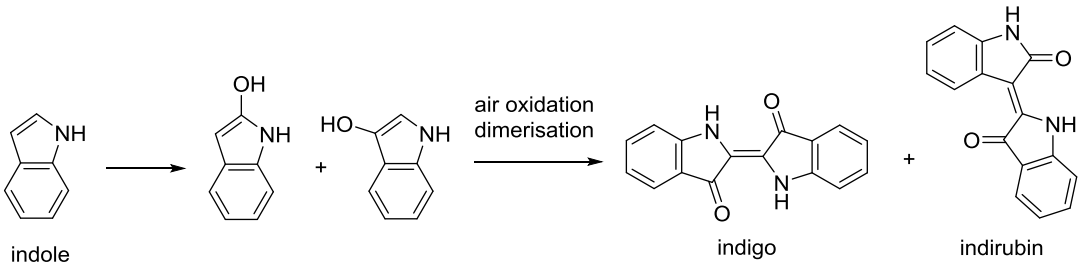

Figure 1-23: The formation of 'blue pigments' caused by indole oxidation. Two possible products are indigo and indirubin.

Arg47 and another residue, Tyr51, at the entrance of the access channel were targeted for mutagenesis. Munro *et al.* reported that the salt bridge between Arg47 and carboxylate, and the hydrogen bond between Tyr51 and carboxylate are important for fatty acid catalysis.[173] The binding of long-chain fatty acids is illustrated by the *N*-palmitoyl glycine (NPG)-bound form of $P450_{BM3}$,[192] where the key amino acids lining the substrate access channel and near the haem are highlighted (Figure 1-24).[193] The carboxylate group near the surface is close to the side-chains of R47 and Y51.

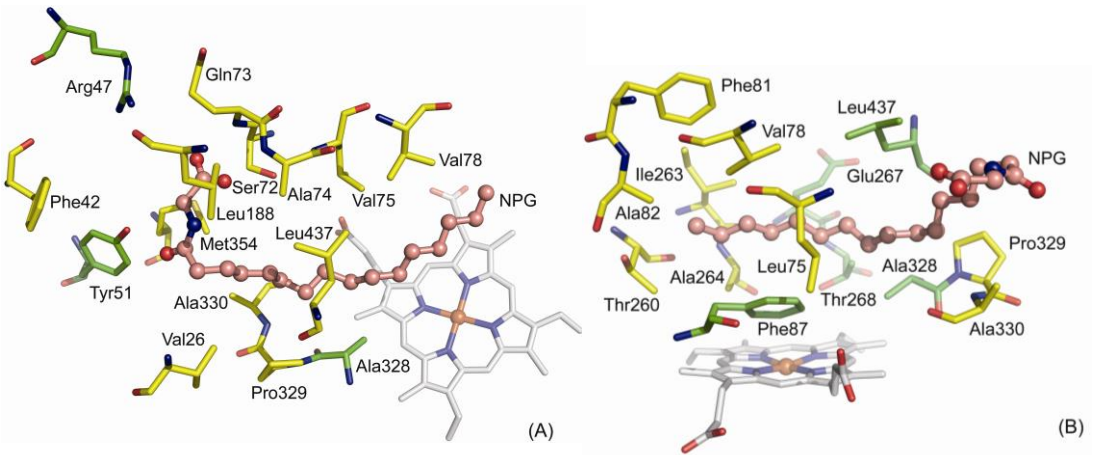

Figure 1-24: The crystal structure of fatty acid-bound WT enzyme. Key residues are highlighted in green. Arg47, Tyr51 are situated at the entrance of the substrate access channel, and Phe87 acts as a gatekeeper to the active site. Ala328 and Leu437 are found near the haem.

Hydrophobic amino acids were introduced at these residues (R47L/Y51F) in order to promote the entry of a hydrophobic PAHs, with test substrates being phenanthrene, fluoranthene and pyrene (Figure 1-25).[194] The R47L/Y51F template was used as the base mutant, and the

subsequent step was to mutate relatively large amino acid residues such as Met354 and Leu437, which are located deeper into the access channel and may be interfering with the PAH binding with the haem. The last step involved performing mutagenesis on residues close to the active site, such as Phe87 and Ala264, to smaller amino acids. Phe87 has been previously targeted and mutated to, e.g. F87V and F87A. The R47L/Y51F couplet greatly improved the product formation rates (PFRs), with the PFR of R47L/Y51F increasing to 22 min^{-1} from 0.5 min^{-1} for phenanthrene oxidation compared to WT. Mutation of Ala264 to glycine further improved the activity to 91 min^{-1}. The RL/YF/A264G mutant showed high activity for pyrene oxidation, with PFR improving from <0.01 to 16.9 min^{-1}. Interestingly, the addition of A264G mutation shifted the selectivity of the products more towards 1-8-pyrenequinone, with 76% of the total products. The effect of the F87A mutation was significant, with a single mutation improving the PFR by more than 100-fold. The RL/YF/F87A/A264G showed high activity towards pyrene with the PFR of 19.5 min^{-1}, with the main product being 1-pyrenol.

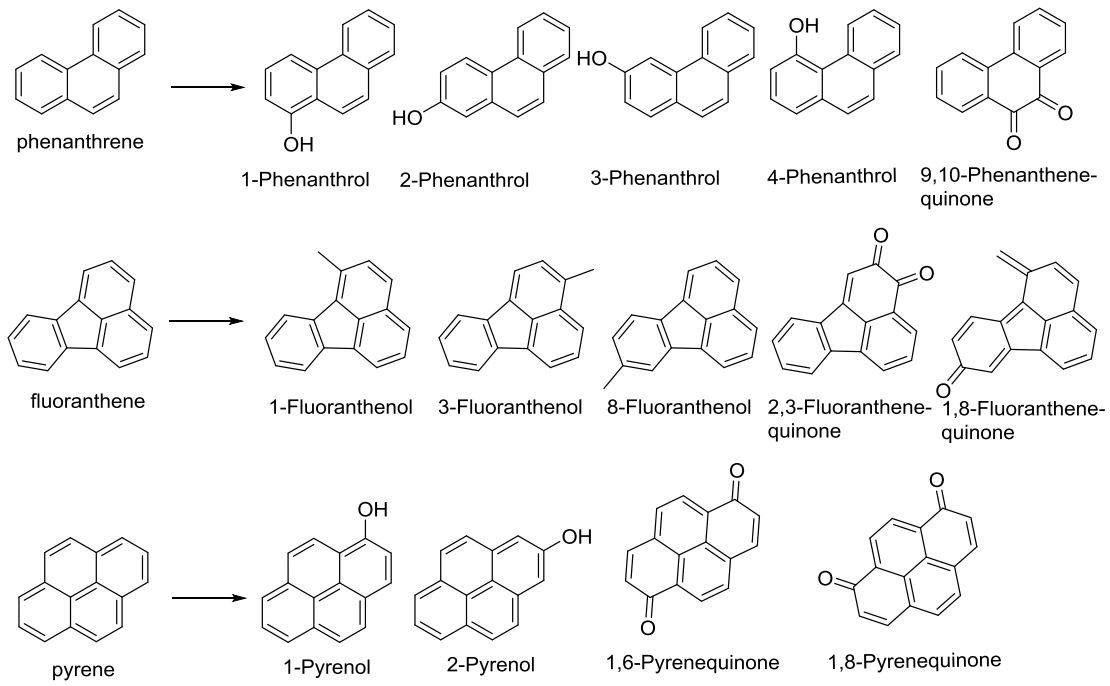

Figure 1-25: The PAH oxidation products by $P450_{BM3}$. Phenanthrene, fluoranthene and pyrene were selected for test substrates.

Directed evolution was performed by Arnold *et al.* by testing the *p*-nitrophenoxy octane (8-pnpane) oxidation activity using the colorimetric assay (see Figure 1-22). The initial step involves transforming $P450_{BM3}$ mutant genes into *E. coli* and plating on agar. Single colonies are picked into 96-well plates, which are grown overnight, and these plates are used to make further 96-well plates to express enzymes. Clones with high activity were identified by looking at their colour, as successful 8-pnpane oxidation leads to the formation of yellow *p*-nitrophenolate and aldehyde (Figure 1-26). Through this method, the activity of the enzyme was improved by five-fold but the mutations were not given.[195] The 8-pnpane was then used as the surrogate substrate to tackle octane oxidation and this is described in section **1.7**.

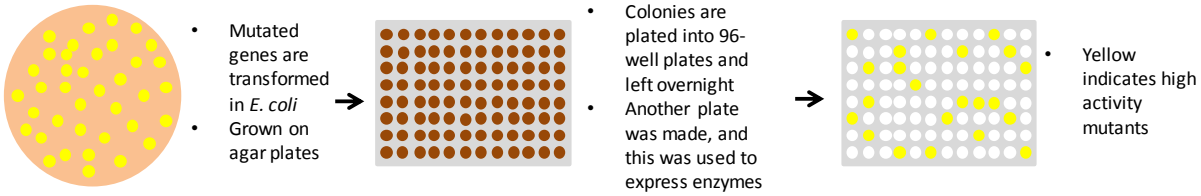

Figure 1-26: The screening process of active $P450_{BM3}$ variants. Yellow colour due to the formation of *p*-nitrophenolate indicates high enzymatic activity.

The oxidation of valencene were performed (Figure 1-27) using WT, R47L/Y51F, R47L/Y51F/F87A and R47L/Y51F/I263A, which opened up the space around the haem for larger substrates.[194] The R47L/Y51F mutant gave 8% β-nootkatol product but no α-nootkatol or nootkatone (WT gave 13% α-nootkatol). The introduction of F87A mutation to R47L/Y51F gave 8% β-nootkatol, 8% nootkatone and 14% nootkatone-13*S*,14-epoxide. The R47L/Y51F/I263A gave mixtures of products, which included both β- and α-nootkatol, nootkatone and *cis*-valencene-1,10-epoxide, indicating the substrate has flexible orientations when bound.[196]

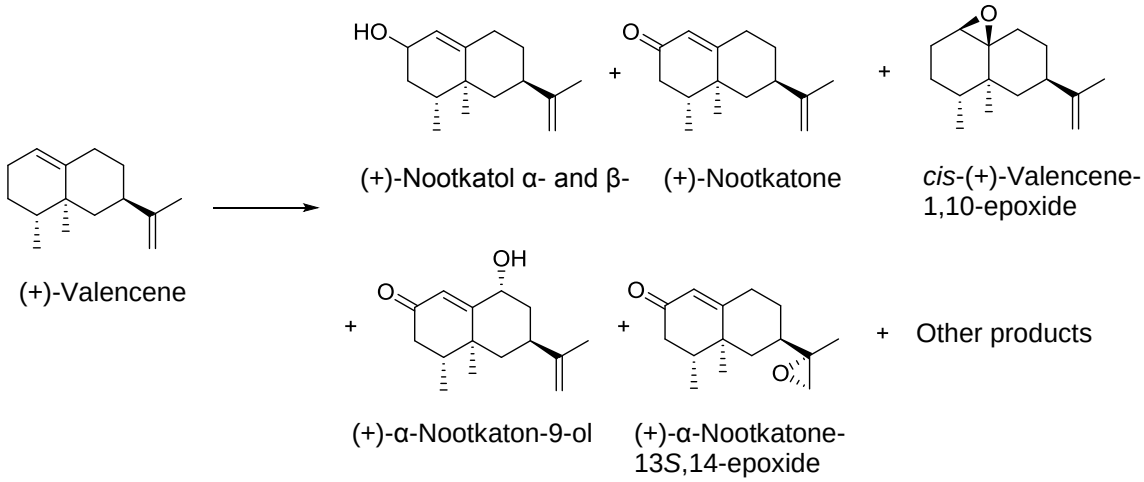

Figure 1-27: The valencene oxidation products.

Vermeulen *et al.* used a fluorescence assay to screen oxidation activities of $P450_{BM3}$ towards drug-like molecules to combat the drawbacks of colorimetric assays such as using pNCAs, which are susceptible to interference from other assay components that absorb at 410 nm, and relatively low sensitivity compared to fluorescence assays. Alkoxyresorufins (methoxy-, ethoxy-, propoxy- and benzyloxy-resorufin) were used as test substrates, as their O-dealkylated products are fluorescent (Figure 1-28).[197] Site-directed mutagenesis was performed to synthesise R47L, R47L/F87V, R47L/L188Q, F87V/L188Q, R47L/F87V/L188Q. R47L/F87V/L188Q showed high activity towards benzyloxyresorufin through fluorescent assay, with the rate of 4.5 nmol min^{-1} (nmol enzyme)$^{-1}$, a 900-fold increase compared to WT. F87V, followed by L188Q, were reported to be the most important mutations for benzyloxyresorufin O-dealkylation (BROD).[198]

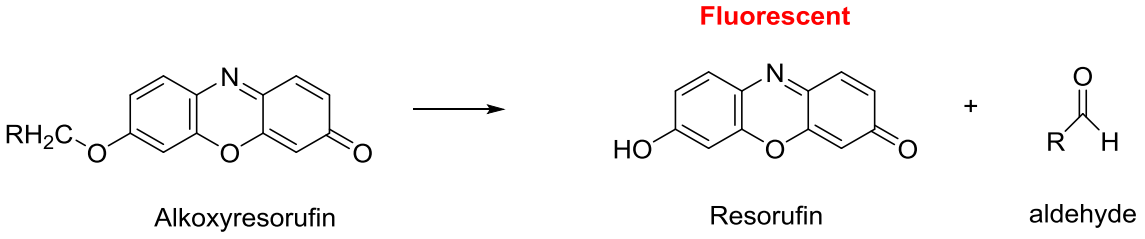

Figure 1-28: The O-dealkylation of alkoxyresorufins. The reaction forms fluorescent resolufin. Methoxy-, ethoxy-, propoxy- and benzyloxyresorufin were used.

The triple mutant, R47L/F87V/L188Q, was used as the base template,[198] and further mutations were introduced randomly by error-prone PCR. Benzyloxyresorufin-O-dealkylation (BROD), pentoxyresorufin-O-dealkylation (PROD), and methoxy/ ethoxyresorufin-O-dealkylation (MROD/EROD) activities were used to screen the activities of variants. Highly active mutants were then tested with dextromethorphan and 3,4-methylenedioxymethylamphetamine (MDMA). Four mutants showed significant activities towards these substrates: R47L/F87V/L188Q/E267V/G415S (M01), R47L/L86I/F87V/L188Q/N319T (M02), R47L/F81I/F87V/L188Q/E267V/G415S (M05), and R47L/E64G/F81I/F87V/E143G/L188Q/E267V/G415S (M11). The mutations L86I and E267V were regarded as highly important. MDMA metabolism by the M02 mutant was four-fold faster than the R47L/F87V/L188Q base mutant. Molecular dynamics (MD) simulations suggested that L86I introduces conformational changes in the nearby residues, leading to a possible opening of the substrate access channel, though it was still not yet clear. The addition of E267V improved the dextromethorphan oxidation activity by 25-fold, relative to the triple mutant, and it was speculated that this may be due to E267V inducing the reshaping of the hydrophobic substrate pocket, changing the orientation of the ligand.[199] Metabolisms of clozapine, diclofenac and acetaminophen were investigated using the same four variants. $P450_{BM3}$ variants oxidised these drugs to generate the same metabolites formed by human and rat liver microsomes, but up to 70-fold more active. M11 showed very high activity towards clozapine, and it was the only variant forming all seven possible products. Similarly, M01 was the only variant to produce all 11 metabolites with diclofenac.[200]

The approach used by Roberts *et al.* was to ‘fill the hole’ of the active site, by closing down the space around the haem. The crystal structure indicated the existence of hydrophobic pocket between residues 81 and 87, where small hydrophobic molecules can bind, leading to non-productive binding. The small alanine at residue 82 was substituted with a larger

hydrophobic amino acid, phenylalanine and tryptophan, and the binding affinity towards laurate improved by *ca.* 800-fold. A82F and A82W were also tested for indole oxidation (see Figure 1-23) and their product concentrations were measured. The total concentrations of indigo and oxindole produced were 75 μM and 70 μM for A82F and A82W, respectively, which were significantly higher than 9.5 μM produced by WT.[201]

Whitehouse *et al.* reported indole oxidation screening of a $P450_{BM3}$ mutant library generated by error-prone PCR on the WT and F87A mutant (Figure 1-23). Colonies that produced the most blue pigment were grown and tested for the oxidation of naphthalene and propylbenzene.[202] Four mutants, A330P, A191T/N239H/I259V/A276T/L353I (KT2), F87A/H171L/Q307H/N319Y (KSK19) and F87A/A330P/E377A/D425N (KT5), were selected for their high activities. The GVQ mutant and F87A were also tested as benchmarks. GVQ showed increased activities compared to WT for both substrates, with PFRs increasing from 3.1 min^{-1} to 487 min^{-1} for naphthalene and from 615 min^{-1} to 1015 min^{-1} for propylbenzene. In comparison, the highest PFR of naphthalene oxidation out of four mutants identified was by the A330P mutant, but PFR was lower than that of the GVQ mutant, with 155 min^{-1}. The KT2 mutant exhibited higher PFR with propylbenzene (2,205 min^{-1}), with 98% 1-phenyl-1-propanol product. F87A, GVQ, KT5, KSK19 produced more 1-phenyl-2-propanol product, with KT5 producing 78% 1-phenyl-2-propanol. The A330P mutant only produced 2% 1-phenyl-2-propanol, but high percentages (30%) of phenol product were observed. The R47L/Y51F mutations, which proved to be important for PAHs oxidations, were added to A330P and KT2, and the resulting PFRs were higher for naphthalene oxidation, with RLYF/A330P reaching 666 min^{-1}. The selectivity towards propylbenzene oxidation was unaffected with the addition of R47L/Y51F. Similar selectivity shifts were observed with *p*-cymene and toluene, and higher activities were observed for pentane oxidation with KT2 and A330P. Further development led to new libraries capable of

oxidising a wide range of compounds, including drugs.[203] More details of A330P and KT2 are given in **1.8**.[202]

Pleiss *et al.* used MD simulations to study the basis of $P450_{BM3}$ selectivity. Bindings of GQ (A74G/L188Q) based variants with (–)-α-pinene and (–)-β-pinene were simulated (possible products shown in Figure 1-29). The effect of mutations at the residue Phe87 was also studied, as the MD simulation suggested this residue acted like a 'gate keeper'. In the (–)-α-pinene oxidation reaction, replacing the F87V of the GVQ mutant with F87G changed the pinene oxide to verbenol product ratio from 70 : 21 to 13 : 77. The shift in selectivity was also observed with (–)-β-pinene, with GVQ giving pinocarveol to myrtanal in a ratio of 68 : 32, to GGQ giving 40 : 60.[204] Pinene oxidation was not detected using WT $P450_{BM3}$.

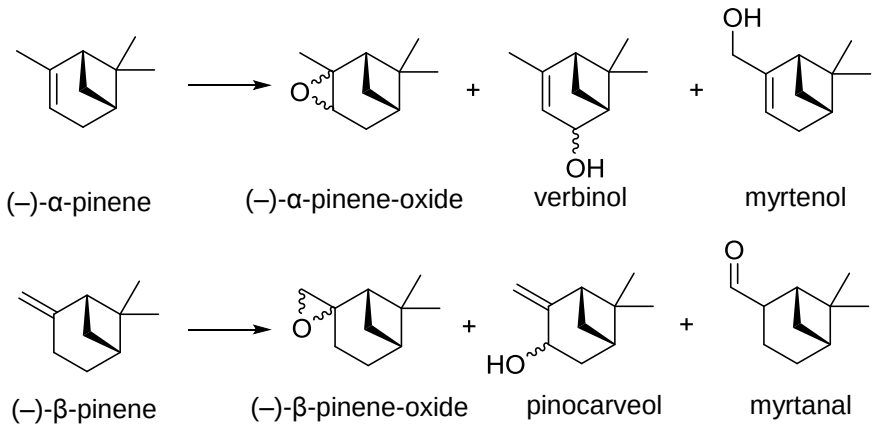

Figure 1-29: Pinene oxidation products. Product selectivity can be controlled by introducing different sets of mutations.

Two positions, Phe87 and Ala328, were mutated to five hydrophobic amino acids (Ala, Val, Phe, Leu and Ile). The position Phe87 was chosen after the work on pinene oxidation. The Ala328 residue was identified as the second 'hot spot' after analysing 31 crystal structures and 6,300 sequences, and Arnold *et al.* introduced mutations at this residue for octane oxidation (see section **1.7**). 24 variants were synthesised and tested with four terpene substrates (Figure 1-30). Only three mutants were inactive towards all four terpenes, and 11 mutants showed different regio- or stereoselectivities to WT. The oxidation of

(4*R*)-limonine by WT gave a total of four products, with carveol being the main product with 54%. The F87V/A328F mutant, however, gave 97% (4*R*)-limonine-8,9-epoxide. Similarly, the F87V/A328V mutant shifted the selectivity of (+)-valencene oxidation, with the percentage of (+)-nootkatol product increasing to 80% from 26%.[205]

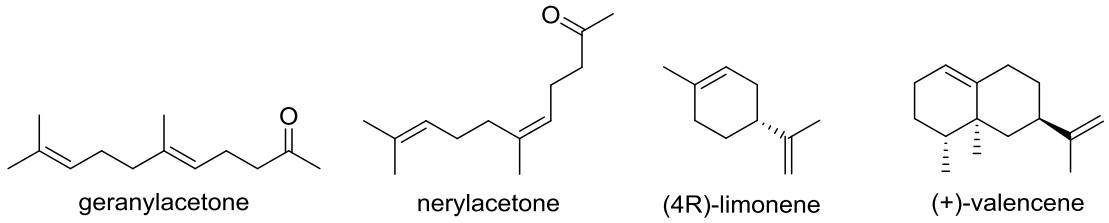

Figure 1-30: Various terpenes with different sizes and shapes used for oxidation.

The variants synthesised for the terpene oxidation work targeting residues Phe87 and Ala328 were used to tackle the oxidation of cycloalkanes (C8, C10 and C12) and n-octane. The mutations to alanine or valine at Phe87 were reported to be the most effective. The F87A mutant oxidised cyclododecane with 20% conversion (WT was inactive towards cyclododecane). The F87A/A328F mutant showed high conversion of 90% towards cyclooctane oxidation and F87A/A328V exhibited 46% conversion with cyclododecane. The F87A showed the highest conversion of 15%, along with F87V/A328F towards n-octane oxidation. The highest selectivity towards 2-octanol product was also achieved by F87V/A328F (92%).[206]

120 $P450_{BM3}$ variants that showed high activities towards non-natural substrates, e.g. straight chain alkanes, cycloalkanes, drug compounds and aromatic compounds, were selected to screen the metabolism of three drugs, verapamil, astemizole and LY294002.[207] The products were analysed using HPLC. These variants are made using techniques such as error-prone PCR and site-directed mutagenesis. Hydroxylations of these drugs were performed, and 12 of 13 known metabolites from mammalian P450 were produced using this $P450_{BM3}$ library, and 7 new oxidation products were also observed, highlighting the versatility of these enzymes.

The D6H10 variant showed high conversion of 78%, with 5 out of 10 possible products formed from verapamil oxidation. The oxidation of LY294002 by the 9-10A F87V mutant showed low conversion of 6%, but the enzyme exhibited high selectivity with only one out of three possible products being formed.[207]

Additional site-directed mutagenesis was performed at the Phe87 residue on the M11 mutant.[206] Initial work involved using the alkoxyresorufins (methoxy- to n-octyloxy- and benzyloxy-) as the substrates (Figure 1-28), and fast NADPH turnover rates up to 6,000 min^{-1} were observed with the M11-F87H with ethoxyresorufin. Couplings were low, with none of the couplings reaching above 1%. The highest couplings were observed for F87A and F87V. NADPH turnover rates were unaffected by the chain length for n-pentyloxy- or shorter resorufins, but NADPH turnover rates dropped with increasing chain length above n-hexyloxyresorufins. Subsequently, testosterone was used as the substrate, and it was found that all mutants produced three expected hydroxylated products (see Figure 1-31), but with different activities and selectivities. The general activity trend towards testosterone was similar to the trend observed for alkoxyresorufins, apart from Phe87 and Thr87, with both showing high enzymatic activities, and their main product was 2β-hydroxytestosterone. Val87, Gly87, Tyr87 and Trp87 containing mutants preferred the formation of 15β-hydroxytestosterone, whereas 16β-hydroxytestosterone product was only synthesised by Ile87 containing variants.[208]

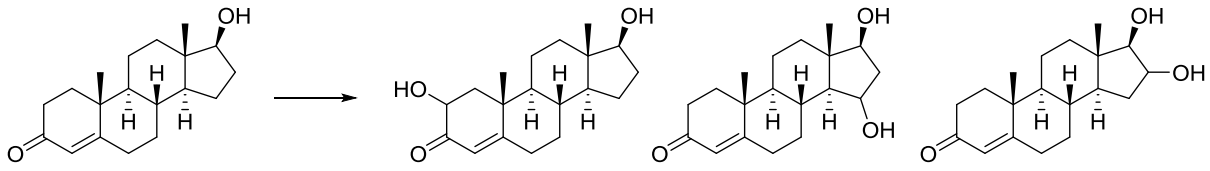

Testosterone | 2β-hydroxy-testosterone | 15β-hydroxy-testosterone | 16β-hydroxy-testosterone

Figure 1-31: Three possible metabolites from testosterone oxidation.

Reetz and co-workers applied directed evolution to $P450_{BM3}$, using saturation mutagenesis which includes the technique called Combinational Active-Site Saturation Test (CAST).[209] Several sets of two or more nearby residues around the active site were mutated randomly, and these mutants were screened for activity. Mutations at multiple residues may lead to unexpected co-operative effects on enzymatic activity. One of the residues mutated in these variants was then introduced with a different amino acid until higher activities were observed. The improved variant was mutated further using saturation mutagenesis at the second residue to achieve the highest enzymatic activity for this set of targeted residues. The starting template was the F87A mutant, as it is well-known that the introduction of smaller residue alanine allowed better substrate binding to the haem for several non-natural substrates by opening up the space around the active site.[194] Testosterone was used as the test substrate. Nine sets of two or three amino acids were screened (Figure 1-32). The F87A variant gave a 1 : 1 mixture of the 2β- and 15β-alcohols. Iterative saturation mutagenesis led to the synthesis of key A330W/F87A and R47Y/T49F/V78L/A82M/F87A mutants, with the former shifting the selectivity towards 2β-alcohol product to 97% with 79% conversion, and the latter giving 96% of the 15 β-alcohol product with 85% conversion. No changes in diastereoselectivity was observed, with all being β-products.[210]

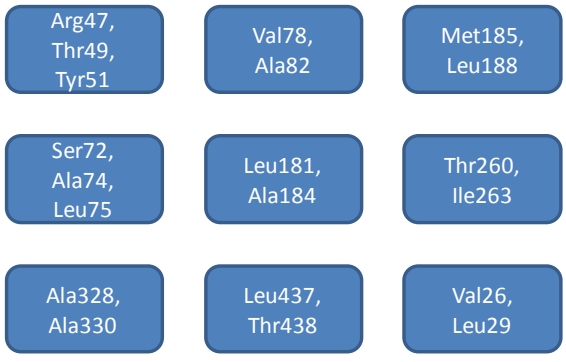

Figure 1-32: Groupings of residues targeted for CAST towards testosterone oxidation.

Cyclopropanations of styrene and ethyl diazoacetate (EDA) were performed using $P450_{BM3}$ variants (Figure 1-33). 92 variants, such as 139-3, 35E11 and $P450_{PMO}$ variants which previously showed to be effective at oxidising octane, propane and ethane,[195,211,212] were screened with $Na_2S_2O_4$ under aerobic conditions. H2A10, H2-5-F10 and H2-4-D4 variants, which all have three to five mutations to alanine around the active site, were identified as key variants, and each mutant was studied in more depth. The $P450_{BM3}$ WT gave a TTN of 5, and 1% yield with 37 : 63 (*cis* : *trans*) product ratio towards EDA, but the introduction of T268A mutation gave mainly the *trans* product (99%) with the TTN of 323 and 65% yield. The introduction of I263A on the 9-10A-TS-F87V/T268A variant reversed the diastereoselectivity, with *cis* : *trans* ratio changing from 71 : 29 to 19 : 81. Five other active site residues were targeted by site-directed mutagenesis, and A328G, T438A, T438S and T438P shifted the selectivity towards the *cis*-product, with A328G also reversing the enantioselectivity. The BM3-CIS-T438S mutant, containing V78A, F87V, P142S, T175I, A184V, S226R, H236Q, E252G, T268A, A290V, L353V, I366V, E442, shifted the selectivity towards the *cis* product (92%), with TTN of 293 and 59% yield.[213]

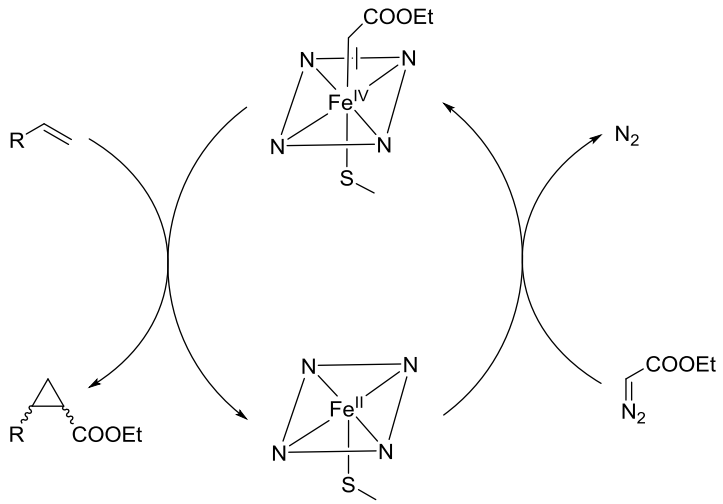

Figure 1-33: Cyclopropanation (carbine transfer) mechanism via a iron^{IV}-carbenoid species using diazoester reagents.

1.7 Alkane oxidation by P450

Screening with 8-pnpane as a surrogate was used as a basis to select $P450_{BM3}$ base mutants for C_3 – C_8 alkane oxidation.[195] The initial work by Arnold *et al.* led to the 139-3 variant after five generations of mutagenesis and screening, which contains V78A, H138Y, T175I, V178I, A184V, H236Q, E252G, R255S, A290V, A295T and L353V mutations. The NADPH turnover rate of 139-3 increased from 2,170 min^{-1} to 3,020 min^{-1} for octane oxidation, with greater percentages of products being 2-octanol (66% from 17%) compared to the WT. The turnover rate of 860 min^{-1} for propane oxidation was reported for the 139-3 mutant, which was almost a 60-fold increase over the WT.[71]

Further work on octane oxidation was performed to shift the selectivity towards the terminal position using hexyl methyl ether (HME) as an octane surrogate and the Purpald assay (Figure 1-34). The purple colour was observed when the hydroxylation takes place at the methyl group and forms formaldehyde (route A), and similarly the pink colour indicated the oxidation at the ω–2 position, forming hexanal (route B). Oxidation at any other positions led to colourless products (route C). The starting template was the mutant 9-10A, containing the mutations R47C, V78A, K94I, P142S, T175I, A184V, F205C, S226R, H236Q, E252G, R255S, A290V and L353V, which showed a TTN of 3,000 and gave 1% 1-octanol.[214] The introduction of A328L and A328M shifted the selectivity more towards the terminal position, with 13% and 24% 1-octanol, respectively, and no 3-octanol or other internal oxidation products were detected. However, the TTN dropped to 700 for the 9-10A/A328M mutant. A82L and A328V mutations were added to 9-10A, and the resulting 1-12G mutant showed high activity, with a TTN of 7,500, but only 3% of 1-octanol. The highest proportion of 1-octanol was observed for the 77-9H mutant (52%), which contains all the mutations in 9-10A, and additionally the A78T, A82G and A328L mutations. The TTN, however, was lower with 1,300.[215]

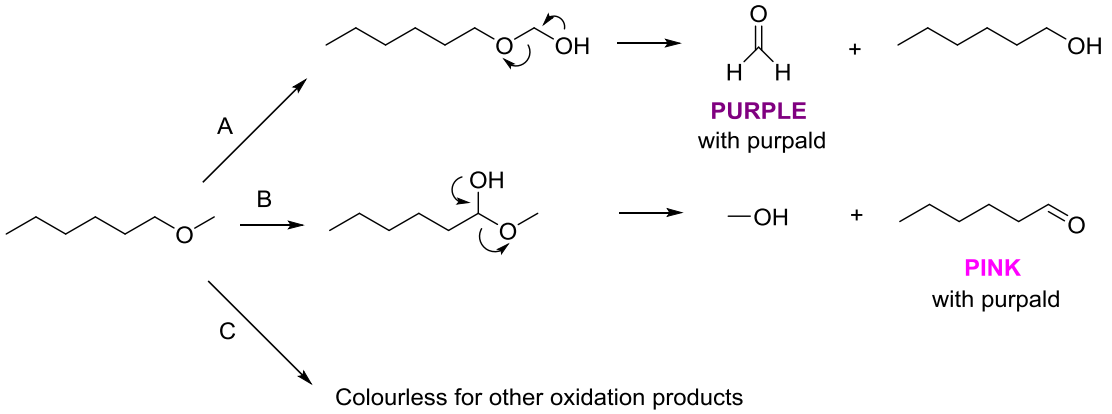

Figure 1-34: The hydroxylation of hexyl methyl ether (HME) is detected by Purpald dye. Aldehyde products react with Purpald to give purple/pink colour.

Hydroxylation of small alkanes down to ethane was studied using directed evolution, site-directed and site-saturation mutagenesis. Dimethyl ether (DME) was used for one of the screening techniques due to its similarity in size and C–H bond strength to propane (Figure 1-35). The formaldehyde product was then detected with the Purpald dye as described in Figure 1-35.[216] The 9-10A mutant was chosen to develop further variants, and saturation mutagenesis on residues around the active site was performed. V78F, A82S, A328F were identified as key mutations. Combinations of screening and random mutagenesis led to another two important mutations, the linker E464G mutation and reductase domain I710T mutation. The TTN of the resulting mutant 35E11, was 250 and 6,000 for ethane and propane oxidations, respectively.[211]

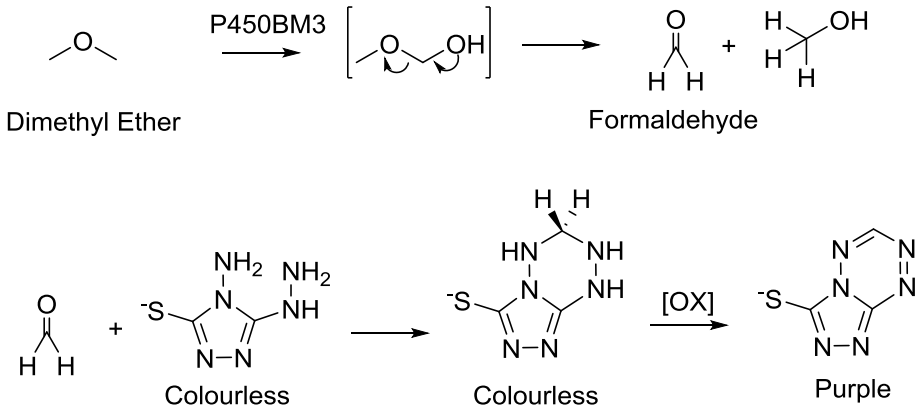

Figure 1-35: The hydroxylation of dimethyl ether (DME) is detected by Purpald dye. Formaldehyde reacts with Purpald to give a purple colour.

Further protein engineering was performed on the 35E11, with its haem, FMN and FAD being targeted (Figure 1-36). These domains were mutated separately and the best mutations were combined. DME screening was used (Figure 1-35), and mutations were introduced using random, saturation and site-directed mutagenesis. The initial mutagenesis step was to improve the stability of the enzyme (route **A**), where the stabilising mutations from $P450_{BM3}$ peroxygenase were introduced.[217] Thermostability of the enzyme was found by heating to high temperatures and measuring the temperature when half of the enzyme has denatured using the standard ferrous-CO P450 assay (see **1.2.1**).[218] Mutagenesis by error-prone PCR was performed on the thermostable ETS8 to synthesise 19A12 (route **B**), which gave two-fold increase in TTN. Further engineering by saturation mutagenesis along the substrate channel and around the active site led to various mutants such as the 11-3 variant with higher activities (route **C**). The key mutations identified after route **C** were then combined and finely tuned by recombination and site-saturation techniques (route **D**). The resulting 7-7 mutant gave a TTN of 20,500. Random mutagenesis was performed on FMN and FAD domains (routes **E** and **F**) and G443D, V445M, T480M, T515M, P654Q, T664M, D698G and E1037G were identified as important mutations. Further optimisation of these key mutations by saturation mutagenesis led to 11-3 based variants containing mutations in the FMN and FAD domains except T515M (routes **G** and **H**). These mutations were also introduced to the 7-7 mutant (route **I**), resulting in $P450_{PMO}R2$ which reportedly gave the TTN of 45,800 with 10% 1-propanol product.

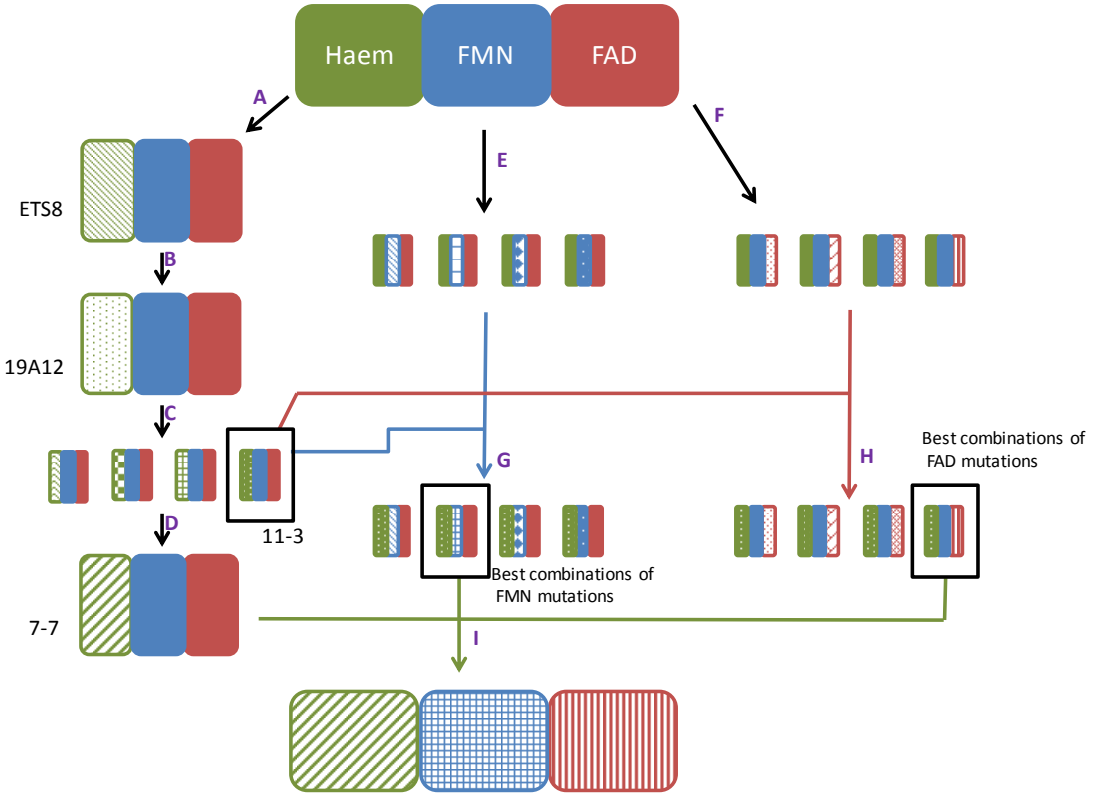

Figure 1-36: The synthetic route from 35E11 to $P450_{PMO}$ variants. Thermostability of the enzyme was improved in step A, whilst the best set of mutations was found through random and site-saturation mutagenesis in steps B – D. Random mutagenesis was performed on FMN and FAD in steps E and F, and the variant was further optimised in steps G – I.

Combinatorial site-saturation mutagenesis (CSSM), C^{orbit} and Challenge Response Authentication Mechanism (CRAM) were used to synthesise further variants.[219–221] The DME screening technique (Figure 1-35) was again used to identify key variants, and these were tested towards propane and ethane oxidations. 0.5 mL reaction mixtures containing, 50 –200 nM $P450_{BM3}$, 20 mM isocitric acid trisodium salt, 400 µM $NADP^+$ and 0.5 U mL^{-1} isocitrate dehydrogenase and 0.1 M phosphate buffer were used for propane and ethane oxidation reactions. The reaction mixtures were pressurised to 30 psi, and left stirring for 20 hours at 4 °C. The A74W/V78I/A82L/A184V/L188W/A328F/A330W mutant was reported to give a TTN of 16,800 for propane oxidation. This mutant, and the analogous mutant with A74L in place of A74W were reported to oxidise ethane with a TTN of 1,200.[222]

Reetz and co-workers have reported that the addition of a chemically inert perfluorocarboxylic acid (PFC) as a dummy substrate promotes the hydroxylation of propane and methane by WT $P450_{BM3}$ at 10 bar total pressure (7% alkane, 8% O_2, and 85% N_2).[223] The inert dummy substrate fills the space in the P450 binding pocket, pushing the substrate closer to the haem to enforce alkane oxidation. 2.5 mL reaction mixture was prepared containing 0.1 M D-glucose, 1 mM $NADP^+$, 1 U mL^{-1} glucose dehydrogenase (GDH), 1 mM PFC, 2.3 µM/2.9 µM $P450_{BM3}$ for propane/methane, and 100 mM KPi, pH 8.0. Reaction mixtures were stirred at 100 rpm for 21 hours and 14.5 hours for methane and propane, respectively. Propanol was analysed using the GC, but the LaCourse method of pulsed amperometric detection, and GC/MS were used to identify the methanol product.[224] The addition of PFC11 led to 3 mM of 2-propanol formed, giving a TTN of 1,020. Reetz also reported methane oxidation (TTN = 2,470).

The hydroxylation of n-butane at various temperatures using the glucose/GDH cofactor regeneration system and the 19A12 $P450_{BM3}$ mutant has been reported.[71] The boiling point of n-butane is –0.5 °C. Reactions were run at room temperature, 8 °C, 0 °C, –1 °C, and –5 °C for 8 hours, and the reaction mixtures were warmed up to room temperature over 16 hours. One more reaction was set up at 0 °C, but this was worked up immediately after 8 hours.
0.06 g L^{-1} of 2-butanol product was observed at room temperature, but higher concentrations of 2-butanol were observed at 0 °C, with 0.16 g L^{-1} (2.2 mM) for normal work-up (warmed up to room temperature over 16 hours) and 0.14 g L^{-1} (1.88 mM) for direct work-up. The increase in activity at low temperatures is due to an increase in the aqueous alkane solubility. Product concentrations did not increase below the boiling point, due to the frozen reaction mixtures.[225]

Work performed by Watanabe *et al.* was on butane, propane, ethane and methane oxidation with WT $P450_{BM3}$. Initially, C_8 – C_{14} PFC were tested with the WT, and propane as the

substrate. 500 nM $P450_{BM3}$, 100 µM PFC and alkane/O_2- saturated 20 mM Tris-HCl buffer, pH 7.4, were prepared, and 5 mM NADPH was added to initiate the reaction. During the reaction, an alkane- and O_2- containing balloon was attached to pressurise the reaction mixture which was kept at 20 °C. 1 mL of the reaction mixture was extracted after 10 minutes as the nitrite. The addition of PFC10 to WT $P450_{BM3}$ led to a PFR of 67 min^{-1}, with 18% coupling efficiency.[226] Another set of reactions was performed under 5 bar (propane and ethane) and 0.7 bar (methane) partial pressure with the PFC10 decoy molecule. The propane oxidation reaction mixture was set up in the same manner as before, but with a 1-hour reaction time. 2,170 µM 2-propanol and 50 µM 1-propanol were detected for propane oxidation (TTN = 4,440). Ethane hydroxylation was also studied under the similar condition, but $P450_{BM3}$ and NADPH concentrations were increased to 1 µM and 5 – 15 mM, respectively, and the reaction mixtures were stirred for 1 – 3 hours. Up to 80 µM ethanol product was observed on the GC with ethanol background taken into account. Methane oxidations were performed using NADPH as described for ethane reaction, and a $NADP^+$ recycling system (1 unit GDH, 100 mM glucose) to mimic the reaction condition used by Reetz and co-workers.[223] No methanol product was observed (TON = 0.02 – 0.05).[227]

Watanabe also altered decoy molecules for a better 'fit' around the active site. It was previously reported that *N*-palmitoyl glycine was a better substrate than palmitic acid for WT $P450_{BM3}$, as the newly formed hydrogen bond between the carboxylate group of *N*-palmitoyl glycine, and Gln73 and Ala74 led to stronger binding.[228] The resulting increase in enzymatic activity from the R47L/Y51F mutations (see **1.6**) also led to the idea that increasing hydrophobicity at the entrance of the substrate access channel may improve activities towards hydrophobic substrates. The synthesis of various *N*-perfluoroacyl amino acids with hydrophobic side chains were performed, and their effects on propane and ethane activities

were monitored. The addition of PFC9-*L*-Leu achieved PFR of 279 min^{-1} and 45 min^{-1}, for propane and ethane respectively.[229]

1.8 Base mutants of this work towards alkane oxidation by $P450_{BM3}$

New mutants of $P450_{BM3}$ were discovered by Whitehouse *et al.* using a simple screening procedure on a random mutagenesis library, where only colonies that showed blue indigo pigment from indole oxidation after 36 hours of incubation were considered relevant (see **1.6**).[230] Further screening and activity studies have identified a number of 'generic accelerator' variants showing fast turnovers for a wide range of substrates. Residues previously targeted are highlighted in Figure 1-37. R47L/Y51F, which itself increased catalytic activity,[194] was combined with the accelerator variants KT2, A330P, and I401P.

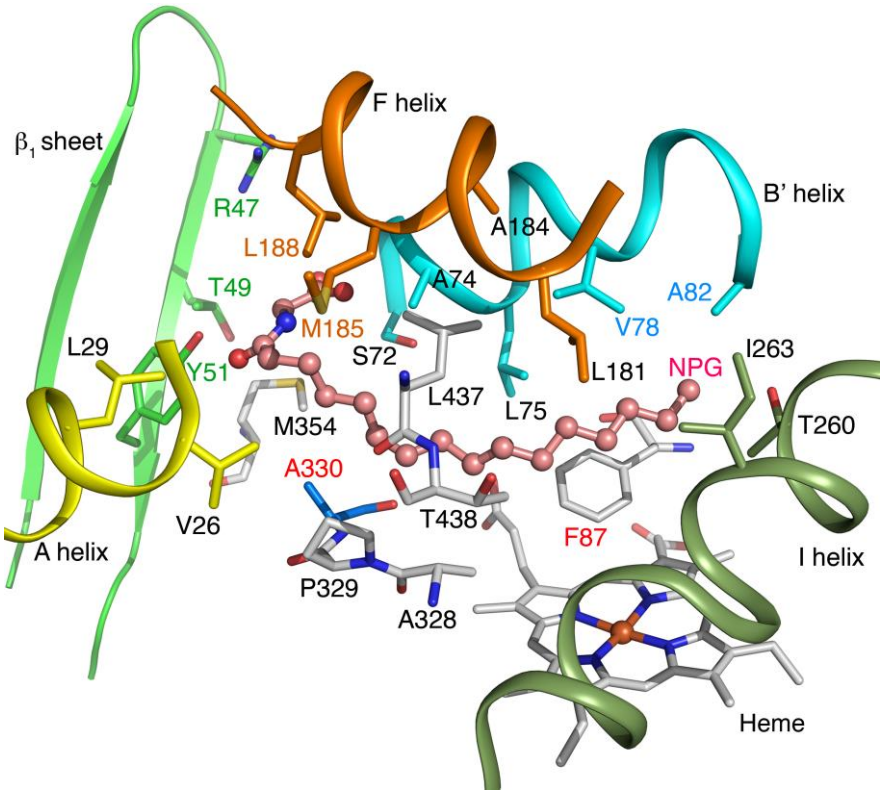

Figure 1-37: The key amino acid residues around the $P450_{BM3}$ active site. R47 and Y51 are found at the entrance of the substrate access channel, and mutations at Phe87 have been targeted by various groups. Different sets of mutations were also performed on B′- and I-helices, for e.g. testosterone oxidations (**1.6**). Mutations at Ala328 and Ala330 have improved activities towards smaller alkanes, such as pentane and octane (**1.7 and 1.8.1.1**).

1.8.1.1 A330P

Ala330, found at the end of the K-helix, was mutated to proline (Figure 1-38). This is adjacent to another Pro residue at 329, causing this latter, substrate channel residue to be relocated into the active site, reducing its volume and increasing the activity and coupling efficiency towards smaller molecules, including linear alkanes.[231]

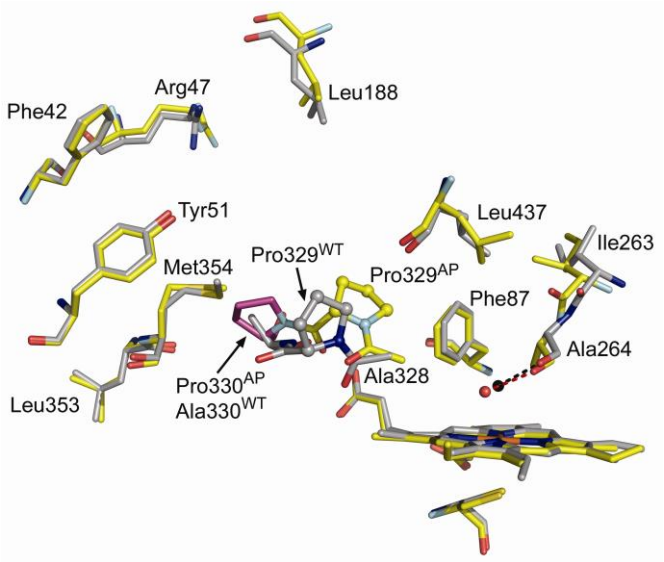

Figure 1-38: The crystal structure of A330P.The mutation A330P causes Pro329 residue to reorient itself into the active site, reducing the volume of the substrate pocket and increasing the coupling with small molecules.

1.8.1.2 I401P

The I401P mutation causes the Ala399–Gly402 loop to drop away from the active site,[232] and this shifts the iron atom to the proximal side, towards Cys400 by 0.5 Å. This movement elongates the Fe–OH_2 bond by 1.1 Å, allowing the water molecule to be displaced more easily, and this lowers the reorganisation barrier to the rate-limiting first electron transfer of the catalytic cycle, thus increasing the turnover frequency (TOF) with non-natural substrates (Figure 1-39).[231]

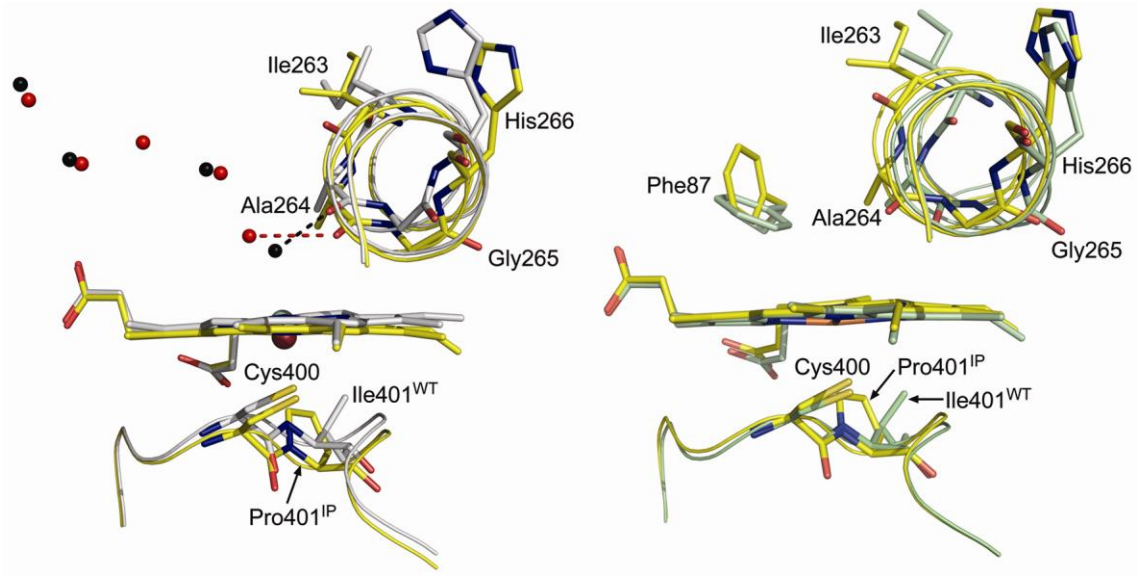

Figure 1-39: Substrate-free (left) and substrate-bound (right) form of I401P. Compared to the substrate-free form (grey) on the left, the I401P (yellow) mutation pulls the haem away from the active site, elongating the Fe–OH_2 bond in the process. The water molecule in WT (black) is directly above the haem, but it is off-axial in the I401P mutant (red). I401P causes the location of the proximal loop and the haem to resemble the substrate-bound form (green) on the right.

1.8.1.3 KT2

KT2 contains five mutations, A191T/N239H/I259V/A276T/L353I, none of which is in the active site (Figure 1-40). The crystal structure revealed that the salt bridge between Asp217 (G-helix) and Arg255 (I-helix) is broken, causing the I-helix to be displaced significantly and breaking the hydrogen bond between the carbonyl oxygen of Ala264 and the axial water. This weakens the Fe–OH_2 interaction and promotes the binding of substrates close to the haem as well as lowering the barrier to electron transfer for the substrate-free form.[233]

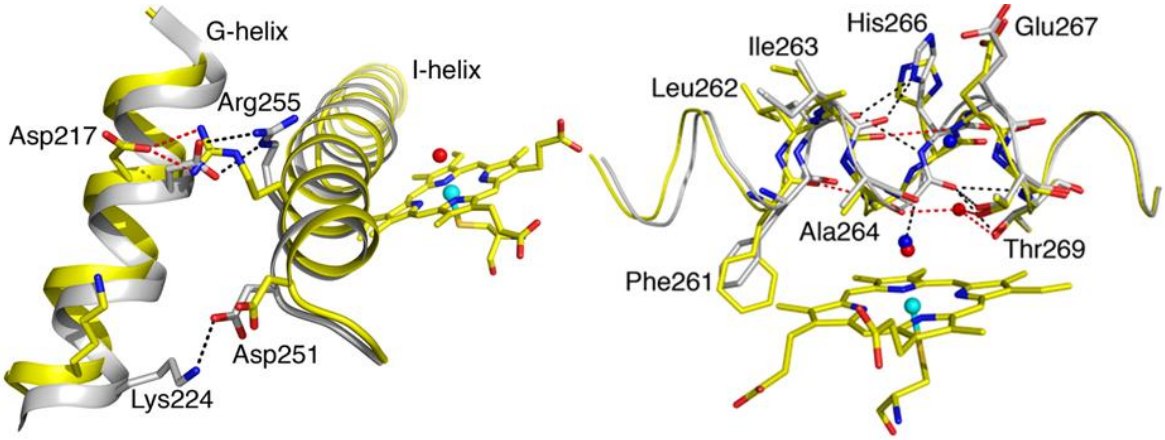

Figure 1-40: The location of the five mutations in the KT2 variant. Five mutations are A191T, N239H, I259V, A276T and L353I. Substrate-free KT2 is in yellow (waters are blue spheres and hydrogen bonds are in red) and the substrate-free WT in grey (waters are red spheres and hydrogen bonds are in black). The figure on the left shows the salt bridge between Asp217 and Arg255 being broken and the I-helix shifting upon introduction of the KT2 mutation. The figure on the right indicates the absence of water molecule between Ala264 and Thr269 in substrate-free KT2.

1.9 NADPH regeneration system

Hydrocarbon oxidation by $P450_{BM3}$ requires two electrons, which are normally derived from a NADPH cofactor.

$$R–H + H^+ + NADPH + O_2 \rightarrow R–OH + H_2O + NADP^+$$

The reaction can be considered as a two-electron oxidation of NADPH to $NADP^+$ and a proton. The two electrons and this proton, together with an external proton, are used to activate O_2 to form water while the second oxygen atom is inserted into a C–H bond. In biocatalytic applications the NADPH cofactor can be regenerated from $NADP^+$ by glucose and GDH,[234,235] which oxidises glucose to gluconolactone that in turn spontaneously hydrolyses to gluconic acid, rendering the reaction irreversible (Figure 1-41).

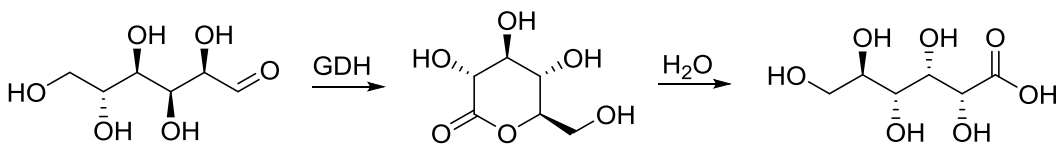

Figure 1-41: The conversion of glucose into gluconic acid via gluconolactone. The formation of gluconic acid may lead to acidification of the reaction mixture.

High substrate conversion TTN by the P450 enzyme will lead to acidification, which can be controlled by simple automated titration with NaOH, while on a small scale the use of 100 – 200 mM phosphate buffer is sufficient.

The bacterium *Ralstonia Eutropha* contains various hydrogenase enzymes that are able to oxidise H_2 for energy synthesis, but of particular interest in this work is soluble hydrogenase (SH). SH is capable of reducing NAD^+ to NADH by coupling with the oxidation of H_2, and thus SH is now being used to supply NADH to a cofactor-dependent enzyme, such as $P450_{BM3}$ – the subject of this thesis. The SH used in this work is active in the presence of O_2, with its activity only dropping by 20% at 60% O_2.[236] The original SH consists of $HoxFUYHI_2$,[237] and it includes one [2Fe-2S] centre, four [4Fe-4S] clusters[238] and two FMN groups.[239]

As the Figure 1-42 suggests, the hydrogenase dimer is used as the electron source for NAD^+-reductase subunits (HoxFU),[240] and therefore direct electron transfer to and from the external source, such as an electrode is possible. This method allows easier extraction and isolation of products, as no reagent is required to provide electrons.[241] However, an electrochemical system may not be favourable in an industrial scale, and thus dihydrogen may be used as an alternative source for both electrons and protons.[242]

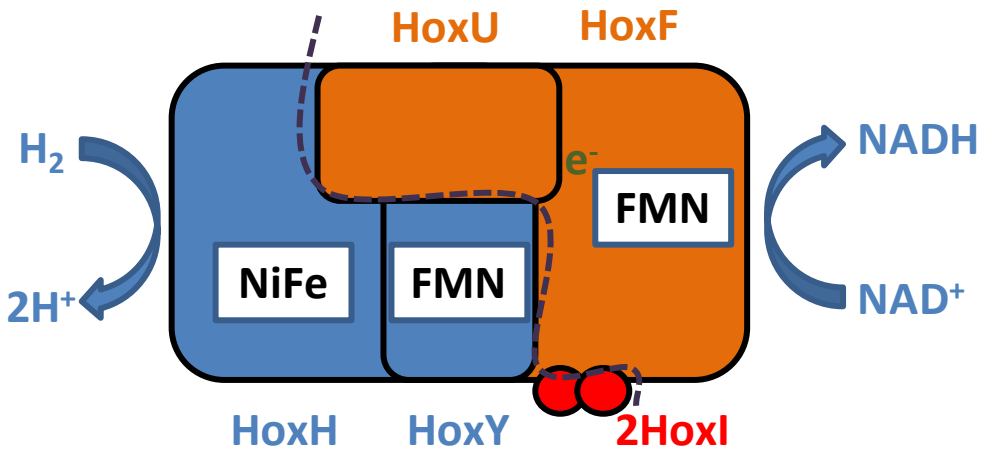

Figure 1-42: A schematic representation of the SH from *Ralstonia eutropha*. The NAD^+ reducing subunits (HoxFU) are in orange and the hydrogenase subunits (HoxHY) are in blue. The enzyme can be split at the purple dotted line. The HoxI subunits (in red) can easily dissociate, especially at high ionic strength, and their functions are not known.[243]

1.10 Thesis objectives

The most widely recognised role of human P450 enzymes is the metabolism of clinical drugs. Ren *et al.* had shown that mutants such as RP/F87V/E267V, oxidised testosterone up to 100% conversion while the WT enzyme has minimal activity.[203,208,244] Similarly, the activity of WT enzyme towards most hydrocarbons is low (PFR = 15 min^{-1} and 0.2 min^{-1} with butane and propane, respectively), mainly due to the low coupling whereby electrons from NADPH entering the catalytic cycle are channelled off to unproductive pathways. Engineering of the active site topology is required for increased activity.

The overall aim of this work is to develop an enzyme cascade (hydrogenase/$P450_{BM3}$) for alkane oxidation, with the long-term aim of performing catalytic methane oxidation. The high bond enthalpy of C–H bonds in methane results in the catalytic oxidation of methane being more challenging, and therefore butane and propane are targeted first. The accelerator variants A330P, I401P and KT2 will be used as a basis to improve the activity towards these substrates. R47L/Y51F/KT2 and R47L/Y51F/A330P mutants reportedly gave higher couplings of 60% and 67% towards pentane oxidation, compared to 21% for the WT.[202] The

crystal structure of fatty acid-bound WT (Figure 1-24) illustrates that the aliphatic chain end of fatty acid stretches within the substrate access channel lined with mainly hydrophobic residues into another hydrophobic active site; 5-coordinated haem indicates that iron centre is HS, but the substrate is still quite far away (>8 Å) from the haem. The most obvious approach will be to use bulky substitutions around the haem to reduce the active site volume so that the small gaseous alkanes are constrained to bind closer to the haem iron for faster substrate C–H bond oxidation. Those mutants with high enzymatic activities towards these substrates will be used as a basis to tackle ethane and eventually methane oxidation. The NADPH turnover rates will be used to initially screen various mutants, and some of these mutants will be selected for TTN assays analysis. Reactions will also be performed under different conditions, such as running the reaction under pressure and with decoy molecules, and their effects are monitored.

The highly active $P450_{BM3}$ mutant, along with the best condition will be used as the basis to perform alkane oxidation using hydrogen-driven cofactor recycling. Octane was selected as the initial substrate, due to its relative ease to being oxidised, and it is not a gaseous alkane. If successful, hydrogen-driven oxidation of a short-chain alkane such as propane will be tested.

Chapter 2

Materials and Methods

2.1 Materials, chemicals and equipment

2.1.1 Chemicals, solvents and enzymes

General chemicals, reagents and media components were from Melford Laboratories, Alfa-Aesar, Fisher Scientific and Sigma-Aldrich. Propane and methane were from BOC Speciality Gases, and ethane was from Air Products. 2-Pentanone used as the internal standard was from Alfa-Aesar, and in earlier work, 1-propanol, which was from Sigma-Aldrich, was used as an internal standard. Anhydrous 1-hexanol used for extraction was from Sigma-Aldrich and Fisher Scientific. K_2CO_3 was also from Fisher Scientific, and kanamycin (Kan) was from Melford Laboratories. $NADP^+$/ NADPH, NAD^+/NADH, glucose and isopropyl-β-D-1-thiogalactopyranoside (IPTG) were from Fisher Scientific. GDH was from Codexis (California), and oligonucleotides were from Eurofins Genetics Services, UK. *E. coli* DH5α and BL21 (DE3) competent cells were from NEB.

2.1.2 Growth media and buffer components

All growth media were autoclaved prior to use. Solutions were filter-sterilised using 0.22 μM syringe filters before being added after autoclaving. Water used for the preparation of growth media, buffers and mutagenesis, was purified by Millipore Elix systems with the resistivity of ≥ 8 MΩ cm^{-1}. All buffers used were at pH 7.3 – 7.5, and media components are shown in Table 2-1. Kan (30 mg L^{-1}) was added to the growth media, after the media was cooled down to ambient temperature.

Table 2-1: Components for all the media and buffers used in this work.

Media and buffers	Components (per Litre)
LB_{agar}	10 g tryptone, 5 g yeast extract, 10 g NaCl, 15 g bacto-agar
LB	10 g tryptone, 5 g yeast extract, 10 g NaCl
$FB_{Glycerol}$	14.7 g K_2HPO_4, 3.6 g NaH_2PO_4, 2.5 g $(NH_4)_2SO_4$, 2 g Na_2SO_4, 1.2 g Na_3citrate.$2H_2O$, 0.5 g NH_4Cl, 5 mL glycerol Post autoclaving – 2 mL 1 M $MgSO_4.7H_2O$, 3 mL trace elements solution, 1 mL 10% w/v thiamine
2YT	16 g tryptone, 8 g yeast extract, 5 g NaCl
Trace elements	20.1 g Na_2EDTA, 16.7 g $FeCl_3.6H_2O$, 0.74 g $CaCl_2.H_2O$, 0.25 g $CoCl_2.6H_2O$, 0.18 g $ZnSO_4.7H_2O$, 0.132 g $MnSO_4.4H_2O$, 0.1 g $CuSO_4.5H_2O$
SOC	20 g tryptone, 5 g yeast extract, 0.5 g NaCl Post autoclaving – 10 mL 1 M $MgCl_2$, 10 mL 1 M $MgSO_4$, 2 mL 20% w/v glucose
Buffer P	4.9 g K_2HPO_4, 1.6 g KH_2PO_4
100 mM KPi	10 mL 1 M Phosphate, 900 mL water (pH 7.4)
1 × TAE (from Millipore)	4.84 g Tris, 1.14 mL glacial acetic acid, 2 mL 0.5 M NA_2EDTA
TFB 1	30 mM potassium acetate, 10 mM $CaCl_2$, 50 mM $MnCl_2$, 100 mM RbCl, 15% glycerol (pH adjusted to 5.8 with 1 M acetic acid)
TFB 2	100 mM MOPS or PIPES (pH 6.5), 75 mM $CaCl_2$, 10 mM RbCl, 15% glycerol (pH adjusted to 6.5 with 1 M KOH)

2.2 Site-directed mutagenesis

2.2.1 DNA mutations

WT, KT2, RT2, GVQ, and RP templates were used as the basis to build the library of mutants listed in Table 2-2. Some mutations within these variants were reversed back to the original amino acid residue of the WT using the designed primers. The CYP102A1 gene was inserted to pET28a, that confers the Kan resistance marker (Figure 2-1).[245]

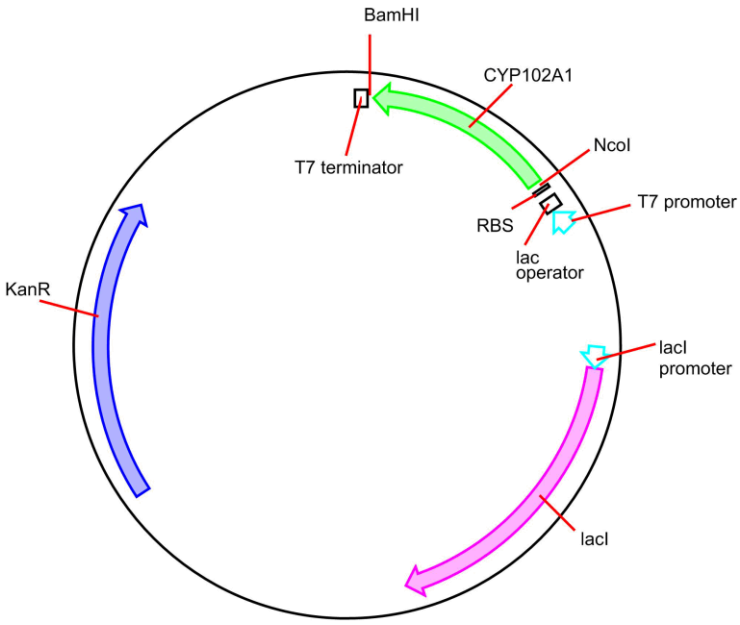

Figure 2-1: pET28a vector map with CYP102A1 gene inserted between NcoI and BamHI.[194]

Table 2-2: A list of $P450_{BM3}$ mutants and DNA codes. The bases in green were changed to bases in red. [a]"/" denotes mutations were added to the backbone simultaneously, and "+" denotes mutations were added individually. Full primer sequences can be found in **Appendix 2**.

Variant Name	Backbone + mutations[a]	Coding DNA
N70S	WT; N70S	AAC → AGC
N70S/M237L	N70S; M237L	ATG → CTG
N70S/M237L/A328V	N70S/M237L; A328V	GCT → GTT
N70S/ M237L/A328V/H171L	N70S/ M237L/A328V; H171L	CAT → CTT
H171L	WT; H171L	CAT → CTT

L188Q	WT; L188Q	CTG → CAG
M237L	WT; M237L	ATG → CTG
A328F	WT;A328F	GCT → TTT
A328V	WT; A328V	GCT → GTT
A330P	WT; A330P	GCG → CCG
A330P/L188Q	A330P; L188Q	CTG → CAG
AP/LQ/A74G	A330P/L188Q; A74G	GCG → GGG
AP/LQ/A191T	A330P/L188Q; L188Q/A191T	CTG → CAG/ GCA → ACA
AP/LQ/I259V	A330P/L188Q; I259V	ATT → GTT
AP/LQ/A328F	A330P/L188Q; A328F/A330P	GCT → TTT/ GCG → CCG
AP/LQ/A328V	A330P/L188Q; A328V	GCT → GTT
AP/LQ/T438F	A330P/L188Q; T438F	ACG → TTT
AP/LQ/T438V	A330P/L188Q; T438V	ACG → GTG
AP/LQ/T438P	A330P/L188Q; T438P	ACG → CCG
AP/LW	A330P; L188W	CTG → TGG
A330W	A330W	GCG → TGG
AVA	WT; A74V/V78I/A82L	GCG → TGG; GTA → ATA; GCA → CTA
AVA/AL	AVA; A184V/L188W	GCA → GTA; CTG → TGG
AVA/AL/AA (E32)	AVA/AL; A328F/A330W	GCT → TTT; GCG → TGG
GVQ	WT; A74G + F87V + L188Q	GCG → GGG; TTT → GTT; CTG → CAG
KT2	WT; A191T + N239H + I259V + A276T + L353I	GCA → ACA; AAC → CAC; ATT → GTT; GCG → ACG; CTA → ATA
KT2/N70S	KT2; N70S	AAC → AGC
KT2/A82G	KT2; A82G	GCA → GGA

KT2/H171L	KT2; H171L	CAT → CTT
KU4/M237L (KT2/M237L without N239H)	KT2; M237L	ATG → CTG
KT2/A328V	KT2; A328V	GCT → GTT
KT2/AP	KT2; A330P	GCG → CCG
KT2/AP/H171L	KT2/AP; H171L	CAT → CTT
KU/AP	KT2/AP; I353L	ATA → CTA
KU/AP/L75Q	KU/AP; L75Q	CTT → CAA
KU/AP/F87W	KU/AP; F87W	TTT → TGG
KU/AP/T88H	KU/AP; T88H	ACA → CAT
KU/AP/L188Q	KU/AP; L188Q/A191T	CTG → CAG/ GCA → ACA
KU/AP/T260L	KU/AP; I259V/T260L	ATT → GTT / ACA → CTA
KU/AP/G402P	KU/AP; G402P	GGT → CCT
KU/AP/A264V	KU/AP; I259V/A264V	ATT → GTT/ GCG →GTG
KU2/AP	KU/AP; V259I	GTT → ATT
KU3/AP	KU/AP; T191A	ACA → GCA
KU3/AP/M185K	KU3/AP; M185K	ATG → AAG
KU3/AP/K391N	KU3/AP; K391N	AAA → AAT
KU3/AP/G443A	KU3/AP; G443A	GGC → GCC
KU4/AP	KU/AP; H239N	CAC → AAC
KU5/AP	KU/AP; T276A	CCG → GCG
I259V/A276T/A330P	KU3/AP; H239N	CAC → AAC
A191T/N239H/I259A/A276T/A330P	KU2/AP; I259A	ATT →GCT
RL/YF	WT; R47L/Y51F	CGT → TTA/ TAC → TTT
RL/YF/AP	RL/YF; A330P	GCG → CCG

RL/YF/AP/A74G	RL/YF/AP; A74G	GCG → GGG
RL/YF/AP/A264G	RL/YF/AP; A264G	GCG → GGG
RL/YF/AP/Q403P	RL/YF/AP; Q403P	CAG → CCG
RL/YF/NMA	N70S/M237L/A328V; RL/YF	CGT → TTA; TAC → TTT
RL/YF/NMA/L188Q	RL/YF/NMA; L188Q	CTG → CAG
RL/YF/H171L	H171L; R47L/Y51F	CGT → TTA; TAC → TTT
RT2	KT2; R47L/Y51F	CGT → TTA; TAC → TTT
RT2/FW	RT2; F81W	TTT → TGG
RT2/FW/AI	RT2/FW; A328I	GCT → ATT
RT2/FW/AI/LV	RT2/FW/AI; L437LV	TTA → TTAGTT
RT2/AP	RT2; A330P	GCG → CCG
RT2/AP/V26M	RT2/AP; V26M	GTT → ATG
RT2/AP/S72A	RT2/AP; S72A	AGT → GCT
RT2/AP/S72Y	RT2/AP; S72Y	AGT → TAT
RT2/AP/V78I	RT2/AP;V78I	GTA → ATA
RT2/AP/F81W	RT2/AP; F81W	TTT → TGG
RT2/AP/A82L	RT2/AP; A82L	GCA → TTA
RT2/AP/A82M	RT2/AP/A82M	GCA → ATG
RT2/AP/A184I	RT2/AP; A184I	GCA →ATA
RT2/AP/E267F	RT2/AP; E267F	GAA → TTT
RT2/AP/P329V	RT2/AP; P329V/A330P	CCT → GTT/ GCG → CCG
RT2/AP/I401P	RT2/AP; I401P	ATC → CCC
RT2/AP/T438L	RT2/AP; T438L	ACG → TTG
RT2/AP/K440L	RT2/AP; K440L	AAA → TTA

RT2/P329W	RT2; P329W	**CCT** → **TGG**
RT2/AP/I401M	RT2/AP; I401M	AT**C** → AT**G**
RT2/AW	RT2; A330W	**GC**G → **TG**G
RT2/AW/A82M	RT2/AW; A82M	**GCA** → **ATG**
RT2/I401P	RT2; I401P	**AT**C → **CC**C
RT2/L437S	RT2; L437S	**TTA** → **AGT**
RP	RL/YF; I401P	**AT**C → **CC**C
RP/A74G	RP; A74G	G**C**G → G**G**G
RP/A82M	RP; A82M	**GCA** → **ATG**
RP/AP	RP; A330P	**G**CG → **C**CG
RP/AP/S72L	RP/AP; S72L	**AG**T → **CT**T
RP/AP/A74W	RP/AP; A74W	**GC**G → **TG**G
RP/AP/A82M	RP/AP; A82M	**GCA** → **ATG**
RP/AP/Q307H/N319Y	RP/AP; Q307H + N319Y	CA**A** → CA**T**; **A**AC → **T**AC
RP/AP/P329V	RP/AP; P329V/A330P	**CC**T → **GT**T/ **GC**G → **CC**G

2.2.2 Primer design

Two oligonucleotides (forward and reverse primers) were designed for each mutagenesis reaction. These oligonucleotides were designed with a minimum overlap and not complementary to each other, so as to maximise the chance of a successful PCR step.[246] Primer sequences must contain at least a 21-base tail, due to the KOD polymerase demonstrating strong 3′→5′ exonuclease activity. The sequences should also contain around 40 – 60% G/C bases. Melting temperatures (T_m) were calculated using the website http://www.biophp.org/minitools/melting_temperature/demo.php and preferably kept below 72 °C.

2.2.3 The PCR step

The concentration of template DNA was set at 10 μg μL^{-1}. Upon mixing the components listed in Table 2-3, the microcentrifuge tube was centrifuged at 2900 rcf for five seconds before being placed in the PCR machine. The following programme was used for PCR: the cycle of 94 °C for 0.5 minutes, (T_m – 5) °C for one minute, and 70 °C for 3.5 minutes, was repeated 30 times, after which the temperature was maintained at 70 °C for 10 minutes before being dropped down to, and held at 10 °C.

Table 2-3: Components added to a thin-walled microcentrifuge tube for the PCR step.

Components	**Volume / μL**
10 × buffer	5
$MgSO_4$	4
dNTPs	5
Forward primer	1.5
Reverse primer	1.5
DNA	1
KOD polymerase	1
DMSO	2
H_2O	29

2.2.4 Gel Electrophoresis

The PCR mixture from **2.2.3** was analysed by agarose gel electrophoresis. 50 mL 1 × TAE buffer was mixed with 0.5 g agarose, which were then microwaved. 2.5 μL of 10 mg mL^{-1} ethidium bromide was added to this solution, before pouring onto the plastic container to solidify. Once the gel had set, the mixtures of 10 μL samples with 2 μL Promega 6 × loading dye, and Promega 1 kbp DNA reference ladder, were separately loaded into 25 μL holes at

the cathodic end of the cell. The running buffer, which contains 250 mL 1 × TAE and 5 μL ethidium bromide, was poured on the gel. A voltage of 90 V was applied for 30 minutes. If an intense band was seen migrating at the same speed as a 8500 bp linear fragment in the DNA ladder standard under UV light, it was indicative of a successful PCR step. 1 μL of DpnI was added to the PCR mixture, which was incubated overnight at 37 °C.

2.2.5 Post-mutagenesis transformation

1 μL of the PCR mix was pipetted into 50 μL of *E. coli* DH5α competent cells, once the cells have thawed out on ice from the –80 °C freezer. These were kept on ice for 45 minutes, and then heat shocked at 42 °C for 45 seconds before returning on ice for further two minutes. 900 μL of SOC media was added and this mixture was shaken at 150 rpm for two hours at 37 °C. 50 μL of the mixture was spread onto the LB_{Kan} agar plate, and the plate was eventually placed in the 37 °C oven with its lid half-open for 30 minutes. The lid was then placed and the plate was flipped upside down. The plate was left overnight.

2.2.6 DNA purification and transformation

DNA purification was performed using the Thermo Scientific GeneJET Plasmid Miniprep kit #502, #503. A single colony from the transformed plate prepared in **2.2.5** was grown in 5 mL LB_{Kan} overnight in a 50-mL centrifuge tube, shaking at 37 °C, 180 rpm. This culture was centrifuged for five minutes at 9,300 rcf. The supernatant was discarded and each pellet was resuspended with 250 μL of the Resuspension Solution. This was transferred to a microcentrifuge tube, and 250 μL of the Lysis Solution was added. The tube was inverted five times until the solution became slightly clear. 350 μL of the Neutralisation Solution was added and again the tube was inverted five times to mix the solution. The tube was then centrifuged for five minutes at 14,800 rcf. The resulting supernatant was decanted to the GeneJET spin column and this was centrifuged at 14,800 rcf for one minute. The

flow-through was removed and the column was put back into the same collection tube. 500 μL of the ethanol-containing Wash Solution was pipetted to the GeneJet column, and the flow-through was discarded after centrifuging at 14,800 rcf for one minute. This step was repeated once more, and the column was centrifuged for an additional one minute to remove any remaining Wash Solution. The inner column was transferred onto a new 1.5-mL microcentrifuge tube, and 40 μL of the Elution Buffer was added to the column. This was left for two minutes at room temperature before centrifuging for the last time at 14,800 rcf for two minutes. The flow-through was this time collected, and DNA was quantitated using UV-Vis spectroscopy. The DNA solution was diluted by a factor of 100, and one absorbance unit at 260 nm had to correspond to 10 μg μL^{-1} or greater, to send the DNA to Eurofins UK, for sequencing. The primers used for DNA sequencing are listed in **Appendix 1**.

2.3 Protein production and purification

2.3.1 Transformation

1 μL of the PCR mix was pipetted into the 50 μL of *E. coli* BL21 (DE3) competent cells. The rest of the protocol was the same as **2.2.6**.

2.3.2 Preparation of cell bank

50 mL of $FB_{Glycerol}$ was made in a 250-mL conical flask, and it was inoculated with a single colony from the agar plate containing transformed *E. coli* BL21 (DE3). The flask was then incubated overnight at 37 °C, 120 rpm. 7 mL of this culture was taken from the flask and mixed with 3 mL glycerol to make a 'cell bank'. This 10-mL cell bank was aliquoted evenly to ten 1.5-mL microcentrifuge tubes and stored in the –80 °C freezer. The remaining culture in the Erlenmeyer flask was used for protein production as described in **2.3.3**.

2.3.3 Protein production

Most mutants were grown by adding 250 μL of the appropriate cell bank per flask to 2 × 600 mL of $FB_{Glycerol}$ in two 2-L Erlenmeyer flasks. The flasks were shaken overnight at 37 °C, 120 rpm. The temperature of incubator was then lowered to 20 °C and the cultures were left shaking for one hour. The culture in each flask was induced with 40 μL 0.4 M IPTG, and supplemented with 600 μL 0.1 M δ-ALA, 600 μL 10 mM $FeCl_2$, and 3 g tryptone. The flasks were left shaking for at least another 48 hours.

The harvesting of cells was initially performed by centrifuging for five minutes at 3,900 rcf. The supernatant was discarded and the cell pellets were resuspended with a total volume of 50 mL Buffer P per 1,200 mL culture by shaking at 180 rpm, 20 °C. Resuspended pellets were then transferred to a beaker kept on ice, and sonicated for 2.5 minutes in total with 15 seconds cooling periods after every 15 seconds of sonication. The amplitude was set at 40%. This lysis mixture was then centrifuged in Oak Ridge tubes at 9,200 rcf for 20 minutes.

Proteins were purified by ammonium sulfate fractionation with the aid of this website, http://www.encorbio.com/protocols/AM-SO4.htm. The volume of the supernatant was *ca.* 60 mL, and 14.0 g of solid $(NH_4)_2SO_4$ was added to initially bring the concentration up to 40% saturation. The solution was stirred at 4 °C until all the solids had dissolved and this was transferred to Oak Ridge tubes for centrifugation for 12 minutes at 9,200 rcf. The resulting supernatant was retained, and another 7.5 g of $(NH_4)_2SO_4$ was added to take the concentration to 60% saturation. The mixture was centrifuged for the last time at 9,200 rcf for 12 minutes, and this time the supernatant was discarded. The pellet was redissolved in a total volume of 10 mL buffer P.

2.4 Alkane oxidation activity assays

2.4.1 Enzyme concentration determination

The enzyme stock stored in the –80 °C freezer was thawed on ice and diluted with H_2O to an absorbance of *ca.* 0.3 at 420 nm. The spectrum was recorded between 250 – 700 nm. A few crystals of sodium dithionite were added to reduce the enzyme, and the spectrum of this reduced enzyme was used as a baseline for the next step. The solution was bubbled gently with a few bubbles of CO and the spectrum was recorded.[91] The absorbance at 450 nm was used to determine the concentration of the protein using ε = 91,000 M^{-1} cm^{-1}.[218]

$$[P450]\mu M = \frac{A_{450} - A_{490}}{91{,}000} \times 10^6$$

2.4.2 NADPH turnover assays for alkane oxidation

A 2AU final concentration of NADPH was used for most turnover reactions. This was determined by diluting the stock NADPH solution of 20 mg mL^{-1} concentration by 100-fold, and recording its spectrum. The absorbance peak at 340 nm, along with the following formula, was used to calculate the volume required for 2AU final concentration.

$$(Volume\ of\ NADPH)\mu L = \frac{2}{Absorbance_{340} \times 100} \times 2400$$

The volume used for turnover assays was 2,400 μL and this was prepared in the cuvette sealed with a screw cap and a silicone rubber septum. The turnover assays were performed in triplicates. The turnover mixture contained 0.5 μM enzyme, and the rest of the incubation mixture was filled with equal volumes of oxygen- and alkane- saturated buffers. DMSO was added to KPi to make 2% v/v final concentration. The buffer was saturated for more than 20 minutes with oxygen in a water bath at 30 °C while alkane saturation was performed on ice. The cuvette containing the incubation mixture was sealed and left in the cuvette holder at

30 °C for one minute, before adding 2AU of NADPH using a Hamilton syringe piercing through the silicone septum to initiate the reaction. The cuvette was quickly flipped twice and placed back in the UV-Vis spectrometer to measure the NADPH consumption rate by monitoring the absorbance at 340 nm and using ε = 6.22 mM^{-1} cm^{-1}.

The reaction mixture was then aliquoted into two 1.5-mL microcentrifuge tubes; one with 1 mL and another with 1.4 mL. The 1 mL turnover mixture was extracted and injected on the GC as described in **2.6.1** and the 1.4 mL mixture was stored at –20 °C as a back-up.

The Beer-Lambert law was used to convert NADPH consumption rate gradients into standard units. N is measured in nmol min^{-1} (nmol-P450) $^{-1}$, Δ is the measured gradient, Δ_{LR} is the gradient of the leak rate.

$$N = \frac{(\Delta - \Delta_{LR}) \times 1000}{[P450] \times \varepsilon_{340}}$$

Coupling efficiency was calculated by dividing the concentration of products by the concentration of NADPH added to the reaction. The PFR was found by multiplying the NADPH turnover rate by the coupling efficiency and exposed as a percentage.

2.4.3 TTN determinations for short-chain alkanes

A total volume of 1,500 μL was used for this reaction and this was carried out in a clean 2-mL GC vial (9 mm diameter), with the lid on at atmospheric pressure and ambient temperature.

Table 2-4: Components used to determine TTN for short-chain alkanes (methane – butane). 2% v/v final concentration of DMSO was added to KPi to improve the alkane aqueous concentration. Catalase was added to break down any H_2O_2 produced to minimise inhibition.

Components	Concentration
P450 enzyme	0.5 μM
GDH	10 U mL^{-1}
Glucose	200 mM
KPi, pH 7.4	100 mM
Catalase	20 mg mL^{-1}
NADPH	320 μM

KPi buffer was pre-saturated with both oxygen and alkane for 30 minutes, as described in section **2.4.2**. The reaction mixture containing components listed in Table 2-4 was stirred for two hours. 1 mL of this mixture was extracted for analysis (**2.6.1**).

2.4.4 High pressure systems

The reaction components in Table 2-4 were mixed in a 6-mL (23 × 38 mm) open-top clear glass vial from Stratlab and placed in the pressure system using a pair of tweezers. A Tinyclave was used for reactions performed under a total pressure of 10 bar, and a Parr autoclave was used for total pressures above 10 bar. The overall oxygen partial pressure was kept *ca.* 2% unless stated otherwise, when the Parr autoclave was used. The reaction mixture was stirred for two hours, at 4 °C or ambient temperature, before pressure was carefully released in a fume hood. 1 mL of this mixture was extracted for analysis (**2.6.1**).

2.4.5 Decoy systems

A similar protocol was used as described in **2.4.3** for TTN assays under atmospheric pressure**,** with the addition of 200 μM perfluorocarboxylic acids (PFCs). The appropriate PFC (PFC9 –

PFC12) was added as a 10 mM DMSO stock for each reaction. The reaction was also performed under pressure, and the protocol described in **2.4.4** was used.

2.5 Hydrogen-driven NADPH regeneration system

2.5.1 Soluble hydrogenase (SH) with octane as the substrate

The total volume of 1,500 µL consisting of components in Table 2-5 was set up in a 6-mL (23 × 38 mm) open-top clear glass vial from Stratlab. Oxygen was removed from all components in Table 2-5 before mixing. KPi was pre-saturated with hydrogen for 30 minutes, and KPi, P450 enzyme, soluble hydrogenase, $NADP^+$ and catalase were mixed in the glove box. The glass vial was sealed with a suba seal, and the reaction mixture was bubbled with hydrogen for a further 30 seconds and into the headspace for 15 seconds. The glass vial was then taken out of the glove box, and the substrate was added. The glass vial was then injected with 10% air to give 2% oxygen overall in both the solution and the headspace, and the glass vial and suba seal were wrapped up with Parafilm to prevent the loss of gases from the reaction vial. The reaction mixture was stirred and left for two hours before being extracted as described in **2.6.2**.

Table 2-5: Components and their concentrations used to perform hydrogen-driven octane oxidation. 2% v/v final concentration of DMSO was added to KPi to improve the saturation. Catalase was added to break down any H_2O_2 produced to minimise inhibition. *100 µL of soluble hydrogenase was added. The $H_2 \rightarrow NADH$ activity of soluble hydrogenase was *ca.* 0.001 µmol min^{-1} (µL-enzyme)$^{-1}$, but its concentration was not determined.

Components	**Concentration**
P450 enzyme	0.5 µM
Octane	5 mM
Soluble hydrogenase*	–
KPi, pH 7.4	100 mM
Catalase	20 mg mL^{-1}
$NADP^+$	1 mM

The control experiment was set up in the same manner as with SH, but 200 mM glucose and 10 U mL^{-1} GDH were added instead of the SH (see Table 2-6).

Table 2-6: Components used to determine TTN for octane oxidation using a glucose/GDH cofactor regeneration system. 2% v/v final concentration of DMSO was added to KPi to improve the saturation and it was maintained at pH 7.4. Catalase was added to break down any H_2O_2 produced to minimise inhibition.

Components	**Concentration**
P450 enzyme	0.5 µM
Octane	5 mM
GDH	10 U mL^{-1}
Glucose	200 mM
KPi, pH 7.4	100 mM
Catalase	20 mg mL^{-1}
$NADP^+$	1 mM

2.5.2 Soluble hydrogenase with propane as the substrate

The total volume of 1 mL consisting of the components in Table 2-7 was set up in a 6-mL (23 × 38 mm) open-top clear glass vial from Stratlab. KPi buffer was pre-saturated with hydrogen for 30 minutes, and oxygen was removed from all components before they were mixed in the glove box. The reaction mixture was placed in the Tinyclave pressure system in the glove box. The Tinyclave was taken out of the glove box and charged up to 2 bar propane, 2 bar hydrogen and 0.5 bar air. The reaction mixture was stirred for 20 hours at ambient temperature. 1 mL of the reaction mixture was extracted, as described in **2.6.1**.

Table 2-7: Components and their concentrations used to perform hydrogen-driven propane oxidation. 2% v/v final concentration of DMSO was added to KPi to improve the saturation and it was maintained at pH 7.4. Catalase was added to break down any H_2O_2 produced to minimise inhibition. *100 µL of soluble hydrogenase was added. The $H_2 \rightarrow$ NADH activity of soluble hydrogenase was *ca.* 0.001 µmol min^{-1} (µL-enzyme)$^{-1}$, but its concentration was not determined.

Components	Concentration
P450 enzyme	0.5 µM
Soluble hydrogenase*	–
KPi, pH 7.4	100 mM
Catalase	20 mg mL^{-1}
$NADP^+$	320 µM

The control experiment was set up in the same manner as with SH, but 200 mM glucose and 10 U mL^{-1} GDH were added instead of the SH (Table 2-8).

Table 2-8: Components used to determine TTN for propane oxidation reaction using a glucose/GDH cofactor regeneration system. 2% v/v final concentration of DMSO was added to KPi to improve the saturation. Catalase was added to break down any H_2O_2 produced to minimise inhibition.

Components	Concentration
P450 enzyme	0.5 μM
GDH	10 U mL^{-1}
Glucose	200 mM
KPi, pH 7.4	100 mM
Catalase	20 mg mL^{-1}
$NADP^+$	320 μM

2.6 Data and product analysis

2.6.1 Extraction and analysis for short chain alkanes

100 μL of 1-hexanol and the appropriate amount of internal standard (IS) was added to the 1-mL turnover mixture (Table 2-9).

Table 2-9: The amount of internal standard added for TTN reactions. The 25 mM internal standard stock was made in 1-hexanol.

Alkane used	IS used	Volume added / μL
Butane	1-propanol	10
Propane	2-pentanone	2.5
Ethane	2-pentanone	2.5
Methane	2-pentanone	2.5

0.5 g of K_2CO_3 was added to this turnover mixture (0.5 g mL^{-1}) for better extraction. The mixture was vortexed for 10 seconds, then centrifuged at 14,800 rcf for five minutes, before 30 μL of the organic layer was transferred to a 200 μL flat bottom MicroSert glass vial.

2.6.2 Extraction and analysis for octane oxidation reactions

200 µL of ethyl acetate was added to 1 mL of reaction mixture in a 1.5-mL microcentrifuge tube, and the mixture was vortexed for 10 seconds. The microcentrifuge tube was centrifuged and the organics were analysed as described in **2.6.3**. No internal standard was added.

2.6.3 Gas chromatography

2 µL of the organic layer from the MicroSert glass vial obtained in **2.6.1** and **2.6.2** were injected to the GC. The GC profile, described in Table 2-10, was used.

Table 2-10: Oven and column regimes (hold times in parentheses) for short-chain alkanes (methane – butane) and octane.

	GC 8000^{Top}	**Thermo Finnigan Trace (methane – butane)**	**Thermo Finnigan Trace (octane)**
Injector Temperature	230 °C	230 °C	230 °C
FID Temperature	250 °C	250 °C	250 °C
Initial Temperature	40 °C (one minute)	45 °C (three minutes)	100 °C (40 minutes)
Ramp	4 °C min^{-1}	3 °C min^{-1}	40 °C min^{-1}
Holding Temperature	112 °C (no holding)	84 °C (no holding)	220 °C (two minutes)
Ramp	40 °C min^{-1}	40 °C min^{-1}	–
Final Temperature	220 °C (five minutes)	220 °C (three minutes)	–

Product concentrations were calculated using the product peak area relative to the internal standard peak area, and multiplying by the calibration factor (see **2.6.4**). The product peak was identified by running 1 mM authentic product in 1-hexanol on the GC and matching the retention times. However, some products coeluted and their peaks could not be separated, e.g. acetone and propanal.

2.6.4 Calibration

Initially, a single stock of *ca.* 25 mM product was made and the appropriate alcohol samples were made up to a range of concentrations in 1-hexanol. For 2-propanol calibration, 9 samples between concentrations of 50 µM to 10 mM were made by weighing the amount of 2-propanol and using the density of 2-propanol to calculate the actual volume of 2-propanol added, and the ratio of 2-propanol and IS peak area was plotted against the concentration (Figure 2-3). Similarly, butane and ethane oxidations were calibrated by making 7 samples up to a concentration of 300 µM for 2-butanol (Figure 2-2), and 6 samples up to a concentration of 150 µM for ethanol (Figure 2-4).

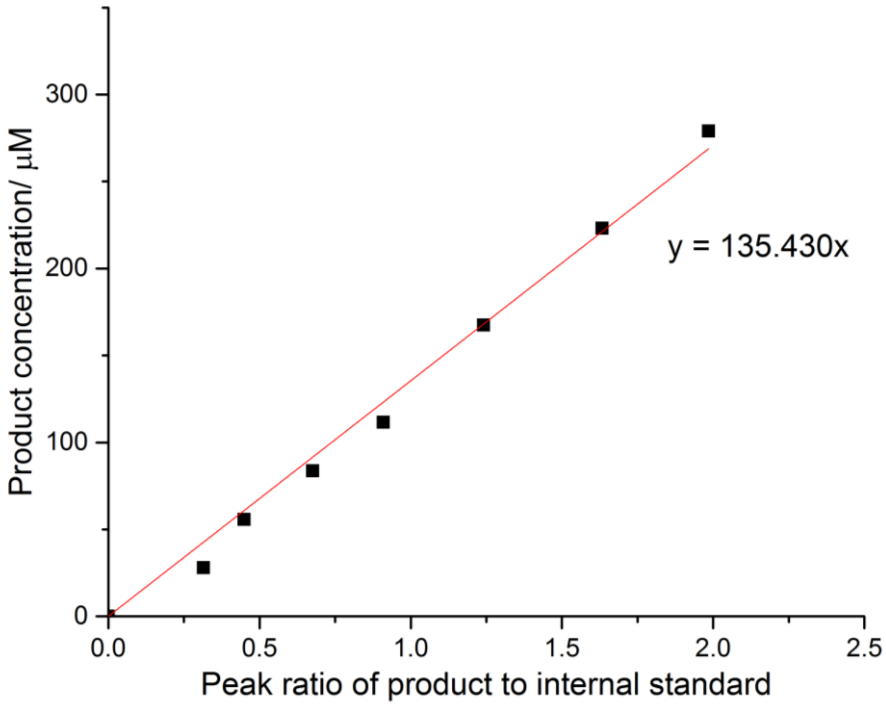

Figure 2-2: The calibration plot of 2-butanol.

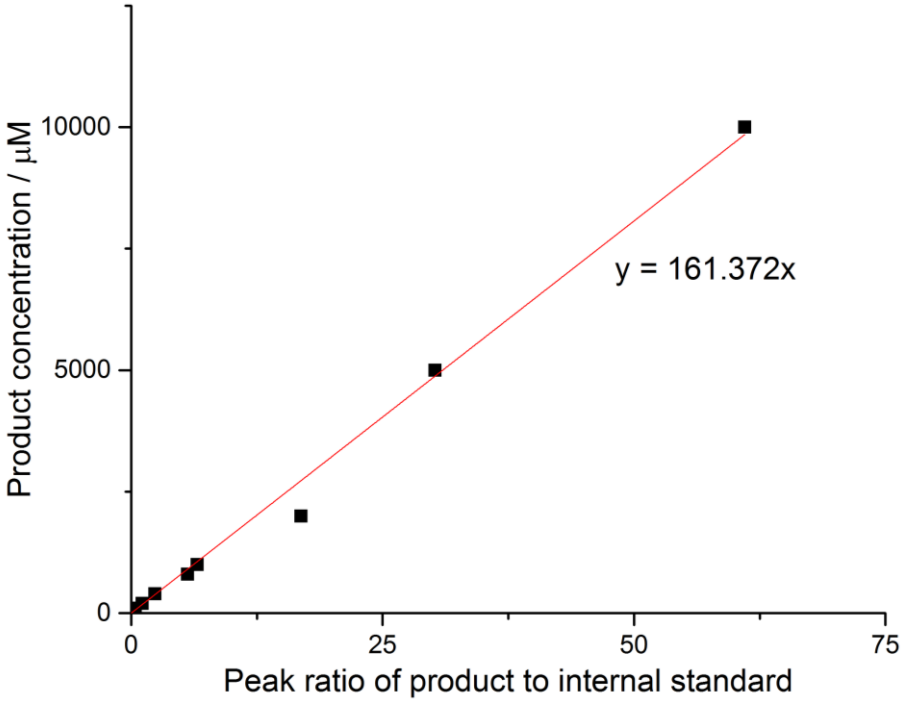

Figure 2-3: The calibration plot of 2-propanol.

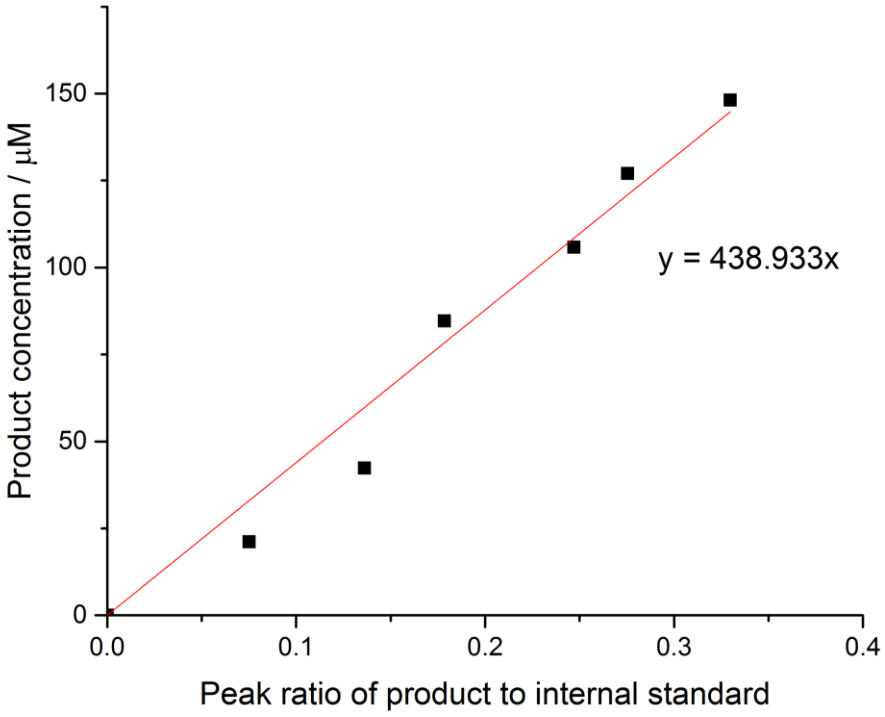

Figure 2-4: The calibration plot of ethanol.

Chapter 3

Alkane turnover assays

3.1 Introduction

The natural substrates for $P450_{BM3}$ are believed to be medium-chain fatty acids, and high activity has been reported towards C_{15} – C_{17} branched chain fatty acids, with 96% coupling for the oxidation of *anteiso* C_{17} fatty acid.[247] The activity towards the oxidation of short-chain alkanes (four carbons or less) by the WT, however, was found to be low.[248]

Arnold and co-workers have reported a TTN of 16,800 for propane hydroxylation with the mutant E32, containing A74W, V78I, A82L, A184V, L188W, A328F and A330W mutations, under 2 bar propane partial pressure.[222] Higher TTN values of 33,400 and 45,800 for in vivo propane oxidation were reported for $P450_{PMO}$ and $P450_{PMO}$R2, respectively with 9 : 1 ratio of 2- and 1-propanol, formed.[249] $P450_{PMO}$ was discovered through saturation-recombination and site-directed mutagenesis. Haem domain substitutions included R47C, L52I, A74E, V78F, A82G, K94I, P142S, T175I, A184V, L188P, F205C, S226R, H236Q, E252G, R255S, A290V, A328F, L353V, I366V, and G443A, as well as the E464G and I710T mutations in the reductase domain. The structurally destabilising L188P mutation was also reported to significantly increase propane oxidation activity on its own.[212] $P450_{PMO}$R2 contains an additional mutation in the reductase domain, D698G, which was reported to lead to a distortion of the electrostatic charge distribution and increasing its activity.[249] These TTN values will be used as benchmarks in this thesis.

3.2 Mutation design

A library of mutants was produced using site-directed mutagenesis. Butane and propane were initially chosen as test substrates due to their weaker C–H bonds relative to ethane and methane. The NADPH consumption and product formation rate (PFR) were used to assess the activity of each mutant.

Residues R47 and Y51 are found at the entrance of the substrate access channel, and mutations on these residues were previously performed. The R47L/Y51F mutant (RL/YF) showed improved activity towards a variety of substrates, including 3-methylpentane, where the PFR increased to 234 min^{-1} from 17 min^{-1} for the WT.[250] Residues between Ser72 to Ala82 in B′-helix, which is located on one side of the active site, were substituted with bulkier amino acids with the aim to reduce the active site volume and constrain the substrate to bind closer to the haem. Further mutations were introduced from above the active site, such as introducing isoleucine to the Ala184 residue. Residues located on the other side to the B′-helix were also targeted, and these include mutations at Ala328, Pro329 and Ala330, as well as Leu437 and Thr438 (Figure 3-1).

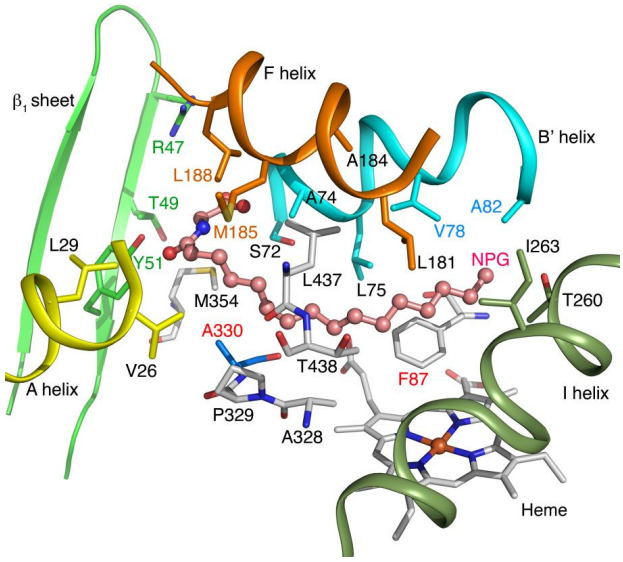

Figure 3-1: The key amino acid residues around the $P450_{BM3}$ active site. Residues on B′-helix were initially targeted such as Ser72, Ala74, and Phe81, as well as residues found in the F- (Ala184) and K-helices (Ala328, Pro329 and Ala330).

The mutants RT2 (R47L/Y51F/KT2) and RP (R47L/Y51F/I401P) were chosen as the starting template for this work. Both contain the mutations R47L and Y51F, but RT2 also includes the KT2 mutations (A191T/N239H/I259V/A276T/L353I), whereas RP has the I401P mutation.[131,230] KT2 is a generic accelerator variant, which showed good activity without altering product profiles, and the I401P mutation may help improve the turnover rate.

The reaction mixture with the total volume of 1.5 mL contained 0.5 μM enzymes and 100 mM KPi buffer, pH 7.4, with 2% v/v DMSO. The buffer was saturated with alkane and oxygen for 30 minutes. DMSO was added to improve the aqueous alkane solubility. NADPH (2 AU, 320 μM) was added, and the initial NADPH consumption rate (5 seconds) was measured. 1 mL of the reaction mixture was extracted using 100 μL 1-hexanol, with an appropriate internal standard; after centrifugation to separate the phases, 2 μL of the 1-hexanol layer was injected on the GC.

3.3 NADPH turnover assays

3.3.1 The RT2 series

The Phe81 residue, located in the C-terminus end of the B′-helix, with the side-chain pointing directly towards the active site, was initially targeted. The F81W mutation (FW) greatly improved the activity of the RT2 mutant towards both butane and propane (Table 3-1), where the PFR for propane oxidation increased from 0.6 ± 0.2 min^{-1} to 30 ± 5 min^{-1}, and 290 ± 50 min^{-1} to 2,060 ± 420 min^{-1} for butane oxidation. NADPH consumption rate and coupling improved for both substrates, with the coupling improving to 77.0 ± 6.2% for butane oxidation. The A328I mutation was added to the RT2/FW mutant, but the coupling of the RT2/FW/AI mutant towards propane dropped unexpectedly from 4.1 ± 0.5% to 2.6 ± 0.4%. The decrease for butane was even more striking, with coupling dropping from 77.0 ± 6.2% to just 9.3 ± 1.1%. This may be due to the active site being too constricted in the immediate vicinity of the haem with the introduction of the bulky isoleucine at the 328 position (Figure 3-1).

The A330P mutation greatly improved coupling percentages, where PFR improved from 0.6 ± 0.2 min^{-1} to 240 ± 20 min^{-1} relative to the parent RT2 mutant towards propane oxidation. The NADPH consumption rate improved by 10-fold, and the coupling reached

25.7 ± 0.9%. The bulkier amino acid, tryptophan, was introduced at this position since enzymes containing the A330W mutation (AW) have been reported to give high propane oxidation activity (CC2: A74W, V78F, A82L, A184V, A328F, A330W, TTN = 12,600; E30: A74W, V78I, A82L, A328F, A330W, TTN = 16,600; E32: A74W, V78I, A82L, A184V, L188W, A328F, A330W, TTN = 16,800).[222] The RT2/AW mutant, however, showed poor enzymatic activity towards both alkanes, with a NADPH consumption rate of $190 \pm 90\ min^{-1}$ for propane, and therefore coupling efficiencies were not measured for both alkanes. RT2/AW was expressed to relatively high levels (40 mg L^{-1}) and active towards larger substrates, such as lauric acid, where the TTN reached 4,250 with ω–3 being the major product (36%).[251]

The I401P mutation (IP) was found to promote the elongation of the Fe–OH_2 bond, allowing the water molecule to be displaced more easily and lowered the reorganisation energy for electron transfer in the substrate-free form.[131] The high NADPH turnover rate of $3{,}950 \pm 210\ min^{-1}$ was observed for butane oxidation with the RT2/IP, but the coupling remained low, at 3.0 ± 0.9%, for propane oxidation. A valine residue was inserted between Leu437 and Thr438 in the flexible loop between the two β4 strands as a potentially novel means to reduce the active site volume to promote propane oxidation. L437LV was thus added to the RT2/FW/AI mutant, but there was no obvious effect on activity.

Table 3-1: Butane and propane oxidation activity of the RT2 series. *N* = NADPH turnover rate; PFR = initial product formation rate was calculated by multiplying the NADPH turnover rate by the coupling efficiency; coupling efficiency was found by dividing the concentration of total product by the concentration of NADPH added to the reaction and expressed as a percentage. Rates are in nmol (nmol-P450)$^{-1}$ min^{-1} (abbreviated to min^{-1}). All data are given as mean ± S.D. for $n \geq 3$. All assays contained; 500 nM $P450_{BM3}$, 320 μM NADPH and 2% v/v DMSO in 100 mM, pH 7.4 phosphate buffer in a total volume of 2,400 μL. 1 mL of the turnover assays were extracted with 100 μL 1-hexanol, and an internal standard was added (10 μL of a 25 mM stock of 1-propanol in 1-hexanol for butane assays and 2.5 μL of a 25 mM stock of 2-pentanone in 1-hexanol for propane). Mutations: RT2 = R47L/Y51F/KT2, FW = F81W, AI = A328I, AP = A330P, AW= A330W, IP = I401P, LV = L437LV. –: not investigated.

	Butane oxidation		**Propane oxidation**	
Mutant	***N* / min^{-1}**	**PFR / min^{-1} (Coupling)**	***N* / min^{-1}**	**PFR / min^{-1} (Coupling)**
RT2	620 ± 40	290 ± 50 (47.1 ± 5.5%)	95 ± 2	0.6 ± 0.2 (0.7 ± 0.2%)
RT2/FW	2,670 ± 330	2,060 ± 420 (77.0 ± 6.2%)	790 ± 30	30 ± 5 (4.1 ± 0.5%)
RT2/FW/AI	1,550 ± 100	140 ± 20 (9.3 ± 1.1%)	1180 ± 60	30 ± 5 (2.6 ± 0.4%)
RT2/FW/AI/LV	1,790 ± 10	140 ± 1 (7.7 ± 0.0%)	1,070 ± 40	30 ± 3 (3.1 ± 0.4%)
RT2/AP	3,380 ± 90	1,540 ± 50 (45.6 ± 2.7%)	940 ± 100	240 ± 20 (25.7 ± 0.9%)
RT2/AW	320 ± 10	–	190 ± 90	–
RT2/IP	3,950 ± 210	1,330 ± 350 (33.4 ± 6.9%)	2,050 ± 330	60 ± 10 (3.0 ± 0.9%)

3.3.2 The RT2/AP series

The RT2/AP variant gave the highest PFR for propane in the initial work (Table 3-1) and good haem incorporation meant that further mutations were added to this mutant. The mutation S72A was added to RT2/AP, but protein folding was a problem. Val78, Phe81 and Ala82 all lie in the B′-helix, and bulkier amino acids were introduced at these positions to reduce the active site volume. RT2/AP/V78I had low oxidation activities for both alkanes (Table 3-2). F81W was introduced to the RT2/AP template, but the yield of protein was low.

Mutations at the Ala82 position to leucine and methionine led to lower PFRs for both sets of alkanes, but the turnover rate with propane improved from 940 ± 100 min^{-1} to 2,340 ± 290 min^{-1} and 2,020 ± 140 min^{-1} for RT2/AP/A82L and RT2/AP/A82M, respectively. However, the coupling dropped as far as 7.2 ± 1.2% for the RT2/AP/A82M mutant.

The A184I mutation was intended to close down the active site from above. The RT2/AP/A184I mutant led to lower couplings (from 45.6 ± 2.7% to 29.7 ± 1.7% for butane), but only a small change with propane. The NADPH consumption rate for propane oxidation improved to 2,930 ± 130 min^{-1}, resulting in *ca.* three-fold increase in PFR to 670 ± 70 min^{-1}. The introduction of A184L may similarly increase the activity, as it was found with the A82L mutation, and this needs to be investigated in the future work.

The P329V mutation alongside A330P was intended to improve protein folding by preventing two rigid proline residues from being adjacent to each other. This additional mutation, however, had a negative effect on its activity with the coupling for propane oxidation dropping to 2.5 ± 0.2%. The side-chain Glu267 forms a salt-bridge with Lys440 and is hydrogen bonded to two water molecules, one of which forms a H-bond to Thr268.[252] The introduction of bulkier phenylalanine was intended to close down the active site. The PFR for propane oxidation, however, dropped to 4.0 ± 0.5 min^{-1}, mainly due to low coupling of 1.0 ± 0.2%. Thr438 is located above Ala328, and it was altered to leucine with a longer side-chain, but the expression level of this mutant was very low. The introduction of K440L mutation was intended to break the salt bridge with Glu267, but this drastically decreased the turnover rate and coupling, with the coupling dropping to 1.0 ± 0.1% for propane oxidation.

The I401P mutation increased the NADPH turnover rate as shown by the RT2/I401P mutant (Table 3-1), and this mutation was added to the RT2/AP variant, but protein folding and haem incorporation was again an issue. The RT2/AP/IP mutant was eventually expressed in

TB media but enzymes made in TB had low activity, and growth in this media was therefore avoided. The I401M mutation was introduced instead, but the expression yield of RT2/AP/I401M was still low, at 6 mg L^{-1}. However, the coupling of the RT2/AP/I401M mutant towards propane oxidation was especially high, at 62.0 ± 18.0%, leading to the highest PFR of 1,090 ± 390.

This set of data indicates that A330P and I401M mutations are important in achieving high PFRs. The A330P mutation led to high NADPH consumption rates, and high propane coupling of 25.7 ± 0.9%, and I401M showed higher coupling of 62.0 ± 18.0% towards propane. The mutation at Ala82 may be important for achieving high NADPH consumption rates, as both RT2/AP/A82L and RT2/AP/A184I mutants gave >2,000 min^{-1}. The RT2/AP/A184I mutant led to a high NADPH consumption rate of 2,930 ± 130 min^{-1}, whilst coupling did not drop significantly towards propane.

Table 3-2: Butane and propane oxidation activity of the RT2/AP series. *N* = NADPH turnover rate; PFR = initial product formation rate was calculated by multiplying the NADPH turnover rate by the coupling efficiency; coupling efficiency was found by dividing the concentration of total product by the concentration of NADPH added to the reaction and expressed as a percentage. Rates are in nmol (nmol-P450)$^{-1}$ min^{-1} (abbreviated to min^{-1}). All data are given as mean ± S.D. for $n \geq 3$. All assays contained; 500 nM $P450_{BM3}$, 320 μM NADPH and 2% v/v DMSO in 100 mM, pH 7.4 phosphate buffer in a total volume of 2,400 μL. 1 mL of the turnover assays were extracted with 100 μL 1-hexanol, and an internal standard was added (10 μL of a 25 mM stock of 1-propanol in 1-hexanol for butane assays and 2.5 μL of a 25 mM stock of 2-pentanone in 1-hexanol for propane). RT2 = R47L/Y51F/KT2, AP = A330P. –: not investigated. ND: no detectable activity. ‡Protein did not fold.

	Butane oxidation		**Propane oxidation**	
Mutant	***N*** **/ min^{-1}**	**PFR / min^{-1} (Coupling)**	***N*** **/ min^{-1}**	**PFR / min^{-1} (Coupling)**
RT2	620 ± 40	290 ± 50 (47.1 ± 5.5%)	95 ± 2	0.6 ± 0.2 (0.7 ± 0.2%)
RT2/AP	3,380 ± 90	1,540 ± 50 (45.6 ± 2.7%)	940 ± 100	240 ± 20 (25.7 ± 0.9%)
RT2/AP/V78I	ND	ND	ND	ND
RT2/AP/A82L	2,750 ± 300	900 ± 120 (32.8 ± 1.4%)	2,340 ± 290	300 ± 40 (13.7 ± 0.8%)
RT2/AP/A82M	1,840 ± 230	590 ± 100 (31.8 ± 1.5%)	2,020 ± 140	150 ± 20 (7.2 ± 1.2%)
RT2/AP/A184I	4,660 ± 450	1,390 ± 190 (29.7 ± 1.7%)	2,930 ± 130	670 ± 70 (22.7 ± 2.6%)
RT2/AP/P329V	320 ± 20	150 ± 5 (45.5 ± 4.7%)	95 ± 10	2.0 ± 0.6 (2.5 ± 0.2%)
RT2/AP/E267F	–	–	440 ± 20	4.0 ± 0.5 (1.0 ± 0.2%)
RT2/AP/K440L	–	–	110 ± 20	1.0 ± 0.1 (1.0 ± 0.0%)
RT2/AP/I401M	–	–	1,740 ± 110	1,090 ± 390 (62.0 ± 18.0%)
RT2/AP/S72A‡	–	–	–	–
RT2/AP/F81W‡	–	–	–	–
RT2/AP/I401P‡	–	–	–	–
RT2/AP/T438L‡	–	–	–	–

3.3.3 The RP series

The RP mutant consists of R47L/Y51F/I401P, and this mutant showed higher NADPH consumption rate compared to RT2, mainly due to the introduction of I401P (4.5-fold increase for propane oxidation). Series of mutants were made using the RP template as the basis to allow direct comparison with RT2 based variants (Table 3-3). Mutations were introduced at Ser72, Ala74, Ala82, Pro329 and Ala330 to explore the effect of reducing active site volume. The addition of A330P to RP highlighted the importance of A330P with over 20-fold increase in PFRs of RP/AP and RP/AP/A82M compared to their precursors. The RP/AP mutant showed 30% higher NADPH consumption rate than the RT2/AP mutant, but the coupling was lower, with 17.1 ± 2.5%. The expression levels of the RP/AP series, however, were lower than the RT2/AP series, with significant P420 formation observed in the ferrous-CO spectrum. The A82M mutation on RP/AP significantly improved the NADPH turnover rate, but lowered the coupling; nevertheless the PFR was increased almost two-fold. The RP/AP/A82L was not made, but this enzyme may also give high PFR. The introduction of P329V again did not increase the enzymatic activity. The A74W mutation on RP/AP drastically reduced its NADPH turnover rate and coupling for propane. The RP/AP/S72L mutant did not fold.

Table 3-3: Butane and propane oxidation activity of the RP series. *N* = NADPH turnover rate; PFR = initial product formation rate was calculated by multiplying the NADPH turnover rate by the coupling efficiency; coupling efficiency was found by dividing the concentration of total product by the concentration of NADPH added to the reaction and expressed as a percentage. Rates are in nmol (nmol-P450)$^{-1}$ min^{-1} (abbreviated to min^{-1}). All data are given as mean ± S.D. for $n \geq 3$. All assays contained; 500 nM $P450_{BM3}$, 320 μM NADPH and 2% v/v DMSO in 100 mM, pH 7.4 phosphate buffer in a total volume of 2,400 μL. 1 mL of the turnover assays were extracted with 100 μL 1-hexanol, and an internal standard was added (10 μL of a 25 mM stock of 1-propanol in 1-hexanol for butane assays and 2.5 μL of a 25 mM stock of 2-pentanone in 1-hexanol for propane). RP = R47L/Y51F/I401P, AP = A330P. –: not investigated. ‡Protein did not fold.

	Butane oxidation		**Propane oxidation**	
Mutant	***N* / min^{-1}**	**PFR / min^{-1} (Coupling)**	***N* / min^{-1}**	**PFR / min^{-1} (Coupling)**
RP	1,390 ± 20	540 ± 100 (38.5 ± 7.1%)	430 ± 20	10 ± 3 (2.2 ± 0.8%)
RP/AP	2,600 ± 30	1,890 ± 230 (72.8 ± 8.1%)	1,770 ± 160	300 ± 30 (17.1 ± 2.5%)
RP/AP/A74W	360 ± 60	270 ± 50 (76.4 ± 2.8%)	240 ± 30	28 ± 4 (11.7 ± 1.0%)
RP/A82M	2,940 ± 220	710 ± 70 (24.2 ± 0.7%)	1,670 ± 340	24 ± 3 (1.5 ± 0.3%)
RP/AP/A82M	4,150 ± 120	2,070 ± 150 (49.9 ± 2.4%)	4,480 ± 100	560 ± 80 (12.6 ± 1.9%)
RP/P329V/AP	1,160 ± 20	440 ± 50 (38.2 ± 4.2%)	660 ± 60	26 ± 3 (3.9 ± 0.5%)
RP/AP/S72L‡	–	–	–	–

3.3.4 Discussion

The coupling and PFR data indicate that the A330P mutation is important in achieving high activity towards butane and propane. The coupling increased significantly when the A330P mutation was introduced, with an increase from 2.2 ± 0.8% to 17.1 ± 2.5% when A330P was added to RP. This is consistent with a more spatially constrained substrate pocket arising from the Pro329 ring being relocated into the pocket. The mutations at Ala82 and Ala184 generally led to higher NADPH consumption rate, with the RP/AP/A82M mutant showing 4,480 ± 100 min^{-1} for propane. RT2/AP/A82L/A184I and RT2/AP/A82M/A184I may be

promising combinations for future work. The introduction of I401P mutation generally led to good activities, with I401P providing fast NADPH turnover rates, e.g. 4,480 ± 100 min^{-1} with RP/AP/A82M for propane oxidation. The insertion of amino acid after the Leu437 residue did not improve the PFR, and the introduction of P329V next to A330P led to significantly reduced alkane oxidation activity; with PFR dropping from 240 ± 20 min^{-1} to 2.0 ± 0.6 min^{-1}, when P329V was added on RT2/AP. The 2-propanol product was clearly visible on GC, but the peak of terminal oxidation product, 1-propanol, was negligible. It is likely that the local conformation of the P329V/A330P combination does not have the 329 side-chain relocated into the pocket, and the P329/A330P combination gave rise to the effect of the A330P mutation.

3.4 Total turnover number (TTN) assays

The NADPH turnover rates were analysed and used as the basis to select mutants for TTN assays, which gave better indications of enzymatic activities towards short-chain alkane hydroxylation. The TTN of RT2/AP was initially investigated, as it showed reasonable expression levels (50 mg L^{-1} of *E. coli* culture – Figure 3-2), and high PFRs towards propane and butane, with 240 ± 24 min^{-1} and 1,540 ± 50 min^{-1}, respectively.

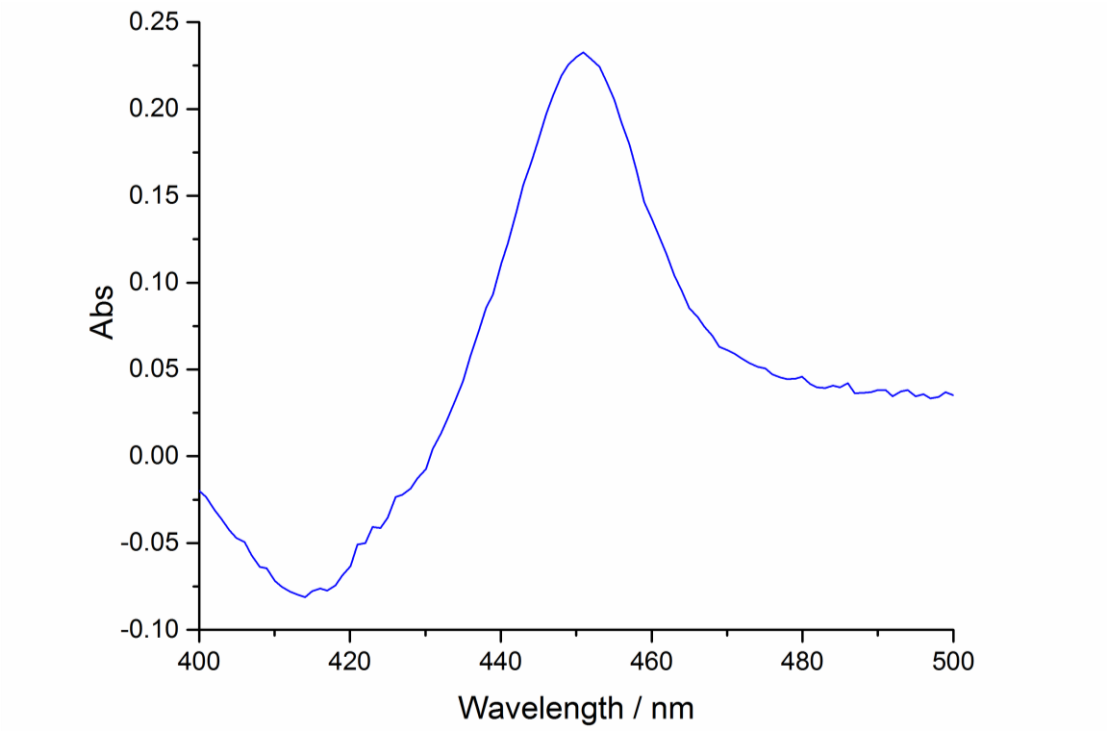

Figure 3-2: The ferrous-CO difference spectrum of RT2/AP, illustrating absence of inactive P420 form.

3.4.1 Extraction techniques

Higher activities for propane oxidation by $P450_{BM3}$ variants containing mutations such as A74W, A330W, A82L, A82M and A328V have been reported, without the generic accelerator mutations also present.[222] This may be due to issues with poor extraction of low molecular weight alcohols from the aqueous phase in our work. Other workers added sodium nitrite and sulphuric acid to convert propanol to the nitrite which was readily extracted into hexane; this method was first described by Maeda[253] who reported >85% recovery of 2-propanol from water samples.

$$H_2SO_4 + NaNO_2 \rightarrow HONO + Na_2SO_4$$

$$ROH + HONO \rightarrow RONO + H_2O$$

Whilst the nitrite method was applicable to propanol (and higher alcohols), it was not suitable for ethanol because ethyl nitrite has a boiling point of 17 °C. Moreover, alkyl nitrites RONO are highly hazardous and hence alternative methods were sought.

It has been long known that addition of sufficient concentrations of metal salts (NaCl, Na_2SO_4, K_2CO_3, $CaCl_2$, $CuSO_4$, etc.) to aqueous : organic mixtures caused the phases to separate. KF was shown to be the most effective in salting out ethanol (dehydrating it to 98%) and acetone from water. However, highly hazardous HF was formed in the process. A good compromise was K_2CO_3 which dehydrated ethanol to 96.5%. When 1 g of anhydrous K_2CO_3 was added to 1 mL phosphate buffer and 500 µL 2-propanol, the solution turned cloudy and there was solid K_2CO_3 in the mixture, but a second phase was readily seen. When 0.5 g was used, all K_2CO_3 was soluble and two clear layers were observed (Figure 3-3). Hence K_2CO_3 at 0.5 g mL^{-1} caused a 2-propanol/phosphate buffer mixture to separate into two layers. This effect might greatly improve extraction of light alcohols, such as propanol and ethanol, into 1-hexanol.

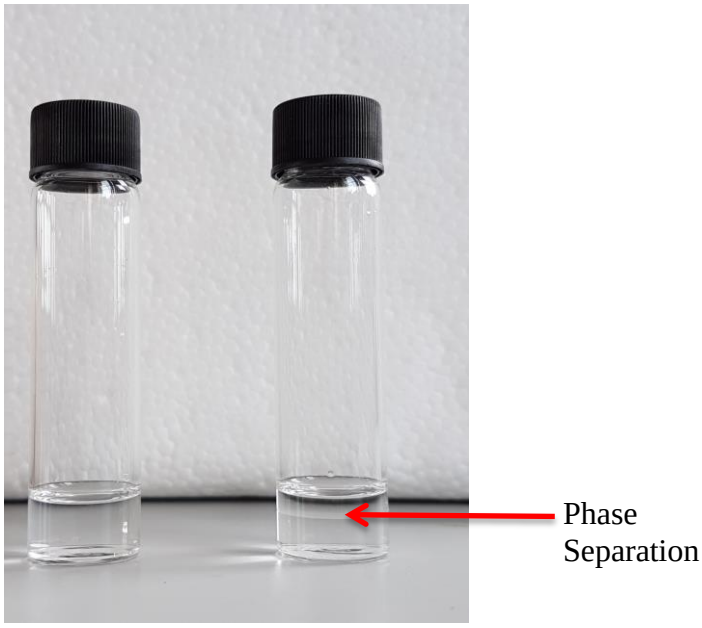

Figure 3-3: Salting out method by K_2CO_3. Both vials contain 1 mL phosphate buffer and 500 µL 2-propanol. 0.5 g of K_2CO_3 was also added to the right vial, and two phases were clearly visible.

3.4.2 Propane TTN with and without K_2CO_3

Two reaction mixtures were prepared in a 2-mL GC vial (9 mm diameter), with each totalling a volume 1.5 mL, consisting of propane- and oxygen-saturated 100 mM KPi buffer, pH 7.4, 0.5 µM RT2/AP, 20 mg mL^{-1} catalase, 10 U mL^{-1} GDH, 0.2 M glucose and 320 µM $NADP^+$. Vials were sealed, and reaction mixtures were stirred for two hours at ambient temperature. 1 mL of reaction mixtures were each extracted with 100 µL 1-hexanol, and 2.5 µL of a 25 mM stock of 2-pentanone in 1-hexanol was added as an internal standard. One of the samples was then supplemented with 0.5 g K_2CO_3. When a test sample of RT2/AP TTN mixture with K_2CO_3 added was analysed, both the 1- and 2-propanol product peaks, as well as the internal standard peak, were higher than the control without K_2CO_3 added as shown in Figure 3-4 (410%, 300%, 150% of the control for 2-propanol, 1-propanol and 2-pentanone, respectively). The resulting propane TTN by the RT2/AP mutant was 680 ± 10, and this value will be used as the benchmark. This simple method did not involve the formation of volatile and hazardous alkyl nitrites and should allow the products peaks to be integrated with greater certainty, which should lead to more consistent and reliable results. Product concentrations were determined by plotting the ratio of product to internal standard peak against the samples of known 2-propanol concentrations (**2.6.4**).

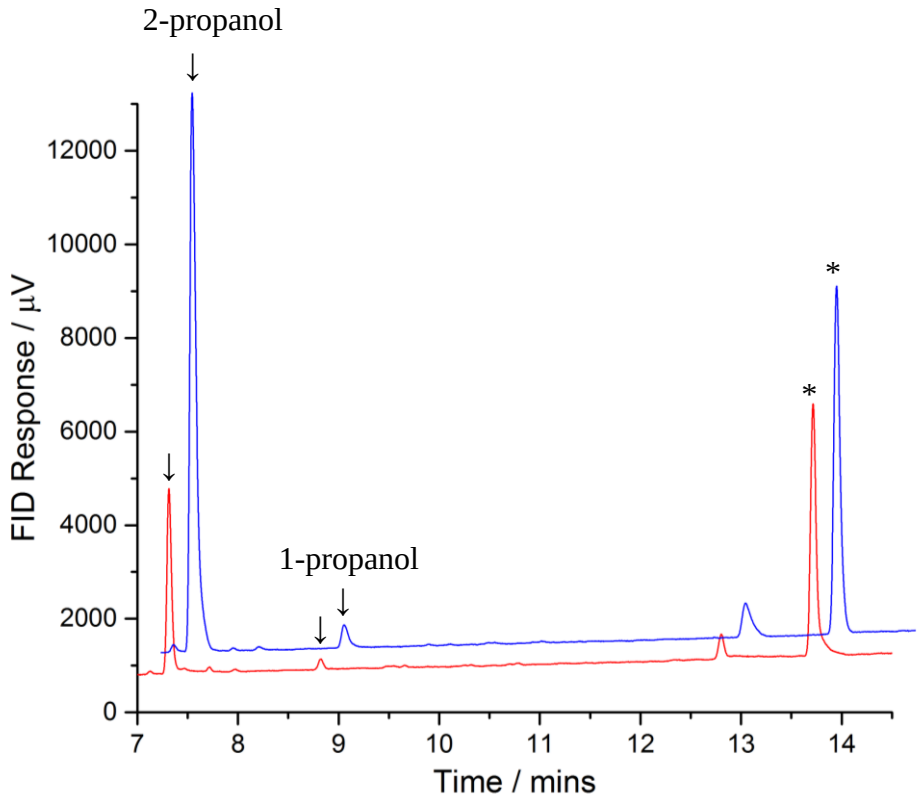

Figure 3-4: GC analysis of a RT2/AP propane oxidation TTN assay after two hours showing an increase in the peak area of both the 2-pentanone internal standard and propanol products upon addition of K_2CO_3 to aid extraction. *denotes the 2-pentanone internal standard.

3.4.3 Propane

The TTN of WT $P450_{BM3}$ was investigated as a reference. The activity of WT towards propane was low, as expected, with no significant propanol products above background. Similarly, the KT2 mutant was unable to produce high enough propanol products above background. TTN values of RL/YF, RT2 and A330P mutants were low, with all under 25.

Further mutagenesis was performed at the Ala82 residue, where alanine was replaced by the bulkier methionine amino acid in order to close down the active site. This mutant gave a higher turnover rate (2,020 ± 140 min^{-1} vs. 940 ± 100 min^{-1}) than RT2/AP, but its low coupling (7.2 ± 1.2% vs. 25.7 ± 0.9%) led to lower TTN of 200 ± 10. The selectivity shifted slightly towards the terminal position, with 8% 1-propanol product observed compared to the

typical value of 5%. The addition of the A184I mutation dramatically increased the NADPH turnover rate ($2{,}930 \pm 130\ min^{-1}$ from $940 \pm 100\ min^{-1}$) and the coupling did not drop significantly (22.7 ± 2.6% from 25.7 ± 0.9%). The TTN, however, dropped by over three-fold from 680 ± 10 to 200 ± 30.

RT2/IP contains key mutations KT2 and I401P, and gave a NADPH turnover rate of $2{,}050 \pm 330\ min^{-1}$ (**3.3.1**). Coupling, however, was low with 3.0 ± 0.9%, and TTN was also low at 100 ± 1. The low TTN of RT2/IP also reflected the importance of A330P in the activity of $P450_{BM3}$ towards propane. The RP/AP mutant, which contains A330P and showed the coupling of 17.1 ± 2.5%, gave a TTN of 350 ± 30. The introduction of I401M to the RT2/AP mutant gave a high PFR of $1{,}090 \pm 390\ min^{-1}$ due to high coupling (62.0 ± 18.0% with propane), but the TTN was similar to the RT2/AP mutant.

The coupling trend observed towards propane oxidation generally followed the trend observed in TTN. The only exceptions were RT2/AP/A184I and RT2/AP/I401M mutants, which showed lower TTN than predicted relative to their couplings. Other mutants gave four- to six-fold higher product concentrations in the cofactor regeneration system than NADPH assays (Table 3-4).

Table 3-4: Propane hydroxylation TTN for various mutants performed under atmospheric pressure at ambient temperature. TTN is defined as the maximum number of moles of substrate converted per 1 mol of $P450_{BM3}$. –: not investigated. ND: no detectable activity. The data are given as mean ± S.D, $n \geq 3$.

	Coupling (N / min^{-1})	**Product concentration from 320 µM NADPH / µM**	**[Product] / µM (TTN)**	**% 2-ol**
WT	–	–	ND	ND
RL/YF	–	–	12 ± 0 (23 ± 0)	95
KT2	–	–	ND	ND
RT2	0.7 ± 0.2% (95 ± 2)	2.2	2 ± 1 (4 ± 1)	93
A330P	–	–	4.5 ± 1 (9 ± 2)	96
RT2/AP	25.7 ± 0.9% (940 ± 100)	82	340 ± 5 (680 ± 10)	96
RT2/AP/A82M	7.2 ± 1.2% (2,020 ± 140)	23	100 ± 5 (200 ± 10)	92
RT2/AP/A184I	22.7 ± 2.6% (2,930 ± 130)	73	100 ± 20 (200 ± 30)	95
RT2/AP/I401M	62.0 ± 18.0% (1,740 ± 110)	200	290 ± 50 (570 ± 50)	97
RT2/IP	3.0 ± 0.9% (2,050 ± 330)	9.6	50 ± 1 (100 ± 1)	95
RP/AP	17.1 ± 2.5% (1,770 ± 160)	55	175 ± 20 (350 ± 30)	97

3.4.4 Ethane and methane oxidation

No enzymes were able to perform ethane or methane hydroxylation under atmospheric pressure at ambient temperature.

3.5 Conclusions

R47L/Y51F, KT2, A330P and I401P were used as templates to build a library of mutants for engineering butane and propane oxidation. The approach was to introduce bulky amino acids at residues around the active site. Overall, the results showed that mutation of residues in the far region of the active site (Figure 3-5) such as Val78, Phe81 and Ala82 mostly led to reduced alkane oxidation activities, even though high NADPH turnover rates were observed, with RT2/AP/A82L and RP/AP/A82M showing 2,340 ± 290 min^{-1} and 4,480 ± 100 min^{-1} for propane, respectively. It appears that these mutations resulted in non-productive alkane binding, in sharp contrast to what is known and expected from data in the literature where a more constrained substrate pocket tended to increase alkane oxidation activity. The most striking example of this is the A330P mutation which causes a conformation change at the adjacent Pro329 such that the Pro329 ring is re-directed into the active site and reduces the volume of the substrate pocket, greatly increasing the $P450_{BM3}$ alkane oxidation activity. The RT2/AP mutant showed good expression levels (50 mg L^{-1}) and coupling of 25.7 ± 0.9% for propane oxidation, resulting in TTN of 680 ± 10. The I401P mutation was added to RT2/AP, but haem incorporation was poor (2 mg L^{-1}). The I401M mutation gave improved but still low expression level (6 mg L^{-1}), and the RT2/AP/I401M mutant gave the highest coupling of 62.0 ± 18.0% and PFR of 1,090 ± 390 min^{-1} with propane. The TTN, however, was slightly lower than RT2/AP with 570 ± 50.

One explanation is that the far region of the substrate pocket is actually required for the binding of small alkanes, perhaps more than one molecule of alkane, before the alkane comes to the vicinity of the haem iron and is oxidised. If this space is blocked by mutations, alkane binding is weakened or the alkane is in a non-productive location such that the probability of the alkane being close to the haem iron is lowered and both activity and coupling are reduced (Figure 3-5).

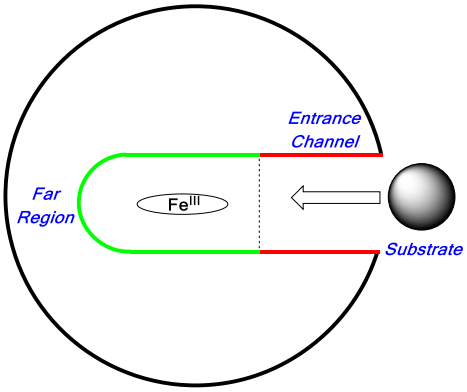

Figure 3-5: Schematic illustration of residues in the 'far region' (green) and 'entrance channel' (red).

The highest TTN achieved in this chapter was around 25-fold lower than those published in the literature. One way to circumvent this problem might be to perform alkane oxidation under moderate pressure or use a decoy filler substrate, as reported by Watanabe,[254] and the results of these studies are described in chapters 4 and 5.

Chapter 4

The effect of pressure

4.1 Introduction

It has been claimed that applying pressure along with the addition of a PFC decoy to WT $P450_{BM3}$ led to some ethanol from ethane oxidation,[254] and methanol production from methane.[223] With the addition of PFC10 under 5 bar ethane, Watanabe reported ethane hydroxylation by the WT with a product formation rate (PFR) of 0.67 min^{-1}.[254] A total turnover number (TTN) of 2,470 for methane oxidation to methanol supported by a glucose-6-phosphate/glucose-6-phosphate dehydrogenase cofactor regeneration system has also been reported by Reetz with the addition of PFC10 under 10 bar total pressure (0.7 bar methane, 0.8 bar O_2 and 8.5 bar N_2).[223] Arnold and co-workers performed propane and ethane oxidation under 30 psi (*ca.* 2 bar) alkane partial pressure at 4 °C for 20 hours, with high TTN values of 16,800 and 1,200 for propane and ethane oxidation, respectively.[222] The high-pressure condition was used to overcome, at least partially, the high K_M by increasing the concentration of gaseous alkane substrates in the reaction mixture. The solubilities of propane are 1.74 mmol L^{-1} at 20 °C and 3.46 mmol L^{-1} at 4 °C.[255]

As described in Chapter 3, propane oxidation at ambient temperature under atmospheric pressure by a series of $P450_{BM3}$ mutants has been observed. However, the TTN values remained relatively low, and the activities did not correlate with those observed with longer-chain alkanes. Nonane, for example, was oxidised by WT $P450_{BM3}$ under atmospheric pressure with a PFR of 5.8 min^{-1}.[250] The oxidative activity of WT $P450_{BM3}$ dramatically dropped for alkanes with four carbons or less.[248] The highest TTN achieved with propane without applying pressure in chapter 3 was 680 ± 10 by the RT2/AP mutant. In this chapter, the effect of applying pressure on the oxidation of propane, ethane and methane is described. The effect of PFC will be explored in Chapter 5.

4.2 Experimental set up

For experiments under a total pressure of up to 10 bar, the Tinyclave apparatus shown in Figure 4-1 was used. The main advantage of this system is its ease of use. Stirring speed can be closely monitored, and its ease of assembly due to the single hand-tight screw design makes this apparatus attractive.

Figure 4-1: The Tinyclave apparatus used for alkane oxidation under a total pressure below 10 bar.

For the application of pressures higher than 10 bar, a Parr autoclave was used. The Parr vessel, with a larger diameter (Figure 4-2) allowed up to five reactions to be run simultaneously but this set up was more complicated compared to the Tinyclave. Glass vials containing the TTN assay mixtures were placed inside the Parr autoclave using a pair of tweezers, and the lid was secured by tightening the bolts using spanners.

Figure 4-2: The Parr high-pressure system. The system was harder to assemble compared to the Tinyclave, but higher pressure (> 10 bar) can be applied to the reaction mixture.

The total reaction volume of 1.5 mL, in 100 mM phosphate buffer, pH 7.4, contained 2% v/v DMSO, 10 U mL^{-1} GDH, 320 µM $NADP^+$, 20 mg mL^{-1} catalase, and 0.5 µM $P450_{BM3}$. Compressed air was charged into the pressure vessel to 10% of the desired total pressure, thus keeping the overall oxygen partial pressure to 2%, and then the vessel was pressurised with the gaseous alkane to the appropriate pressure. After the reaction, the pressure was slowly released, before unscrewing the bolts to take vials out of the autoclave with tweezers. 1 mL of the reaction mixture was extracted with 100 µL 1-hexanol in the presence of 0.5 g mL^{-1} K_2CO_3, and 2.5 µL of a 25 mM stock of 2-pentanone internal standard in 1-hexanol was added. After centrifugation, the 1-hexanol layer was removed and immediately analysed by GC.

4.3 Initial studies with WT $P450_{BM3}$

For propane oxidation, the reaction mixtures were stirred at room temperature. A reaction time of two hours was selected from a series of experiments with different reaction times; no significant increase in TTN was observed after two hours. The TTN for propane oxidation increased slightly from no product under atmospheric pressure to 24 ± 9 when the reaction was carried out under 5 bar propane and 2 bar air. 1-Propanol was also observed for the first

time in this work (Figure 4-3). Although the peak on the GC was small, and corresponded to a concentration of just 0.5 µM, it nevertheless constituted 5% of the total product.

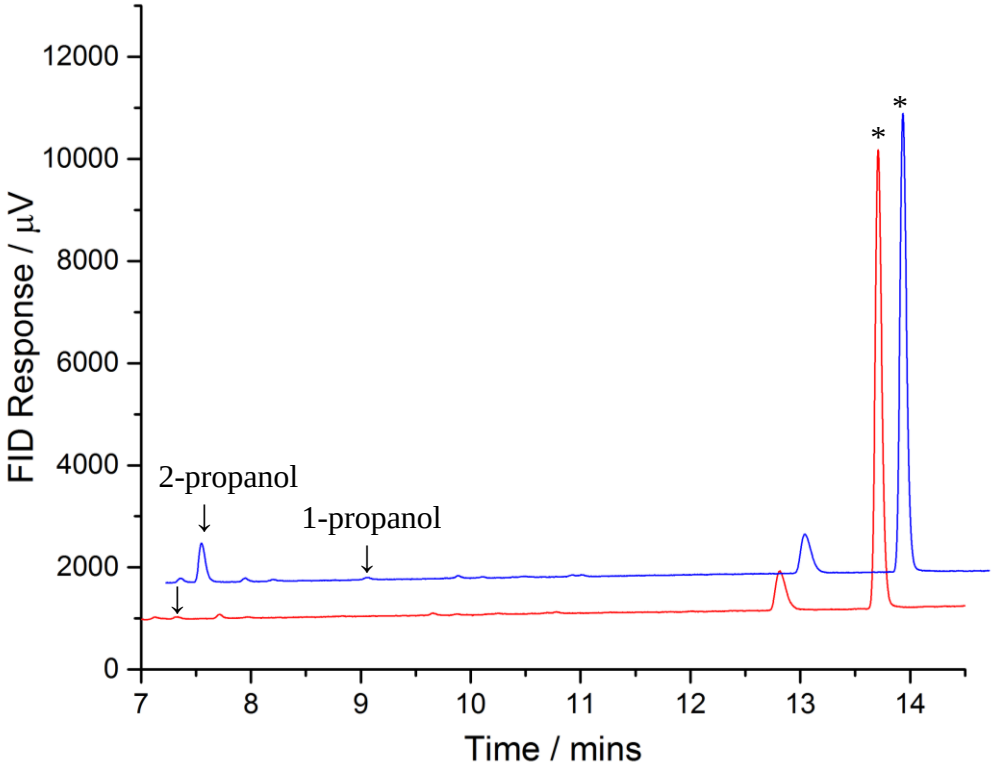

Figure 4-3: The chromatographic analysis of reactions by WT $P450_{BM3}$. The reaction performed at ambient temperature under atmospheric pressure is in red, and under 5 bar propane and 2 bar air is in blue. *denotes the 2-pentanone internal standard.

Under atmospheric pressure, no ethanol peak above background was detected with the WT or any of the mutants listed in Table 3-4 (Chapter 3). Ethane oxidation with WT was also attempted under 5 bar ethane and 2 bar air, but ethanol was again not detectable above background. The partial pressure of ethane was raised to 8 bar, but again no ethanol peak was observed.

The gas chromatograms for control reactions, and indeed the ethane reaction, gave a clean background at the retention time for 1- and 2-propanol (Figure 4-3). The simple and efficient extraction method using K_2CO_3 allowed any differences in peak size of the propanol products to be clearly detectable. The increase in TTN from 0 to 24 ± 9 corresponded to increased

activities observed by Arnold at 30 psi (*ca.* 2 bar) without the use of PFC, and by Watanabe and Reetz in the presence of PFC under 5 bar propane partial pressure.[222,223,227] The effect of applying pressure on short-chain alkane oxidation was then explored for mutants that showed high activities under atmospheric pressure at ambient temperature. Small but consistent peaks of ethanol (*ca.* 15 µM) and methanol (*ca.* 1 µM) background were observed, and they were taken into account when a TTN was calculated.

4.4 Evaluation of the RT2/AP mutant

The RT2/AP mutant showed an expression yield of 50 mg L^{-1} of *E. coli* culture, and a TTN of 680 ± 10 was observed for propane oxidation under atmospheric pressure at ambient temperature.

The effect of pressure was thus investigated further with this variant, initially under a total pressure of 7 bar (5 bar propane, 2 bar air). GC analysis showed a dramatic increase in 2-propanol product concentration (Figure 4-4), with the TTN increasing by almost 16-fold to 10,900 ± 420 (Table 4-1). With this large increase in propane turnover, the 1-propanol peak was clearly observed although its proportion of products remained at *ca.* 5%. There was no evidence of further oxidation products such as propanal or acetone, which virtually co-eluted under the oven temperature conditions (Figure 4-4). Oven and column regimes of GC are described in Table 2-10.

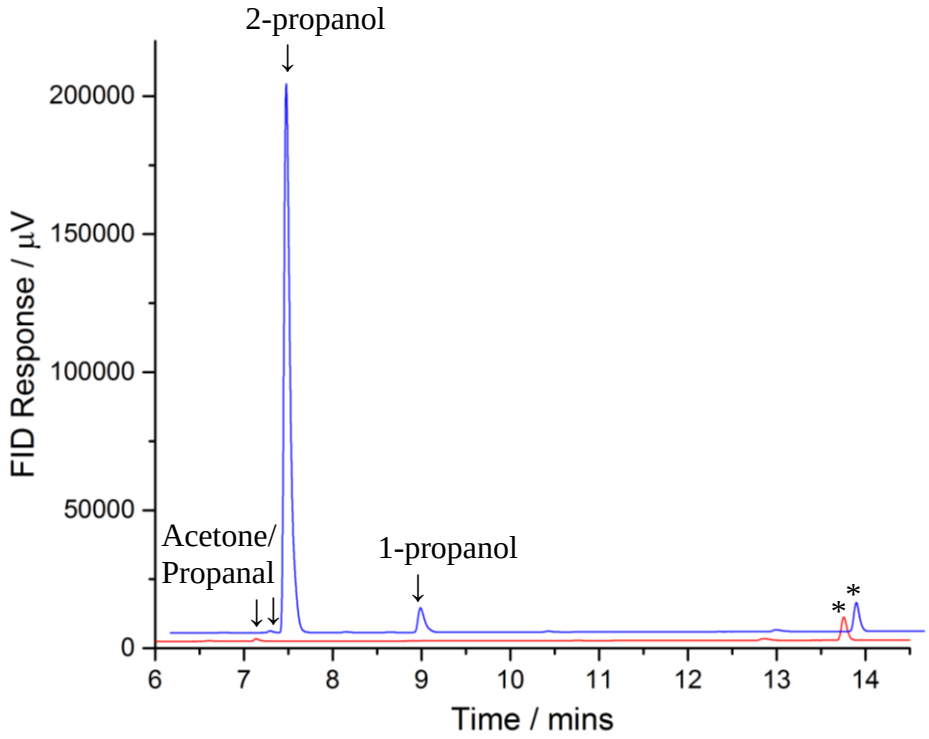

Figure 4-4: The GC illustrating a propane oxidation by the RT2/AP variant under mild pressure after two hours at ambient temperature. In blue is the data for propane oxidation under 5 bar propane and 2 bar air, and in red is the background. *denotes the 2-pentanone internal standard.

Table 4-1: The effect of pressure on the TTN and selectivity for propane oxidation by RT2/AP and the WT at ambient temperature. ND: no detectable activity. All data are given as mean ± S.D. for $n \geq 3$.

	Atmospheric pressure		**5 bar propane/2 bar air**	
	TTN	**% 2-ol**	**TTN**	**% 2-ol**
WT	ND	ND	24 ± 9	95
RT2/AP	680 ± 10	96	10,900 ± 420	95

Another set of reactions was therefore performed, where the partial pressure of propane was varied, whilst the partial pressure of air was kept to 2 bar under ambient temperature. GC analysis showed that increasing the propane partial pressure to just 2 bar dramatically raised the TTN, from 680 ± 10 to 8,220 ± 270 (a 12-fold increase). At 5 bar propane there was a further increase in TTN of 25%, to 10,900 ± 420 but no significant increase in TTN was observed when the partial pressure of propane was increased to 7 bar.

The effect of the total pressure was then investigated. The partial pressure of propane was kept at 2 bar, but the total pressure was varied. No obvious gain in TTN was observed when the partial pressure of air was increased from 2 bar to 7 bar, highlighting the importance of partial pressure of propane over the total pressure. The product selectivity was unaffected by pressure, where the percentages of 2-propanol and 1-propanol remained at 95% and 5%, respectively.

No ethane oxidation product was observed under atmospheric pressure with the RT2/AP mutant. A series of reactions utilising different partial pressures of ethane was carried out. As shown in Figure 4-5, a clear ethanol peak above background was observed at 6.7 minutes in the reaction under 8 bar ethane and 2 bar air, leading to a TTN of 350 ± 30. The formation of acetaldehyde was observed at 5.7 minutes, corresponding to 2% of the overall products.

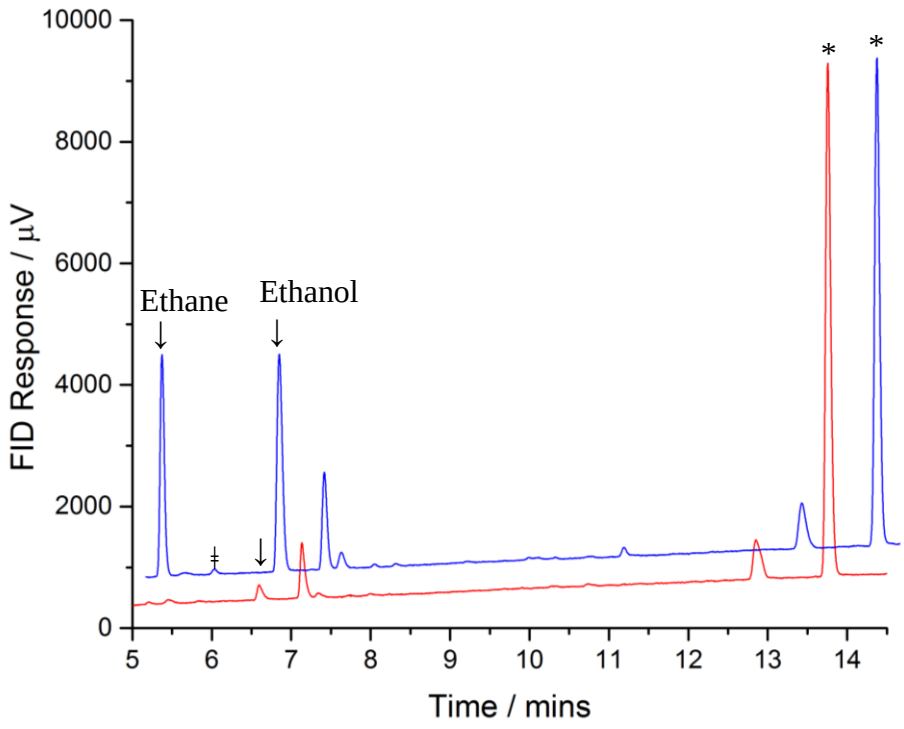

Figure 4-5: The GC illustrating an ethane oxidation by the RT2/AP mutant under pressure. ǂdenotes acetaldehyde formation and *denotes 2-pentanone internal standard. The blue chromatograms represent the reaction under 8 bar ethane and 2 bar air at ambient temperature after two hours, and red chromatograms represent the background.

The RT2/AP mutant showed enhanced TTN for both propane and ethane oxidation with the application of pressure, with the TTN for propane oxidation improving from 680 ± 10 to 10,900 ± 420 under 5 bar partial pressure of propane at ambient temperature. A clear ethanol product peak above background was also observed, with the TTN of 350 ± 30, under 8 bar ethane and 2 bar air. The activity of RT2/AP was therefore directly compared with the previously reported, highly active E32 mutant of $P450_{BM3}$.[222]

4.5 The $P450_{BM3}$ mutant E32

Arnold and co-workers reported the $P450_{BM3}$ mutant E32 discovered by the technique of Challenge Response Authentication Mechanism (CRAM).[222] This variant contained the mutations A74W, V78I, A82L, A184V, L188W, A328F and A330W. TTN values of 16,800 and 1,200 were reported for propane and ethane oxidation, respectively. Mixtures were assayed in 100 mM phosphate, pH 8.0, with 25 – 250 nM E32 mutant, 100 μM $NADP^+$, 20 U mL^{-1} isocitrate dehydrogenase, 10 mM isocitrate, and the mixtures were stirred for 20 hours under 30 psi propane or ethane at 4 °C. The reactions were quenched with 15 μL of 5 M HCl then neutralised with 75 μL 1 M phosphate, pH 8.0. However, no details were provided on the analysis method, such as whether and what solvent was used for extraction, and gas chromatograms were not provided. Apart from the different alkane pressure, the reaction temperature was also different (ambient vs. 4 °C) from the present work.

The mutations included in the E32 variant, such as V78I, A82L and A330W, had already been individually added and the mutants were tested under atmospheric pressure (see Chapter 3), but no significant increase in propane oxidation activity was observed. Given the different conditions, these assays were repeated under propane pressure. In addition, the E32 variant as well as combinations of its constituent mutations were prepared to allow direct comparison with the data from this work.

The A74W/V78I/A82L (AVA) triple mutant was tested first under the conditions of the present work, i.e. 5 bar propane and 2 bar air at ambient temperature with stirring for two hours. The TTN was 300 ± 80 (Table 4-2), 13-fold higher than the WT. Two more mutations, A184V and L188W, were then added to the AVA mutant. The A74W/V78I/A82L/A184V/L188W (AVA/AL) variant gave a TTN of 2,070 ± 150, which was seven-fold higher than the AVA mutant. The E32 mutant, A74W/V78I/A82L/A184V/L188W/A328F/A330W, was 2.5-fold more active still, with a TTN of 5,170 ± 450. However, under the same conditions this is only 50% of the activity of the RT2/AP mutant, and 30% of the reported activity. The difference in TTN values may be due to a calibration effect.

The effect of some mutations within the E32 variant was examined. The A330W mutation improved the activity towards propane, with the TTN of 270 ± 10. The L188Q mutation increased the TTN to 890 ± 50. Leu188 had been targeted for mutagenesis since the report of the high activity of the A74G/F87V/L188Q mutant by Schmid and co-workers.[256] The A328F mutant led to a TTN of 1,040 ± 20, almost 50 times the activity of WT $P450_{BM3}$. It may be concluded that the L188W and A328F mutations were mainly responsible for the increased propane oxidation activity of the E32 variant. The AVA/AL/AA mutant also shifted the product selectivity slightly towards terminal oxidation, with 9% of the total products being 1-propanol, again due to the introduction of A328F mutation which gave 8% 1-propanol.

Table 4-2: Comparison of propane and ethane hydroxylation TTN, and selectivity data of A330P and RT2/AP, along with the E32 mutant and some of its component mutations. Reactions were performed under 5 bar propane and 8 bar ethane, respectively, for two hours at ambient temperature. AVA = A74W/V78I/A82L, AL = A184V/L188W, AA = A328F/A330W. –: not investigated. ND: no detectable activity. All data are given as mean ± S.D. for $n \geq 3$.

	Propane TTN	**% 2-ol**	**Ethane TTN**	**% ethanol**
WT	24 ± 9	95	ND	ND
L188Q	890 ± 50	96	–	–
A328F	1,040 ± 20	92	–	–
A330P	3,730 ± 40	96	ND	ND
A330W	270 ± 10	96	–	–
AVA	300 ± 80	95	–	–
AVA/AL	2,070 ± 150	95	ND	ND
AVA/AL/AA (E32)	5,170 ± 450	91	290 ± 20	97
RT2/AP	10,900 ± 420	95	350 ± 30	98

The reported TTN of 16,800 for propane oxidation by the E32 mutant was under 30 psi (just over 2 bar) propane pressure at 4 °C, and the reaction mixture was left for 20 hours. A similar experiment was set up, where the propane oxidation reaction by AVA/AL/AA and RT2/AP mutants were run in parallel under 2 bar propane at 4 °C for 20 hours using the Parr autoclave. The TTN of the AVA/AL/AA mutant increased to 6,270 ± 180 from 5,170 ± 450, while the RT2/AP mutant showed a significant increase to 13,170 ± 580 from 10,900 ± 420. The partial pressure of propane was raised to 5 bar at 4 °C in another set of experiment, but the resulting TTNs for both AVA/AL/AA and RT2/AP were slightly lower than under 2 bar propane at 4 °C. The A330P mutant was also tested under three different conditions. Activities of A330P under 5 bar propane and 2 bar air at ambient temperature, and under 5 bar propane pressure at 4 °C, were similar to the activities shown by the E32 mutant (Figure 4-6).

The activity of A330P at 2 bar propane pressure at 4 °C, however, was lower than expected, with TTN of only 2,050 ± 290. Arnold *et al.* reported the value of 590 for this mutant under the similar conditions.[222]

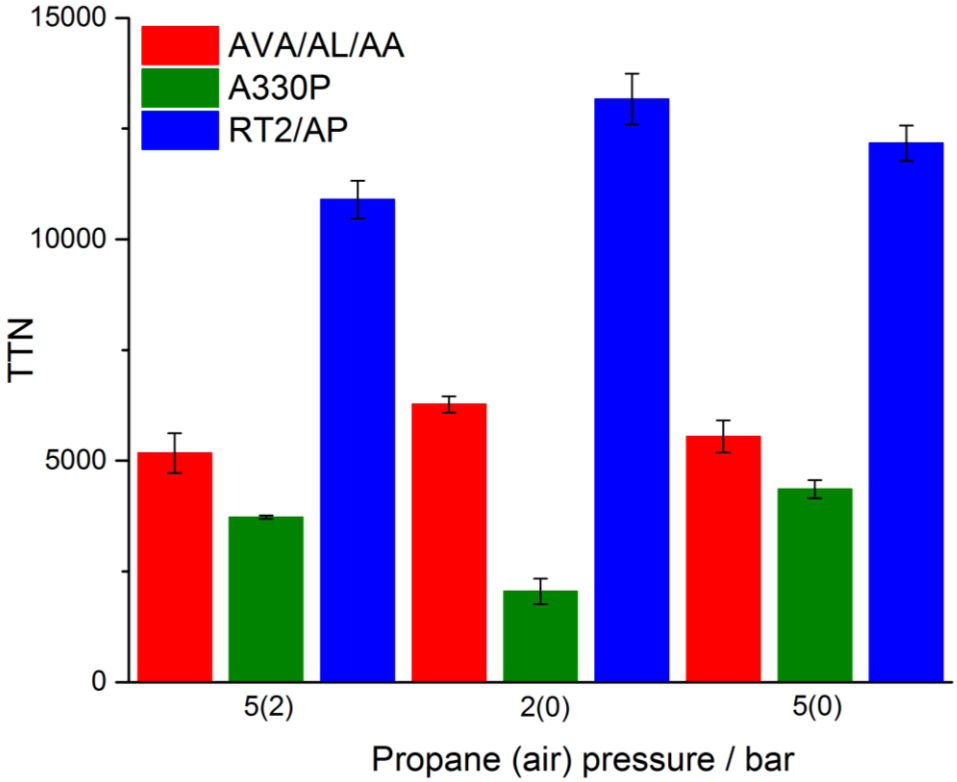

Figure 4-6: Bar chart comparing relative peak sizes of combined 1- and 2-propanol products of A330P, RT2/AP and AVA/AL/AA (E32) mutants for propane oxidation under different conditions. Under ambient temperature, partial propane pressure of 5 bar and 2 bar compressed air was used, and reaction mixtures were extracted after two hours. In the cold room at 4 °C, partial propane pressures of 2 and 5 bar were used, and reaction mixtures were extracted after 20 hours. [$P450_{BM3}$] = 0.5 µM.

Ethane oxidations were performed under different sets of conditions (Figure 4-7). The E32 mutant showed ethane oxidation activity with TTN of 290 ± 20 under 8 bar ethane at ambient temperature, but the reaction under 15 bar ethane at 4 °C improved to TTN of 420 ± 40. In comparison, the TTN of RT2/AP increased from 350 ± 30 to 630 ± 50 at 4 °C. The ethane oxidation was also performed at 2 bar (*ca.* 30 psi) ethane pressure at 4 ºC to allow direct comparison with Arnold's work. Under these conditions, the RT2/AP mutant gave a TTN of 240 ± 50, and the E32 mutant showed lower TTN of 170 ± 10. This value, however, was

below the reported value of 1,200 under 2 bar ethane.[222] In all the GC analysis, the ethanol product peak was high above background and can be integrated accurately (see Figure 4-5), supporting the absolute as well as relative TTN values.

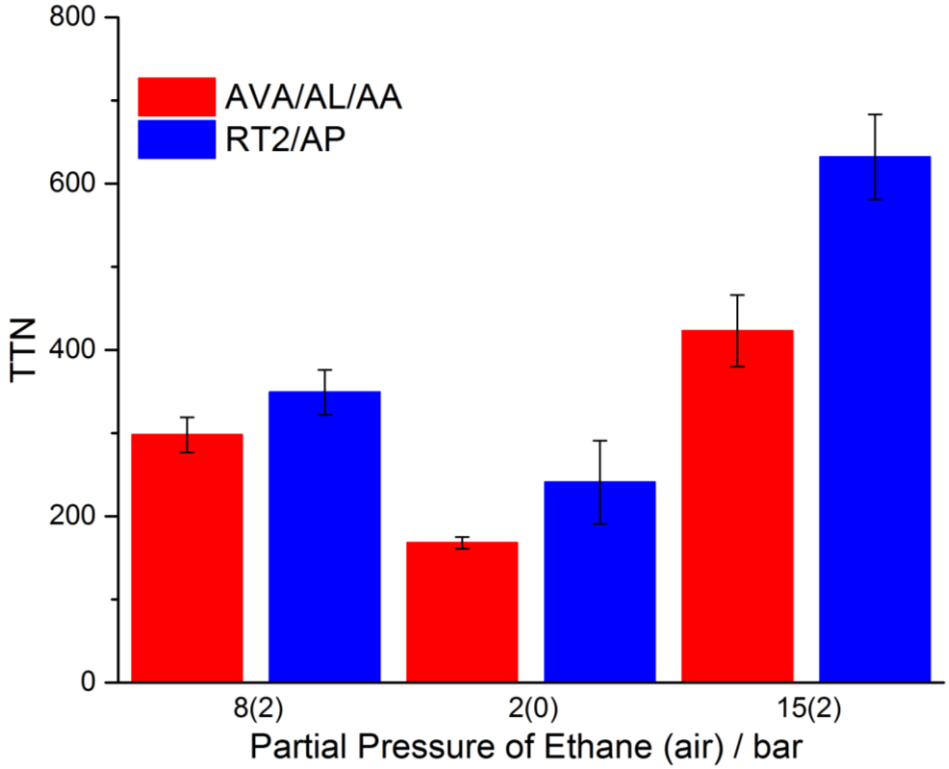

Figure 4-7: Bar chart comparing relative peak sizes of ethane oxidation products of RT2/AP and AVA/AL/AA (E32) mutants under different conditions. Under ambient temperature, partial ethane pressure of 8 bar and 2 bar compressed air was used, and reaction mixtures were extracted after two hours. In the cold room at 4 °C, partial ethane pressures of 8 bar and 15 bar were used, and reaction mixtures were extracted after 20 hours. [$P450_{BM3}$] = 0.5 µM.

In general, the best condition for propane hydroxylation was applying partial pressure of 2 bar at 4 °C, and 15 bar at 4 °C for the ethane oxidation. The increase in TTN by lowering temperature and applying mild pressure indicated that improving saturation of alkanes was important in achieving higher enzymatic activities. No significant gain in TTN values were observed when the partial propane pressure was increased to 5 bar at 4 °C, apart from the A330P mutant.

The condition of 5 bar propane and 2 bar air at ambient temperature was then used to test various mutants, due to the short reaction time and ease of handling. The best mutants would

then be studied for their ethane oxidation activities under 8 bar ethane and 2 bar air at ambient temperature. The key variants identified from these screenings will be used to perform both propane and ethane oxidations at 4 °C to achieve the highest TTN (see Chapter 5).

4.6 The breakdown analysis of the effect of applying mild pressure on propane hydroxylation activities of base mutants

Further analysis of each mutation within the RT2/AP mutants were performed to get a better understanding of the effect of mild pressure on TTN. The A330P mutation is important for propane oxidation activity, as found in chapter 3. The high TTN of 3,730 ± 40 was achieved for the A330P variant alone at 5 bar propane, 2 bar air at ambient temperature. Introduction of the bulkier amino acid, tryptophan at this residue, however, had less significant effect, with TTN of only 270 ± 10 observed for the A330W mutant. Arnold *et al.* did not report the TTN value for the A330W mutant.[222] The TTN of R47L/Y51F (RL/YF), KT2 and RT2 were dramatically improved with the application of mild pressure, with the TTN of RT2 improving to 2,650 ± 420. Activities of these mutants, however, were poor compared to any mutants containing A330P, with the TTN of RT2/AP being four-fold higher than for RT2. For most of mutants described in Table 4-3, a clear 1-propanol product peak above background was observed under 5 bar propane pressure.

Table 4-3: Comparison of propane hydroxylation TTN values and selectivity data for various mutants between reactions performed under atmospheric pressure, and 5 bar propane and 2 bar air. –: not investigated. ND: no detectable activity. All data are given as mean ± S.D. for $n \geq 3$.

	Atmospheric Pressure		5 bar propane/2 bar air	
	TTN	**% 2-ol**	**TTN**	**% 2-ol**
WT	ND	ND	24 ± 9	95
R47L/Y51F	23 ± 0	96	1,130 ± 80	95
A330P	9 ± 2	96	3,730 ± 40	96
A330W	–	–	270 ± 10	96
KT2	ND	ND	1,260 ± 300	96
RT2	4 ± 1	93	2,650 ± 120	96
RT2/AP	680 ± 10	96	10,900 ± 420	96

4.7 Propane hydroxylation reaction under 5 bar partial pressure

The application of higher pressure significantly increased the TTN for most of the mutants listed in Table 4-3 without significantly altering product profiles, and the effect of 5 bar partial pressure of propane was explored with other mutants. New sets of mutations were introduced to these variants targeting residues shown in Figure 4-8, but in some cases, one or more residues were reversed back to the original amino acids of WT from RT2/AP to make new enzymes, such as KT2/AP and KU/AP, where RL/YF and RL/YF/L353I were removed, respectively, to determine the role of each mutation. Other mutations, such as L188Q, which is a part of the GVQ mutant reported by Schmid,[191] were then added to these variants to see if it could improve the TTN of propane hydroxylation. GVQ has previously shown improved activity towards various substrates, such as ethylbenzene and naphthalene, where PFRs improved from 6.7 min^{-1} to 199 min^{-1} and 3.0 min^{-1} to 204 min^{-1}, respectively.[250] Most active mutants were also tested for ethane hydroxylation.

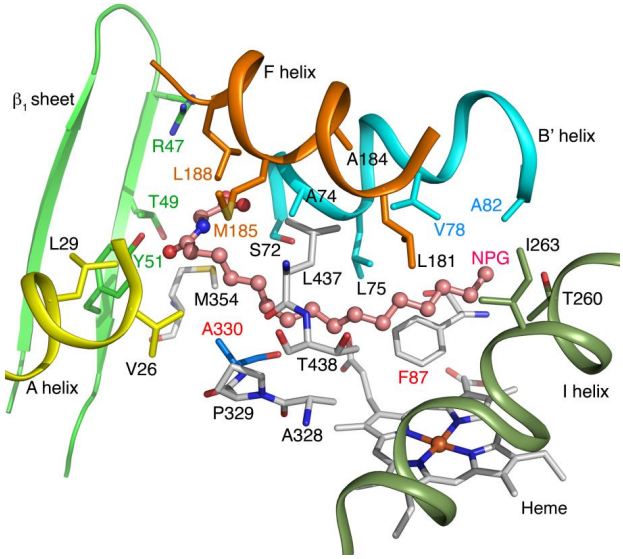

Figure 4-8: The key amino acid residues around the $P450_{BM3}$ active site. Further work on mutating residues on the B′-helix was performed, as well as further analysis on individual mutations within the KT2 set. The effect of mutating Thr438, which is located above the haem, was also investigated.

4.7.1 The R47L/Y51F series

The RL/YF series was the first set of mutants tested under 5 bar partial propane pressure (Table 4-4). The TTN increased by nine-fold, when the A330P mutation was added to the RL/YF variant. This increase was expected from the data in chapter 3. A smaller amino acid, glycine, was then substituted to two alanine residues, 74 and 264, and both mutations were added to RL/YF/AP. A74G is a part of the GVQ mutant. The RL/YF/A74G/AP mutant, however, did not significantly affect the activity towards propane. This is consistent with the small increase in propane oxidation activity for the A74W/V78I/A82L mutant. The RL/YF/A264G/AP mutant showed low activity towards propane with the TTN of 1,300 ± 230. Although a negative result, the data indicated the detrimental effect on alkane oxidation of reducing the side chain volume at residues close to the haem.

The I401P mutation was added to RL/YF to make the RP variant, and this led to a three-fold increase in TTN. The addition of A330P, however, did not lead to a further increase in activity for the RP/AP mutant. The Q403P mutation was added to the RL/YF/AP mutant since

it was previously found to be rate-accelerating, with 39 s^{-1} for propylbenzene.[250] However, no holoenzyme was detected in cultures.

Table 4-4: Propane hydroxylation TTN and selectivity data for the RL/YF series under 5 bar propane and 2 bar air. –: not investigated. ND: no detectable activity. All data are given as mean ± S.D. for $n \geq 3$. ‡Protein did not fold.

	Atmospheric Pressure		**5 bar propane/2 bar air**	
	TTN	**% 2-ol**	**TTN**	**% 2-ol**
WT	ND	ND	24 ± 9	95
A330P	9 ± 2	96	3,730 ± 40	96
R47L/Y51F	23 ± 0	96	1,130 ± 80	95
RL/YF/AP	–	–	9,200 ± 350	96
RL/YF/A74G/AP	–	–	9,010 ± 260	96
RL/YF/A264G/AP	–	–	1,300 ± 230	98
RL/YF/AP/Q403P‡	–	–	–	–
RP	–	–	2,490 ± 310	96
RP/AP	350 ± 30	97	3,110 ± 250	96

4.7.2 The KT2 series

The KT2 base mutant had a TTN of 1,260 ± 280 under 5 bar propane and 2 bar air (Table 4-5). The 10-fold increase in TTN from KT2 to KT2/AP again illustrated the importance of the A330P mutation. His171 residue is located at the start of the F-helix and in close proximity to the Leu215 residue in G-helix. H171L is one of the mutations in the KSK19 variant, and KSK19 previously showed high activities towards various compounds such as *p*-cymene hydroxylation, where the PFR increased from 170 min^{-1} to 1,440 min^{-1} relative to WT.[202] This is partially due to the movement of G-helix caused by the H171L mutation, and thus this mutation was added to the KT2 mutant. Addition of H171L to KT2

led to a two-fold increase, and this mutation was therefore added to KT2/AP. The resulting KT2/AP/H171L variant, however, gave a very low yield. Its activity was five-fold lower than KT2/AP and similar to that of KT2.

Table 4-5: Propane hydroxylation TTN and selectivity data for the KT2 series under 5 bar propane and 2 bar air. All data are given as mean ± S.D. for $n \geq 3$.

	5 bar propane, 2 bar air	
	TTN	**% 2-ol**
KT2	1,260 ± 280	96
KT2/H171L	2,590 ± 240	95
KT2/AP	12,490 ± 1,980	95
KT2/AP/H171L	2,410 ± 20	95

4.7.3 The RT2 series

The R47L/Y51F mutant showed greatly increased activity towards propane oxidation compared to WT, with the TTN of 1,130 ± 80. The activity of RT2 was also higher than KT2 by two-fold (Table 4-6). Unexpectedly, the introduction of I401P to the RT2 template did not improve the activity under 5 bar partial pressure of propane. Other residues were targeted for mutagenesis. The Val26 residue lies in A-helix and near the active site. Glutamine and methionine were added at these positions to reduce the space available at this location further away from the haem. The addition of V26M and S72Y mutations on RT2/AP led to adverse effects towards propane oxidation activities, and the haem incorporation of these enzymes were poor. The addition of A82M and A184I on RT2/AP also reduced enzymatic activities towards propane oxidation, with TTN values dropping to 3,540 ± 340 and 4,190 ± 160 from 10,900 ± 420. The RT2/AP/A82M mutant, interestingly, shifted the selectivity more towards the terminal position, with 8% 1-propanol product. The introduction of I401P or I401M mutations also led to slightly lower TTN, as mentioned in chapter **3.4.3**, and the yield of

protein was also reduced to 6 mg L^{-1} for the RT2/AP/I401M and 2 mg L^{-1} for the RT2/AP/IP mutant.

Table 4-6: Propane hydroxylation TTN and selectivity data for RT2 and RT2/AP series under 5 bar propane and 2 bar air. –: not investigated. ND: no detectable activity. All data are given as mean ± S.D. for $n \geq 3$.

	Atmospheric Pressure		5 bar propane, 2 bar air	
	TTN	**% 2-ol**	**TTN**	**% 2-ol**
R47L/Y51F	23 ± 0	95	1,130 ± 80	95
KT2	ND	ND	1,260 ± 280	96
RT2	4 ± 1	93	2,650 ± 120	96
RT2/IP	100 ± 1	95	2,620 ± 60	96
RT2/AP	680 ± 10	96	10,900 ± 420	96
RT2/AP/V26M	–	–	7,190 ± 440	96
RT2/AP/S72Y	–	–	7,030 ± 500	95
RT2/AP/A82M	200 ± 9	92	3,540 ± 340	92
RT2/AP/A184I	200 ± 30	95	4,190 ± 160	95
RT2/AP/I401M	570 ± 50	97	7,720 ± 860	97

4.7.4 The KT2/AP series

Further analysis of each individual mutation within the RT2/AP mutant is described in this section. The RT2 mutant was constructed by adding the R47L/Y51F couplet to the KT2 mutant (A191T/N239H/I259V/A276T/L353I). Interestingly, the KT2/AP variant gave a similar TTN (12,500 ± 1,980) as RT2/AP (10,900 ± 420) as shown in Table 4-7. Therefore, the L353I mutation was removed from KT2 to see the effect on propane oxidation activity. The Leu353 residue is situated next to the substrate access channel. The KU/AP variant (A191T/N239H/I259V/A276T/A330P) thus generated had similar activity as the KT2/AP

mutant, with a TTN of 13,910 ± 100, clearly showing that not all the KT2 mutations were required for improved propane oxidation. The other mutations in KT2 were then individually removed to see the effect of each mutation for propane hydroxylation.

The removal of I259V, A191T, N239H, and A276T from KU/AP led to the KU2/AP, KU3/AP, KU4/AP and KU5/AP variants, respectively. Ile259 and Ala276 residues both lie in the I-helix and are not in direct contact with the substrate. The elimination of I259V and A276T mutations led to lower activities, with the TTN of KU2/AP dropping to 6,510 ± 670 compared to 13,910 ± 100 for KU/AP. The observed increase in enzymatic activity towards propane oxidation with the I259V mutation in KU/AP led to the idea of substituting I259V with the I259A mutation, which incorporates an even smaller amino acid at this residue. The resulting AT/NH/IA/AT/AP variant, however, had a lower TTN of 9,520 ± 150. The Ala191 residue is found on the outer region of the access channel, and the crystal structure of the palmitate-bound form showed significant displacement of this residue. Asn239 is situated in the H-helix, which is in contact with the N-terminal end of the I-helix, and the N239H mutation may play a role in the displacement of the I-helix observed in the KT2 structure.[233] KU3/AP and KU4/AP mutants led to similar activities to KU/AP towards propane, with TTN values being *ca.* 13,000. Both N239H and I191T were therefore removed from KU/AP, leading to the I259V/A276T/A330P mutant. The resulting TTN, however, was lower than expected, with a TTN of 9,990 ± 260. The difference between KU/AP and KU5/AP was not significant, with both enzymes showing high activities. This set of data indicated that both I259V and A330P mutations were crucial in achieving high propane oxidation activity, whilst the A276T mutation and one of A191T or N239H, were important in maintaining TTN >12,000. A191T and N239H mutations are likely to promote propane oxidation by leading to similar conformational changes and mechanisms, and hence are interchangeable.

The R47L/Y51F couplet and the L353I mutations did not improve the activity in the KU/AP series (A191T/N239H/I259V/A276T/A330P).

The M185K mutation was added to KU3/AP, as PFR increased for propane oxidation by two-fold when this mutation was added to the RT2 set, in the work performed by Knight.[257] The Met185 residue is in the F-helix, and the crystal structure indicates that this helix shifts when a fatty acid binds, allowing the Leu437 residue to move away from the haem. The substitution to lysine at Met185 should minimise the movement of F-helix and prevent the active site opening. The resulting TTN, however, was lower than the KU3/AP mutant, with two-fold decrease in activity. The mutation G443A was added to the KU3/AP template, as the mutant $P450_{PMO}R2$, which contains a total of 23 mutations including G443A, was reported to give a high TTN of 45,800 towards propane oxidation.[249] However, the addition of G443A alone to KU3/AP, did not significantly improve the propane oxidation activity.

Table 4-7: Propane hydroxylation TTN and selectivity data for the KT2/AP series and the KU3/AP series under 5 bar propane and 2 bar air. KU/AP = KT2/AP without the L353I mutation, i.e. A191T/N239H/I259V/A276T/A330P, KU2/AP = KU/AP without the I259V mutation, KU3/AP = KU/AP without the A191T mutation, KU4/AP = KU/AP without the N239H, and KU5/AP = KU/AP without the A276T mutation. AT/NH/IA/AT/AP = A191T/N239H/I259A/A276T/A330P. –: not investigated. All data are given as mean ± S.D. for $n \geq 3$. *TTN of RT2/AP under atmospheric pressure was 680 ± 10, with 96% 2-propanol product. ‡Protein did not fold.

	5 bar propane, 2 bar air	
	TTN	**% 2-ol**
RT2/AP*	10,900 ± 420	96
KT2/AP	12,500 ± 1,980	95
KU/AP	13,910 ± 100	96
KU2/AP	6,510 ± 670	96
AT/NH/IA/AT/AP	9,520 ± 150	95
KU3/AP	13,530 ± 270	96
KU3/AP/M185K	7,680 ± 90	95
KU3/AP/K391N‡	–	–
KU3/AP/G443A	13,700 ± 1,380	96
KU4/AP	14,250 ± 1,370	96
KU5/AP	12,780 ± 970	96
I259V/A276T/A330P	9,990 ± 260	96

4.7.5 The Ala330/Leu188 series

The L188Q mutation alone did not give high TTN (890 ± 50) for propane hydroxylation, but when it was combined with the key A330P mutation, the A330P/L188Q mutant led to a high TTN of 8,550 ± 460 (Table 4-8). The I259V mutation was important in achieving high activity in KU/AP, and this mutation was added to further improve the activity. However, the resulting mutant, A330P/L188Q/I259V, had a lower TTN of 6,760 ± 420. The higher TTN of

13,590 ± 240 was surprisingly achieved by the A330P/L188Q/A191T mutant. Previous work in **4.7.4** indicated that removing I259V from KU/AP had a significant effect on TTN by over two-fold, and removing A191T from KU/AP led to a slight increase (8%) in TTN. This set of results therefore contradicted with the trend observed previously. This may be due to L188Q and I259V mutations promoting propane oxidations by similar mechanisms.

The A328V mutation was added to the A330P/L188Q template, as this mutation improved the activity of $P450_{BM3}$ in the work performed by Arnold's group (A328V alone was reported to give a TTN of 2,300).[222] The resulting A330P/L188Q/A328V mutant showed lower activity towards propane oxidation, with TTN dropping by almost two-fold, probably due to bulky amino acid residues overcrowding around the active site and preventing propane substrate from approaching the haem. Another mutation, A328F, was added to A330P/L188Q, as this was in the E32 mutant.[222] The activity of A330P/L188Q/A328F was drastically lower, with a TTN of just 1,780 ± 30. The mutations at the Ala328 residue interestingly shifted the selectivity towards the terminal position relative to the A330P/L188Q template (8% 1-propanol product for A330P/L188Q/A328F). L188W is also a part of the E32 mutant, and the mutation was added to A330P instead of L188Q. The TTN of 7,150 ± 20 was observed for A330P/L188W, which was *ca.* 15% lower than A330P/L188Q.

Thr438 was targeted for mutagenesis to close off the space higher up the active site. The A330P/L188Q/T438P variant showed good expression levels, but the TTN dropped from 8,550 ± 460 to 700 ± 10 without altering the selectivity. The A330P/L188Q/T438F mutant also led to a significant drop in activity (560 ± 50), but interestingly the selectivity shifted more towards the terminal alcohol, with 12% of 1-ol being formed. The low activity may be due to the primary C–H bond oxidation being slower. The T438V mutation led to an even larger drop in TTN, to 220 ± 20 for the A330P/L188Q/T438V mutant.

Table 4-8: Propane hydroxylation TTN and selectivity data for the Ala330/Leu188 series under 5 bar propane and 2 bar air. All data are given as mean ± S.D. for $n \geq 3$. *TTN of A330P under atmospheric pressure was 9 ± 2, with 96% 2-propanol product.

	5 bar propane, 2 bar air	
	TTN	**% 2-ol**
WT	24 ± 9	95
L188Q	890 ± 50	96
A328F	1,040 ± 20	92
A328V	860 ± 360	93
A330P*	3,730 ± 40	96
A330P/L188Q	8,550 ± 460	96
A330P/L188Q/A74G	9,170 ± 30	96
A330P/L188Q/A191T	13,590 ± 240	96
A330P/L188Q/I259V	6,760 ± 420	96
A330P/L188Q/A328F	1,780 ± 30	92
A330P/L188Q/A328V	5,170 ± 60	93
A330P/L188Q/T438F	560 ± 50	88
A330P/L188Q/T438V	220 ± 20	95
A330P/L188Q/T438P	700 ± 10	96
A330P/L188W	7,150 ± 20	95

4.7.6 The KU/AP series

L75Q and A264V mutations were added to KU/AP to reduce the active site volume from the B′- and I-helices, respectively. The A264G mutation was found to lower propane oxidation activity so a bulkier side chain could be beneficial. The resulting TTN values, however, were very low, with both mutants giving TTN of *ca.* 100 even under 5 bar propane, although the KU/AP/A264V showed a change in selectivity, with 17% 1-propanol produced (the highest of

all mutants in this work). The F87W mutation was added on the basis that the addition of F87A on KT2 led to lower activity towards pentane (PFR dropping from 645 to 136 min^{-1}).[250] Alanine is a small amino acid and the reverse trend was expected with the bulky tryptophan. The activity of KU/AP/F87W was very low (TTN = 60 ± 2) even under 5 bar propane, as shown in Table 4-9. T88H, T260L, and K391N mutations were all designed to push the substrate closer to the haem, but no holoenzyme was obtained. Since the A330P/I401P combination affected protein folding and haem incorporation, the G402P mutation was used, but no holoenzyme was obtained. The addition of L188Q to A330P previously improved the activity, and KU/AP/L188Q was therefore prepared. The resulting TTN was similar to the KU/AP variant (*ca.* 13,500).

Table 4-9: Propane hydroxylation TTN and selectivity data for the KU/AP series under 5 bar propane and 2 bar air. KU/AP = KT2/AP without the L353I mutation, i.e. A191T/N239H/I259V/A276T/A330P. –: not investigated. All data are given as mean ± S.D. for $n \geq 3$. ‡Protein did not fold.

	5 bar propane, 2 bar air	
	TTN	**% 2-ol**
KU/AP	13,910 ± 100	96
KU/AP/T88H‡	–	–
KU/AP/T260L‡	–	–
KU/AP/G402P‡	–	–
KU/AP/L75Q	130 ± 10	95
KU/AP/L188Q	13,560 ± 860	96
KU/AP/A264V	80 ± 5	83
KU/AP/F87W	60 ± 2	97

4.8 Ethane hydroxylation under 8 bar partial pressure

The gain in propane oxidation activity for mutants listed in **4.7** was clear, with several mutants reaching TTN of above 10,000 under 5 bar partial propane pressure. The base mutant RT2/AP gave high propane oxidation activity, with TTN improving from 680 ± 10 to 10,900 ± 420 under 5 bar pressure. The A330P/L188Q variant, containing only two mutations, reached a TTN of 8,550 ± 460, and KU/AP (KT2/AP without the L353I mutation), reached a higher TTN of 13,910 ± 100. A new set of mutations which were added around the active site, such as L75Q, A264V and T438V, significantly lowered the propane hydroxylation activity. Without any substantially increased activity towards propane, the RT2/AP, A330P/L188Q and KU/AP enzymes were used as benchmarks for the screening of ethane hydroxylation under 8 bar partial ethane pressure.

WT gave no detectable ethanol or acetaldehyde above background, even with the aid of 8 bar ethane pressure. The variants in Table 4-10 generally followed the activity trend observed for propane oxidation. The RT2/AP gave the TTN of 350 ± 30 for ethane oxidation under 8 bar ethane pressure. The A330P/L188Q mutant, which contains just two mutations and exhibited high propane oxidation TTN of 8,550 ± 460 under 5 bar partial propane pressure, showed ethane TTN of 540 ± 70. The addition of A191T to this variant also improved the ethane activity, with TTN improving to 740 ± 50. The RL/YF/AP mutant, which showed slightly higher propane activity than A330P/L188Q with TTN of 9,200 ± 350, had lower ethane hydroxylation activity, with the TTN of 260 ± 100.

The mutants with reversions of KT2/AP generally showed high ethane oxidation activity, with the TTN of KT2/AP being 600 ± 40. The KU2/AP mutant, with the I259V and L353I mutations removed from KT2/AP, unsurprisingly showed lower ethane oxidation TTN of 170 ± 20, which mirrored the lowered propane TTN of 6,510 ± 670. The percentage of

acetaldehyde, however, increased to 3%. Similarly, the KU5/AP variant also showed relatively high acetaldehyde formation (4%). KU/AP, KU3/AP, KU4/AP all exhibited enhanced ethane oxidation activity, with TTN of 920 ± 50 observed by KU3/AP under 8 bar ethane at ambient temperature after two hours (Figure 4-9). KU/AP/L188Q and KU3/AP/G443A showed no clear signs of higher ethane oxidation TTN, but 3% of the overall product was acetaldehyde for the latter.

Table 4-10: TTN and selectivity data for ethane hydroxylation reactions performed under 8 bar ethane and 2 bar air for two hours at ambient temperature. Those mutants that showed high activities towards propane oxidation were selected. KU/AP = KT2/AP without the L353I mutation, i.e. A191T/N239H/I259V/A276T/A330P, KU2/AP = KU/AP without the I259V mutation, KU3/AP = KU/AP without the A191T mutation, KU4/AP = KU/AP without the N239H, and KU5/AP = KU/AP without the A276T mutation. AT/NH/IA/AT/AP = A191T/N239H/I259A/A276T/A330P. ND: no detectable activity. All data are given as mean ± S.D. for $n \geq 3$.

	TTN	**% ethanol**	**% acetaldehyde**
WT	ND	ND	ND
RT2/AP	350 ± 30	98	2
A330P/L188Q	540 ± 70	99	1
A330P/L188Q/A191T	740 ± 50	99	1
A330P/L188Q/I259V	400 ± 20	99	1
RL/YF/AP	180 ± 20	96	4
KT2/AP	600 ± 40	98	2
KU/AP	890 ± 1	96	4
KU/AP/L188Q	760 ± 40	99	1
KU2/AP	170 ± 20	97	3
AT/NH/IA/AT/AP	450 ± 20	99	1
KU3/AP	920 ± 50	98	2
KU3/AP/G443A	750 ± 4	97	3
KU4/AP	730 ± 60	98	2
KU5/AP	470 ± 80	96	4
I259V/A276T/A330P	540 ± 70	99	1

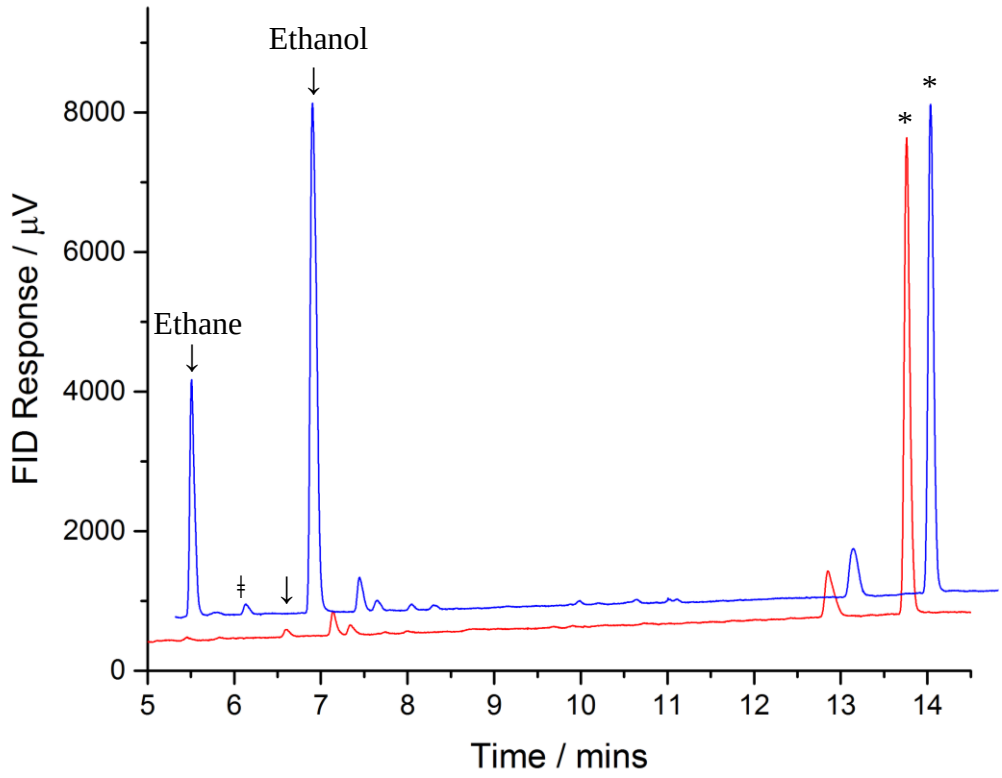

Figure 4-9: The GC illustrating an ethane oxidation by the KU3/AP mutant under pressure. ǂdenotes acetaldehyde formation and *denotes the 2-pentanone internal standard. The blue chromatogram represents the reaction under 8 bar ethane and 2 bar air at ambient temperature after two hours, and red chromatogram is the background.

4.9 Discussion

No significant propanol peaks above background were observed by the WT $P450_{BM3}$ under atmospheric pressure at ambient temperature, even with the efficient K_2CO_3/1-hexanol extraction method (see **3.4.2**). Under these conditions, the highest TTN achieved by $P450_{BM3}$ variants studied in this work was 680 ± 10 by the RT2/AP mutant. The activity, however, was 25-fold lower than the E32 mutant synthesised by Arnold *et al.*, where the TTN of 16,800 was reported. Arnold and co-workers performed reactions under propane partial pressure of 30 psi and at 4 °C to improve the aqueous alkane solubility, and thus the effect of pressure and temperature were initially studied with the WT and the RT2/AP mutant.

The reaction was initially performed under 5 bar propane pressure and 2 bar air at ambient temperature for two hours. Propanol products were observed for the first time by the WT,

with the TTN of 24 ± 9. Similarly, the activity of the RT2/AP mutant improved by 16-fold, reaching the TTN of 10,900 ± 420. No ethanol product above background was seen with the WT even under the ethane partial pressure of 8 bar, but the TTN of 350 ± 30 was observed by the RT2/AP mutant, with a small but clearly detectable acetaldehyde peak observed on the GC. The effect of partial pressure and the total pressure was investigated, and the partial pressure of alkanes was found to be more important over the total pressure in the reaction vessel.

Propane and ethane oxidations were performed at 4 °C, and the RT2/AP mutant was directly compared to the E32 mutant. The best condition for propane oxidation was at 4 °C under 2 bar propane pressure, with TTN of 13,170 ± 580 observed for the RT2/AP mutant. The TTN of E32 mutant was two-fold lower, at 6,270 ± 180. Ethane oxidation reactions were performed using the RT2/AP and E32 mutants, and the best condition was found to be under 15 bar ethane at 4 °C. The RT2/AP mutant similarly showed a higher TTN of 630 ± 50 than the TTN of 420 ± 40 by the E32 mutant.

Series of bulky amino acid substitutions were introduced around the active site of the RT2/AP mutant. Activities of these variants were measured towards propane oxidation under 5 bar propane at ambient temperature. Introductions of V26M and S72Y led to lower propane oxidation activities, with TTN decreasing by *ca.* 30% to 7,030 ± 500 for the RT2/AP/S72Y mutant. RT2/AP/A82M, RT2/AP/A184I and RT2/AP/I401M all showed lower TTN than the RT2/AP under 5 bar propane pressure, mirroring the observed lower activities under atmospheric pressure.

The introduction of new mutations on RT2/AP also often led to lower expression levels, especially in the case of V26M, S72Y and I401M mutations. This problem was tackled by identifying the important mutations within the RT2 set (R47L, Y51F, A191T, N239H, I259V,

A276T, L353I) and reducing the number of mutations of the base mutant, without losing its activity. R47L/Y51F and L353I mutations were initially removed, and the yield of protein improved from 50 mg L^{-1} to 120 mg L^{-1}. Interestingly, higher propane TTN was achieved by the resulting KT2/AP and KU/AP mutants, with the TTN towards propane oxidation increasing up to 13,910 ± 100. Removing either of the A191T and N239H mutations (KU3/AP and KU4/AP, respectively) led to a small change in propane oxidation activity and a further increase in the yield of protein up to 160 mg L^{-1}. The highest TTN towards ethane oxidation under 8 bar ethane pressure at ambient temperature was 920 ± 50 by the KU3/AP mutant, with *ca.* 8 μM acetaldehyde product. Arnold *et al.* reported the TTN of 1,200 with the E32 mutant under the ethane partial pressure of 30 psi at 4 °C, but TTN was found to be 170 ± 7 in this work under the same conditions, and 300 ± 20 under 8 bar ethane pressure at ambient temperature. The difference in TTN values may be due to the effect of the calibration, but the KU3/AP mutant is clearly more active than the E32 mutant, as shown in Figure 4-10. The addition of A74G and G443A seemed to improve the protein folding, but had small effects on the enzymatic activity.

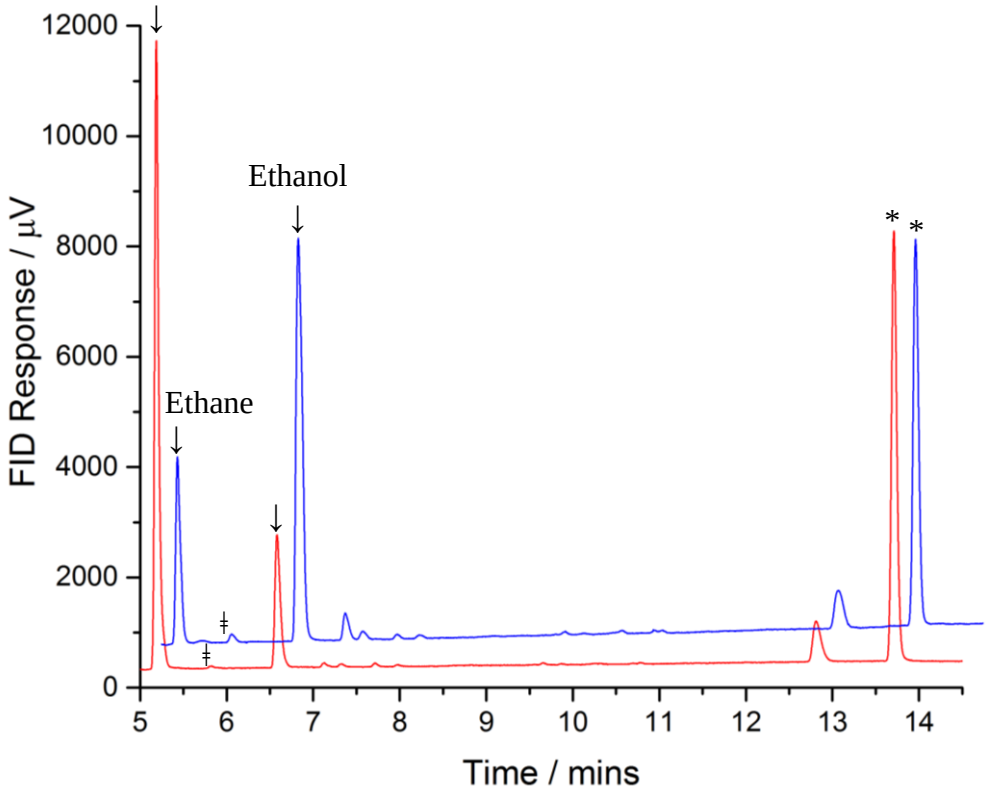

Figure 4-10: The GC comparing ethane oxidation activities of KU3/AP (blue) and the E32 mutant (red) under 8 bar ethane pressure at ambient temperature. ǂdenotes acetaldehyde formation and *denotes the 2-pentanone internal standard.

Further bulky amino acid substitutions of residues around the active site, such as Leu75, Ala264 and Thr438, did not improve the activity towards propane oxidation, with KU/AP/L75Q dropping to 130 ± 10 from 13,910 ± 100 of KU/AP. The A330P mutation continued to be important in achieving high propane TTN, with the A330P mutant alone giving 3,730 ± 40. Another important mutation was L188Q, where the addition of L188Q to A330P led to TTN values of 8,550 ± 460 and 540 ± 70, for propane and ethane, respectively, although the addition of L188Q mutation to KU/AP did not improve the propane oxidation activity further.

The 2-propanol to 1-propanol product ratio remained similar for most of enzymes at 95 : 5, with the only clear exceptions being the A330P/L188Q/T438F and KU/AP/A264V variants. Both enzymes seemed to favour terminal oxidation, with 17% of 1-propanol being produced

for the latter. These enzymes, however, showed low activities towards propane oxidation, especially the KU/AP/A264V mutant giving the TTN value of only 80 ± 5.

Chapter 5

Decoy systems

5.1 Introduction

The addition of "decoy molecules" such as perfluorocarboxylic acids (PFCs) under 5 bar pressure to promote alkane oxidation has been reported by Watanabe[227] and Reetz,[223] including methane oxidation by the WT.[223] The PFC decoys are chemically inert, and their structures resemble those of natural substrates, enabling them to occupy and fill the active site. Smaller substrates such as alkanes may be constrained to bind closer to the haem iron and the alkane oxidation activity may be increased (Figure 5-1).

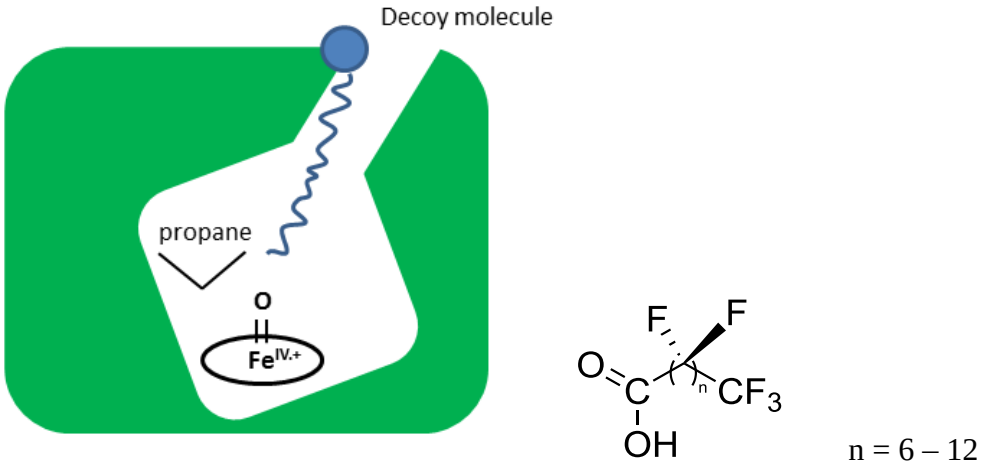

Figure 5-1: Schematic illustration of how the decoy molecule pushes the propane substrate closer to the haem.

The reports by Reetz on propane oxidation did not include any gas chromatographic data on ethane oxidation.[223] The use of RID and LaCourse methods by Reetz, which were claimed to detect small amounts (0.1 ppm, 160 nmol) of methanol,[224] made direct comparison difficult. Reetz reported that oxidation of methane was possible in the presence of PFCs, with the highest TTN of 2,470 for PFC10 under 10 bar pressure (7% CH_4, 8% O_2 and 85% N_2). The application of alkane partial pressure in Chapter 4 also led to large increases in enzymatic activity, where the KU4/AP variant gave a TTN of 14,250 ± 1,370 for propane oxidation under 5 bar propane partial pressure at ambient temperature, compared to 24 ± 9 for the WT.

Watanabe provided chromatograms (reproduced in Figure 5-2) with clear increases in product peaks above background, for the propane oxidation reaction (Figure 5-2a).[227] The effect of PFC with different chain length (PFC8 – PFC14) was investigated. Each reaction contained 20 mM Tris-HCl, pH 7.4, which was pre-saturated with propane and oxygen in 4 to 1 ratio, 0.5 µM $P450_{BM3}$, and 100 µM PFC was added as methanol solution. 5 mM NADPH was then added to initiate the reaction. During the reaction, the reaction mixture was slightly pressurised at 5 to 8 kPa (0.05 to 0.08 bar) using a balloon containing propane and oxygen. A 1 mL aliquot of the reaction mixture was derivatised using 0.15 g sodium nitrite, and 1 mM ethanol was used as internal standard. 1 mL of hexane or dichloromethane was then added before the sample was put on ice, and 150 µL of 20% sulfuric acid was added to generate the 2-propanol nitrite. The addition of PFC8 and PFC14 to WT $P450_{BM3}$ gave no product after 10 minutes, but product concentrations of 330 ± 10 µM (TTN = 660) and 200 ± 20 µM (TTN = 400) were observed with PFC10 and 11, respectively. The turnover rate increased to 67 min^{-1} with 18% coupling efficiency, with the addition of PFC10.[254] The effect of 5 bar propane pressure along with PFC10 under similar conditions gave 2,170 µM 2-propanol and 50 µM 1-propanol (TTN = 4,440). The coupling efficiency under the partial propane pressure of 5 bar improved to 48%, with a clear 1-propanol product peak being observed.[227]

Ethane oxidation under 5 bar pressure was performed for 1 – 3 hours in the same manner as propane oxidation, apart from the concentrations of $P450_{BM3}$ and NADPH were increased to 1 µM and 5 – 15 mM, respectively. 80 µM ethanol product was detected, with ethanol background taken into account. However, the increase in the ethanol peak height and area relative to the background in the gas chromatogram was small (Figure 5-2b). Methane oxidation was also performed under 5 bar methane, but no significant product above background was detected. The reaction condition used by Reetz,[223] (10 bar total pressure, which consisted of 0.7 bar methane, 0.4 bar oxygen, and 8.9 bar nitrogen, and the reaction

mixture contained 1 mM PFC10, 1 mM $NADP^+$, 1 unit GDH, and 100 mM glucose), was also used to perform methane oxidation, but again no methanol product above background was detected, and Watanabe could not reproduce the result reported by Reetz.

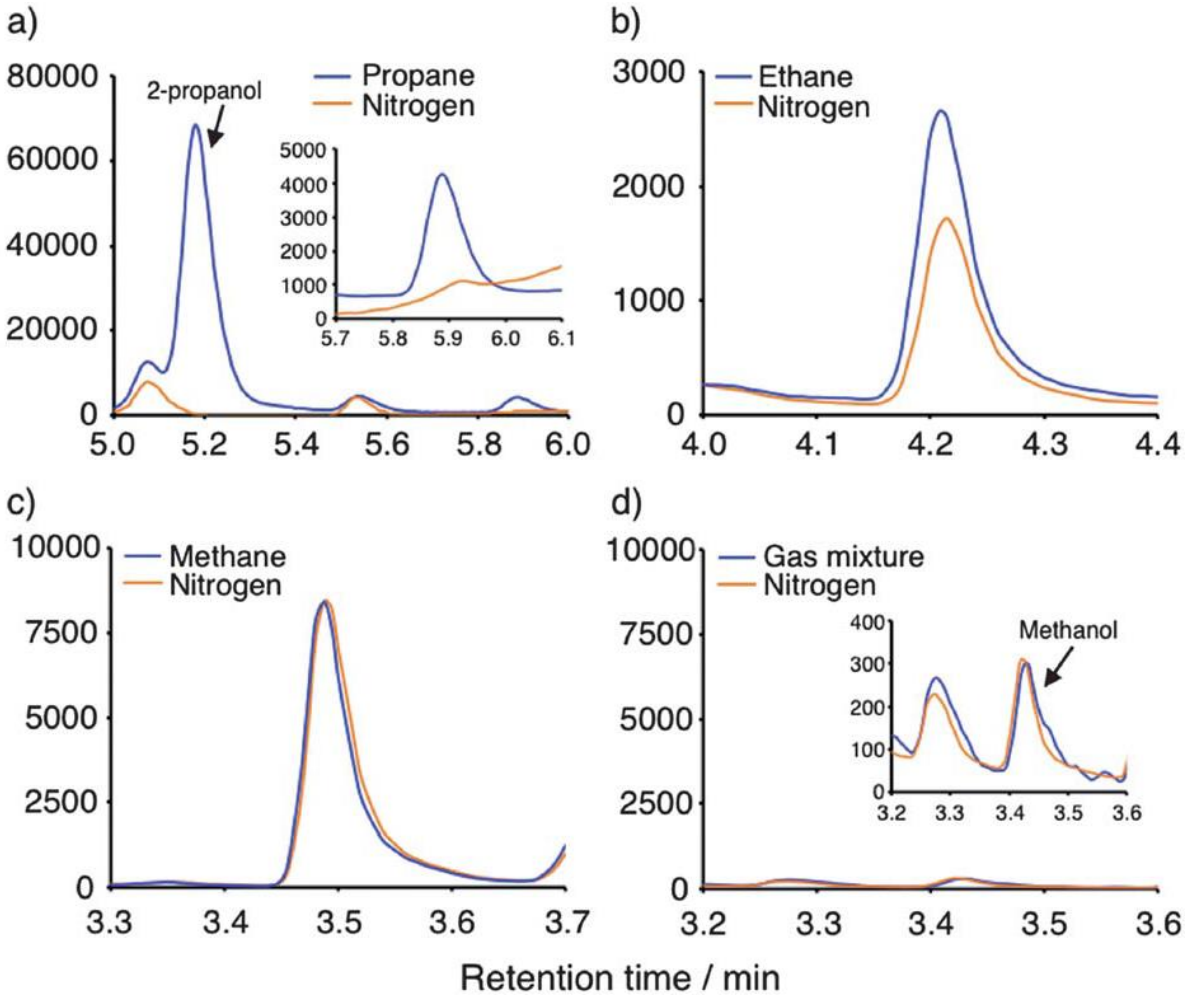

Figure 5-2: The GC analysis performed by Watanabe and co-workers.[227] The hydroxylation of propane (a), ethane (b), and methane (c) with PFC10 were performed under an alkane partial pressure of 5 bar. The GC shown in (d) is the reaction with methane using the total pressure of 10 bar (7% methane, 4% O_2, and 89% N_2). Reproduced with permission.

N-Perfluoroacyl amino acids with hydrophobic side chains ('next generation decoy molecules') were prepared on the basis that the substitution of residues around the substrate access channel entrance to hydrophobic amino acids such as R47L and Y51F led to enhanced catalytic activity (Figure 5-3).[194] The same reaction conditions used for propane hydroxylation with first generation PFCs were used. Various decoy molecules were

synthesised, with different chain length, stereochemistry, and amino acid. The addition of PFC9-*L*-Leu led to the highest PFR of 279 min^{-1}, almost 2-fold increase compared to 159 min^{-1} of PFC9.

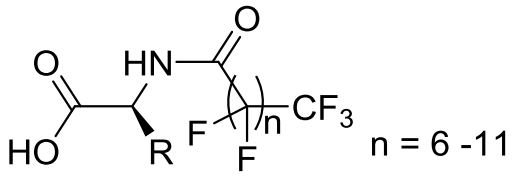

Figure 5-3: The 'next generation decoy molecule'. Hydrophobic side chains are introduced on *N*-perfluoroacyl amino acids to improve short chain alkane oxidation activities.

Ethane oxidation was also studied by Watanabe using PFC9-*L*-Leu with the glucose/glucose dehydrogenase NADPH regeneration system.[229,258] The PFR increased from 15 min^{-1} to 45 min^{-1} with the addition of PFC9-*L*-Leu, leading to the TTN of 90.

5.2 Initial studies with the WT

Initial tests involved measuring the activity of WT with the addition of various PFC with chain length between C_9 – C_{12}. Alkane oxidation assays were performed using 0.5 µM $P450_{BM3}$ enzyme concentration, 200 µM concentration of PFC, 100 mM phosphate buffer, pH 7.4, and a NADPH regeneration system comprising 10 U mL^{-1} GDH, 200 mM glucose and 320 µM $NADP^+$. The activity was measured both under atmospheric pressure and partial pressure of 5 bar propane or 8 bar ethane.

The WT showed negligible propane oxidation activity without any PFCs under atmospheric pressure, but significant 2-propanol formation was detected with added PFCs, especially with the addition of PFC10 and 11, where product concentrations of 240 ± 30 µM (TTN of 470 ± 50) and 200 ± 20 µM (TTN of 390 ± 40) were formed, respectively. The observed trend is in good agreement with the PFR data collected by Watanabe for the series of PFC (Figure 5-4), with the PFR reportedly peaking at PFC10 with 330 µM (TTN = 660).[226]

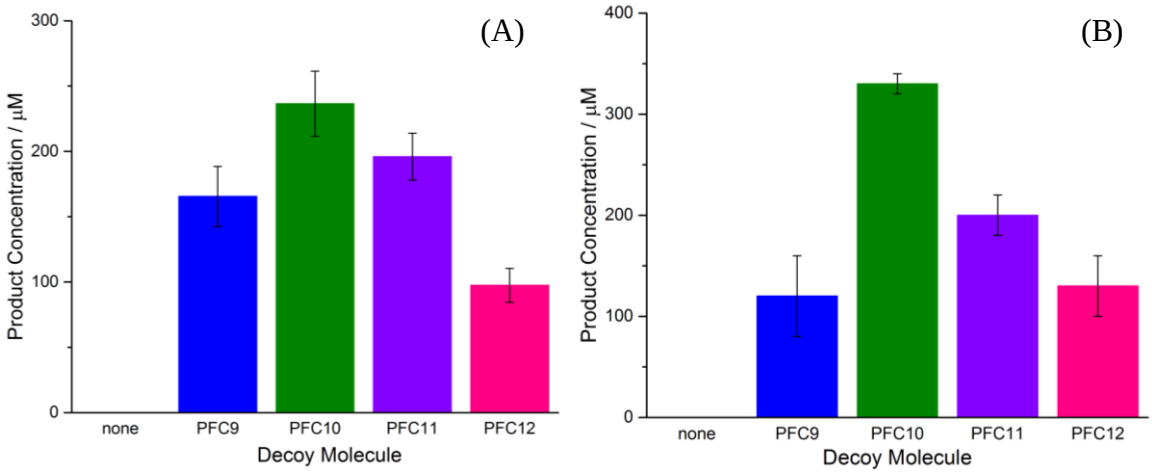

Figure 5-4: The effect of adding PFC of chain length C_9 – C_{12} on the amount of product formed by WT $P450_{BM3}$. Reactions were performed under atmospheric pressure for two hours using a NADPH regeneration system (A). The amount of product formed after 10 minutes using 5 mM NADPH reported by Watanabe (B).[226]

The combination of PFC and 5 bar propane pressure further improved the TTN, as shown in Figure 5-7. The TTN improved by over 250-fold with the addition of PFC10 under 5 bar partial pressure of propane (Figure 5-5), where the combined 1- and 2-propanol concentrations reached 3,080 ± 20 µM (TTN = 24 ± 9 vs. 6,160 ± 30). The total product concentration was higher than the value reported by Watanabe and co-workers (2,220 µM) with the addition of PFC10 under 5 bar propane pressure.

No ethanol was observed under atmospheric pressure without any PFCs, in agreement with previous reports. However, under 8 bar ethane partial pressure, the use of PFC led to some ethanol production. Watanabe reported an ethanol concentration of 80 µM ethanol under 5 bar ethane with PFC10 by 1 µM WT.[227] The amount of ethanol produced in this work was slightly higher, as may be expected due to the higher partial ethane pressure, with 110 µM ethanol (TTN of 230 ± 4) formed (Figure 5-7). Ethanol peak was clearly above background, as illustrated in Figure 5-6. The activity of WT greatly benefited with the incorporation of decoy molecules, especially under pressure. The effect of PFC was therefore tested with the benchmark mutant, RT2/AP.

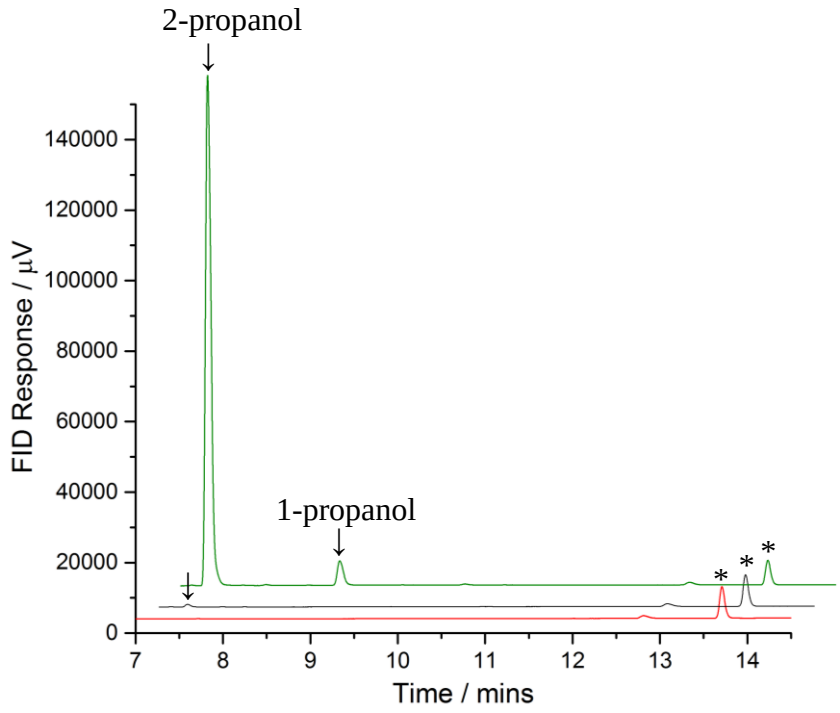

Figure 5-5: The GC illustrating the importance of PFC and applying mild pressure on propane oxidation activities of WT at ambient temperature. No propanol products were observed under atmospheric pressure (red), but small 2-propanol peak was seen under 5 bar propane pressure and 2 bar air (blue). Significant 1- and 2-propanol peaks were observed with PFC10 under 5 bar propane pressure and 2 bar air (green). *denotes the 2-pentanone internal standard.

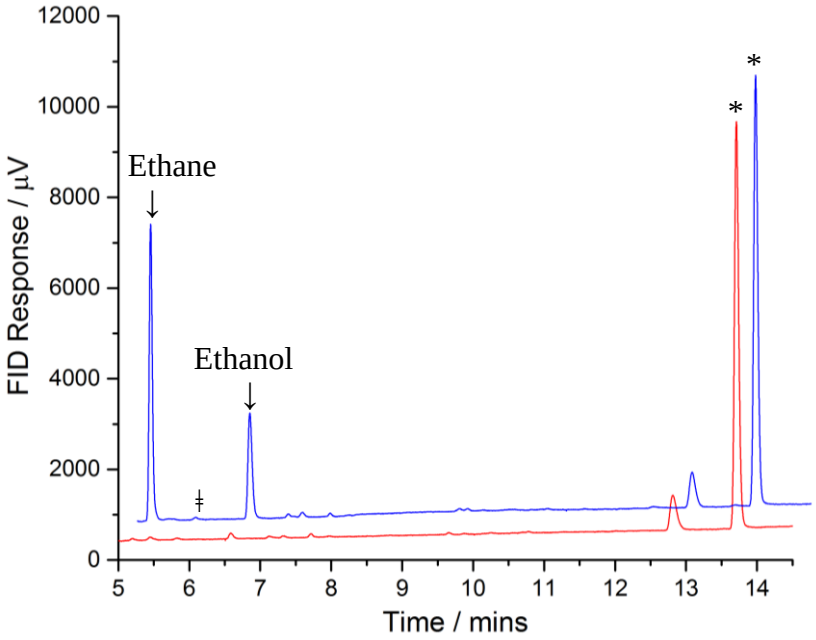

Figure 5-6: The GC illustrating an ethane oxidation by the WT with PFC10. The reaction performed under 8 bar ethane at ambient temperature is in blue and the background is in red. ǂdenotes acetaldehyde formation and *denotes 2-pentanone internal standard.

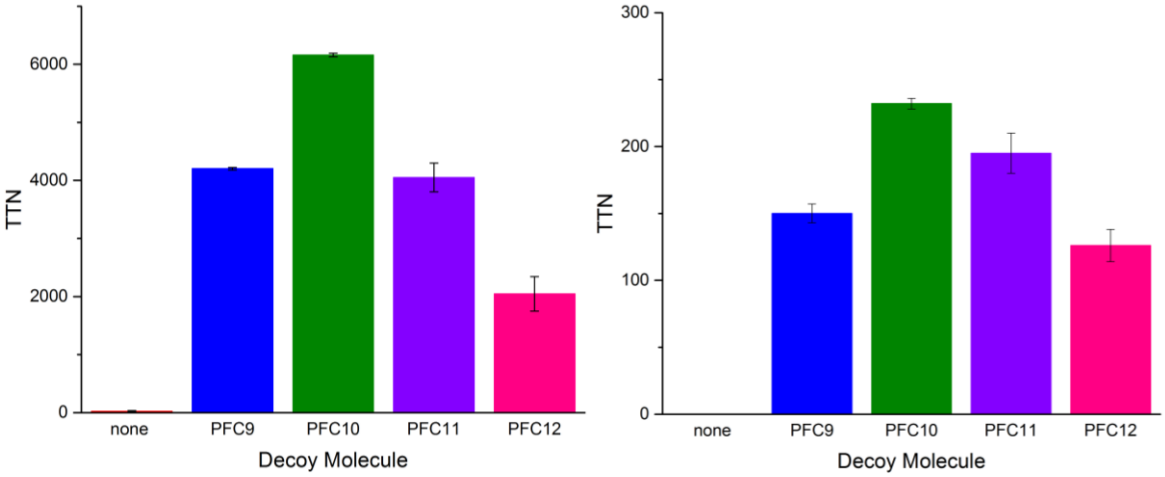

Figure 5-7: The effect of adding various PFCs to the WT at ambient temperature. The bar chart on the left shows propane oxidation TTN under 5 bar propane and 2 bar air, and ethane oxidation TTN under 8 bar ethane and 2 bar air is illustrated on the right.

5.3 The RT2/AP base mutant with decoys

The effect of PFCs was initially investigated with the RT2/AP variant, which showed a TTN of 680 ± 10 for propane oxidation under atmospheric pressure at ambient temperature. The addition of PFC in the same conditions did not have a significant effect on propane oxidation activity, unlike the WT, as illustrated in Figure 5-8.

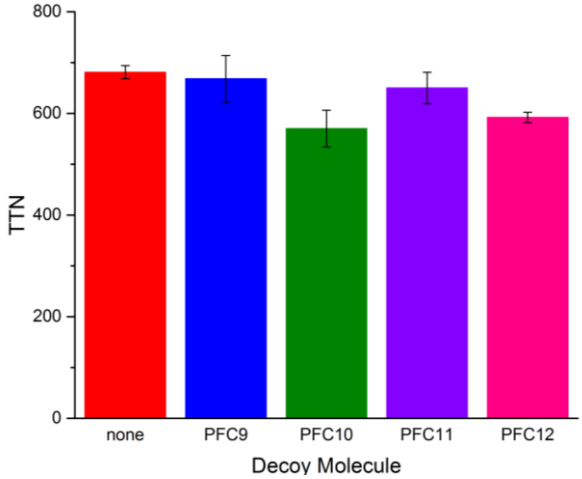

Figure 5-8: The effect of adding various PFCs to the RT2/AP mutant on propane oxidation under atmospheric pressure at ambient temperature.

The combination of applying mild pressure and adding decoy molecules did not improve the propane oxidation activity, with the TTN dropping from 10,900 ± 420 to 5,770 ± 140 in the

case of PFC9. The addition of PFCs under 8 bar ethane pressure did not significantly improve the ethane oxidation activities either, although PFC11 and 12 might have small effects (Figure 5-9).

The lack of increase in activity from the addition of PFCs for the RT2/AP variant may be due to the A330P mutation. The crystal structure of substrate-free A330P showed that the introduction of A330P shifts the adjacent Pro329 residue into the active site, leading to the access channel being too constricted for medium- to long-chain fatty acids and abolishing their oxidation activities.[131,231]

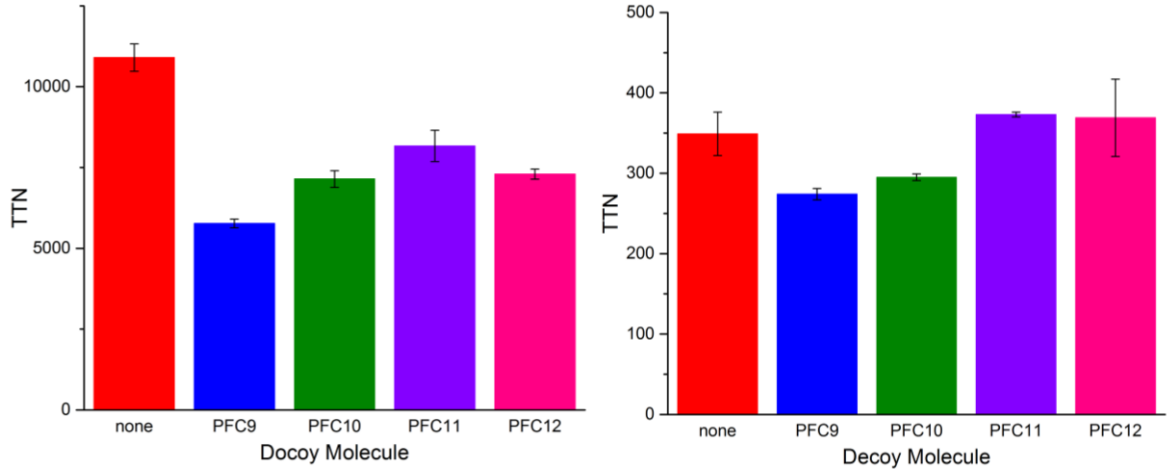

Figure 5-9: The effect of adding various PFCs to the RT2/AP variant at ambient temperature. The bar chart on the left shows propane oxidation TTN under 5 bar propane and 2 bar air, and ethane oxidation TTN under 8 bar ethane and 2 bar air is illustrated on the right.

5.4 Propane hydroxylation reaction with the decoy system under 5 bar partial pressure

The addition of decoy molecules significantly improved WT $P450_{BM3}$ activities towards both propane and ethane at atmospheric and 5 bar propane pressure, with ethanol product being observed for the first time by the WT. The RT2/AP mutant, however, did not gain from the PFCs, due to the A330P mutation shifting the adjacent Pro329 residue towards the active site, and causing a bottleneck that blocks PFCs from entering the substrate pocket above the haem. This needs to be investigated further, and other variants were screened with PFCs to investigate which mutations can be combined with decoy systems to achieve higher alkane oxidation activities. The oxidation of aromatic compounds, such as benzene and cyclohexane, were reported using the KT2 mutant and PFC8 – 10, with the PFR of cyclohexane oxidation improving from 70 ± 5 to 480 ± 30 with the addition of PFC10.[259] The partial propane pressure of 5 bar and 2 bar air at ambient temperature was used for the initial set of screening.

5.4.1 The initial screening

The starting point was to screen variants containing only one mutation to allow direct comparison with the WT. Previous work by Wahler *et al.* created a library of mutants through directed evolution using iterative cycles of random and site-directed mutagenesis.[260] The resulting 29E12 mutant, containing Q55P, N70S, F87I, M185T, A197V, K202R, V216A, M237L, N239T, I263F, A328V, showed strong preference towards the terminal position in palmitic acid oxidation (74%). Some of these mutations were used as the basis of this work with the decoy systems, as PFCs resemble the structure of medium-chain fatty acids. All the single-mutation variants listed in Table 5-1 showed higher propane oxidation activities than the WT, without the addition of decoy molecules. With the exceptions of A328F, A330P and A330W, all of these benefited significantly from the addition of PFC10 or 11. Ala328 and Ala330 both lie on the K-helix and the introduction of bulky mutations at these positions may

have altered the orientation of nearby residues, interfering with the PFC decoy molecules, as mentioned in **5.3**. It has been reported that the mutation at Ala328 residue promoted terminal octane oxidation. Addition of the A328M mutation to the 9-10A variant, containing R47C, V78A, K94I, P142S, T175I, A184V, F205C, S226R, H236Q, E252G, R255S, A290V and L353V led to an increase from 1% to 24% 1-octanol being produced, even though the TTN dropped from 3000 to 700.[215] The A328F mutant showed no significant effect on TTN with PFCs, but led to the formation of higher percentages of 1-propanol with PFC11 (9%). The A328V mutation was the only mutation introduced in the K-helix to benefit from the addition of decoy systems, with TTN improving by four-fold to 3,790 ± 230, with PFC11.

N70S, H171L, L188Q, and M237L mutants showed significant improvements with the addition of PFC under 5 bar propane, with the TTN of H171L (a component of the KSK19 mutant) and PFC11 reaching 9,140 ± 440 (see **4.7.2**). This TTN eclipsed the activity of the RL/YF/AP mutant mentioned in **4.7.1**, which contains key R47L/Y51F and A330P mutations. The GVQ variant (A74G, F87V and L188Q) was tested with and without a decoy molecule. This mutant, however, did not benefit from the addition of PFC11, with the TTN of just under 1,000. The L188Q mutation was tested on its own, and showed higher activity than the WT towards propane oxidation, where the TTN improved by over 37-fold. Remarkably, the TTN of L188Q with PFC11 (1,660 ± 7) was in fact lower than that of the WT (6,160 ± 30) in the presence of the same PFC. It is most likely that the F87V mutation generated space and enabled propane to bind further away from the ferryl oxygen, thus lowering the activity. The highly active double mutant, A330P/L188Q, found in **4.7.5**, was tested with the decoy system but the gain in activity was small from 8,550 ± 460 to 10,370 ± 500. This is consistent with the A330P mutation preventing entry of fatty acids deep into the substrate pocket.

Table 5-1: TTN and selectivity data for variants used in initial screening with and without PFC under 5 bar propane and 2 bar air. All data are given as mean ± S.D. for n ≥ 3.

	No PFC	2-ol (%)	PFC	2-ol (%)
WT	24 ± 9	95	6,160 ± 30 (PFC10)	95
N70S	250 ± 20	96	3,150 ± 580 (PFC11)	95
H171L	1,300 ± 60	96	9,140 ± 440 (PFC11)	95
L188Q	890 ± 50	96	1,660 ± 7 (PFC11)	96
M237L	810 ± 160	96	3,760 ± 300 (PFC10)	95
A328F	1,040 ± 20	92	1,170 ± 160 (PFC11)	91
A328V	860 ± 360	93	3,790 ± 230 (PFC11)	94
A330P	3,730 ± 40	96	3,210 ± 0 (PFC12)	97
A330W	270 ± 10	96	300 ± 40 (PFC11)	95
A330P/L188Q	8,550 ± 460	96	10,370 ± 500 (PFC11)	96
A74G/F87V/L188Q (GVQ)	950 ± 170	93	920 ± 100 (PFC11)	95

5.4.2 The KT2 series

The activity of the KT2 mutant (A191T/N239H/I259V/A276T/L353I) increased with PFCs under 5 bar propane pressure, where the TTN increased to 8,650 ± 110 with PFC10 from 1,260 ± 280, as shown in Table 5-2. The N70S mutant greatly benefited from the addition of PFC and thus N70S was added onto the KT2 set. KT2/N70S showed a six-fold increase in activity from the addition of PFC10, but its activity was half of KT2 with PFC11. Ala82 lies on the B′-helix near the Asn70 residue, and glycine was substituted at this position. The activity of KT2/A82G similarly improved by three-fold with the PFC11 decoy, but the TTN was still low at 2,020 ± 5. The H171L mutation was then added to the KT2 variant, but the

resulting TTN of 7,050 ± 790 was lower than both precursor mutants. The M237L mutant, which showed TTN of 3,760 ± 300 with PFC10 was combined with the KT2 set, but nearby N239H mutation was removed to improve the protein folding. The resulting KU4/M237L mutant showed low propane oxidation activity, with or without PFC10.

The A328V mutant showed four-fold increase with PFC11, and thus it was combined with the KT2 set. The KT2/A328V variant, however, did not significantly benefit from the addition of PFC10, with the low TTN of 1,740 ± 50. Further three mutants containing A330P were tested with decoys, and they all illustrated that PFCs were not required to achieve high propane oxidation activity under 5 bar propane with A330P-containing mutants.

Table 5-2: TTN and selectivity data for the KT2 series with and without PFC under 5 bar propane and 2 bar air. KU4/M237L = KT2/M237L without the N239H mutation. All data are given as mean ± S.D. for $n \geq 3$.

	No PFC	**2-ol (%)**	**PFC**	**2-ol (%)**
WT	24 ± 9	95	6,160 ± 30 (PFC10)	95
KT2	1,260 ± 280	96	8,650 ± 110 (PFC11)	95
KT2/N70S	650 ± 210	94	4,010 ± 650 (PFC10)	95
KT2/A82G	640 ± 50	96	2,020 ± 5 (PFC11)	95
KT2/H171L	2,600 ± 240	94	7,050 ± 790 (PFC11)	95
KU4/M237L	420 ± 4	94	2,290 ± 140 (PFC10)	95
KT2/A328V	990 ± 40	93	1,740 ± 50 (PFC10)	92
KT2/A330P	12,490 ± 1,980	95	9,950 ± 80 (PFC11)	96
KU/AP	13,900 ± 100	96	10,930 ± 900 (PFC11)	96
KU2/A330P	6,510 ± 670	96	3,380 ± 240 (PFC11)	96

5.4.3 The R47L/Y51F series

The effect on R47L/Y51F (RL/YF) was significant with TTN increasing by over three-fold with the addition of PFC11 (Table 5-3). The introduction of I401P to RL/YF improved the activity to 2,180 ± 280 without PFC, but this RP mutant did not seem to benefit from the addition of decoy molecules. The RL/YF/H171L mutant gave TTN of 6,580 ± 70 without the decoy system, but the activity of this enzyme also did not benefit significantly from the addition of PFC11, where the TTN of this mutant was similar to that of the H171L mutant.

Table 5-3: TTN and selectivity data for the RL/YF series with and without PFC under 5 bar propane and 2 bar air. All data are given as mean ± S.D. for n ≥ 3.

	No PFC	**2-ol (%)**	**PFC**	**2-ol (%)**
WT	24 ± 9	95	6,160 ± 30 (PFC10)	95
RL/YF	1,130 ± 80	95	4,970 ± 50 (PFC11)	95
RL/YF/H171L	6,580 ± 70	93	7,330 ± 90 (PFC11)	93
RP	2,180 ± 280	96	2,960 ± 220 (PFC11)	96

5.4.4 The RT2 series

Both RL/YF and KT2 sets combined well with PFC for propane hydroxylation reactions under 5 bar propane pressure, and thus RT2 was tested with the decoy substrate. RT2 benefited from the addition of PFC, with the TTN increasing to 3,630 ± 170 with PFC10, but the activity was unexpectedly low compared to the precursors (Table 5-4). F81W was added to RT2, but the TTN of RT2/F81W was low even with the addition of PFC11. Another residue on the K-helix, Pro329, was targeted, and mutation to bulky tryptophan was introduced to close down the active site like A330P, but the RT2/P329W mutant showed dramatic loss of propane oxidation activity with and without PFC.

RT2/IP contains several key mutations (RL/YF, KT2 and I401P) and the effect of decoy molecules was investigated. The resulting TTN was low, with no significant improvement in propane oxidation activity with the addition of PFC11. Further mutations were performed between the two β4 strands, with the Leu437 residue being the target, but the RT2/L437S variant gave low TTNs with and without PFC.

Table 5-4: TTN and selectivity data for the RT2 series with and without PFC under 5 bar propane and 2 bar air. All data are given as mean ± S.D. for n ≥ 3.

	No PFC	**2-ol (%)**	**PFC**	**2-ol (%)**
WT	24 ± 9	95	6,160 ± 30 (PFC10)	95
KT2	1,260 ± 280	96	8,650 ± 110 (PFC11)	95
RT2	2,650 ± 120	96	3,630 ± 170 (PFC10)	95
RT2/F81W	300 ± 30	96	1,260 ± 40 (PFC11)	96
RT2/P329W	200 ± 8	95	110 ± 30 (PFC11)	96
RT2/IP	2,620 ± 60	96	2,860 ± 50 (PFC11)	96
RT2/L437S	26 ± 2	95	37 ± 9 (PFC11)	96

5.5 Rational design of variants using decoy molecules

Mutants that showed significant increase in propane oxidation with the incorporation of the decoy systems were combined and optimised in this work. N70S and M237L mutations are part of the 29E12 mutant, which reportedly gave 74% terminal oxidation of palmitic acid oxidation, and N70S and M237L mutants individually benefited up to 12-fold for propane oxidation from the addition of PFCs (**5.4.1**). These mutations were combined to make the N70S/M237L mutant, and this variant showed higher activity towards propane, giving TTN of 6,950 ± 160 with PFC11. The N70S/M237L mutant was also combined with the A328V

mutation, which is also within the 29E12 mutant, and the N70S/M237L/A328V (NMA) mutant showed 25% higher propane oxidation activity, with TTN of 8,630 ± 340. H171L, which matched the propane oxidation activity of NMA with PFC11, was also combined with NMA, but the activity of the N70S/M237L/A328V/H171L (NMAH) mutant with PFC11 was lower than both precursor mutants.

The R47L/Y51F couplet showed good activity with the addition of PFC11 (TTN of 4,970 ± 50), and thus this couplet was added to both the H171L and NMA mutants. The RL/YF/H171L mutant, however, gave lower expression levels (35 mg L^{-1}) with significant P420 formation, and the TTN did not significantly improve with the addition of PFC11. The RL/YF/NMA mutant showed high expression levels (150 mg L^{-1}), and the activity greatly improved with the addition of PFC11. The resulting TTN was 13,590 ± 30 under 5 bar propane pressure at ambient temperature, mirroring the highest TTN of 14,250 ± 1,370 by the KU4/AP mutant (see chapter 4). Addition of the activity enhancing mutation L188Q to RL/YF/NMA surprisingly led to poor expression levels of the enzyme. Incorporation of the H171L mutation to generate the RL/YF/NMAH mutant resulted in decreased propane oxidation activity as shown in Table 5-5, and no improvement with the decoy molecule was observed.

Table 5-5: TTN and selectivity data for various key mutants with and without PFC under 5 bar propane and 2 bar air. RL/YF/NMA = R47L/Y51F/N70S/M237L/A328V, RL/YF/NMAH = R47L/Y51F/N70S/M237L/A328V/H171L. –: not investigated. All data are given as mean ± S.D. for n ≥ 3. ‡Protein did not fold.

	No PFC	2-ol (%)	PFC	2-ol (%)
WT	24 ± 9	95	6,160 ± 30 (PFC10)	95
N70S	250 ± 20	96	3,150 ± 580 (PFC11)	95
H171L	1,300 ± 60	96	9,140 ± 440 (PFC11)	95
L188Q	890 ± 50	96	1,660 ± 7 (PFC11)	96
M237L	810 ± 160	96	3,760 ± 300 (PFC10)	95
A328V	860 ± 360	93	3,790 ± 230 (PFC11)	94
RL/YF	1,130 ± 80	95	4,970 ± 50 (PFC11)	95
N70S/M237L	490 ± 80	95	6,950 ± 160 (PFC11)	95
N70S/M237L/A328V (NMA)	4,950 ± 40	93	8,630 ± 340 (PFC11)	93
N70S/M237L/A328V/H171L (NMAH)	5,670 ± 490	92	6,160 ± 310 (PFC11)	92
RL/YF/NMA	4,920 ± 30	95	13,590 ± 30 (PFC11)	95
RL/YF/NMA/L188Q‡	–	–	–	–
RL/YF/H171L	6,580 ± 70	93	7,330 ± 90 (PFC11)	93
RL/YF/NMAH	3,800 ± 90	92	3,540 ± 270 (PFC11)	92

5.6 Optimisation of KU4/AP and RL/YF/NMA mutants

The effect of pressure alone was investigated in chapter 4, and a few variants (KU/AP, KU3/AP, and KU4/AP) showed high TTN of >13,000 under 5 bar propane pressure at ambient temperature, as well as high expression levels of over 150 mg mL^{-1}. The combination

of pressure, decoy systems and mutations led to the RL/YF/NMA mutant that showed similar propane oxidation activity with PFC11 of 13,590 ± 30, under the same conditions.

The results with A330P, RT2/AP, and E32 mutants described in chapter 4 showed performing reactions under 2 bar propane at 4 °C, and 15 bar ethane at 4 °C gave higher monooxygenase activity. Therefore TTN values were measured with KU4/AP and RL/YF/NMA mutants at different enzyme concentrations under these conditions, and the E32 mutant was also investigated as a benchmark. Four different enzyme concentrations (50 nM, 100 nM, 250 nM and 500 nM) and the control reaction, which contains no enzyme, were set up in the same Parr autoclave.

Similar TTN values were observed at different enzyme concentrations for propane oxidation, but the TTN dropped with increasing $P450_{BM3}$ concentration for ethane, with all three enzymes. Control reaction mixtures also contained up to 100 times higher (*ca.* 400 µM) 2-propanol and 1-proanol peaks than background for propane oxidation, and up to 3 times higher (*ca.* 45 µM) ethanol than background for ethane oxidation. Another set of reactions was therefore set up, where two reactions with each containing 0.5 µM KU4/AP, one containing just buffer, and another one containing 10 mM 2-propanol and buffer. The Parr autoclave was pressurised to 15 bar ethane at 4°C, and left stirred for 20 hours. All four mixtures were extracted, and GC analysis showed that both KU4/AP reaction mixtures and the buffer sample contained *ca.* 1 mM 2-propanol in each, and higher than background ethanol was detected in the vial containing the buffer only, and that with buffer and 10 mM 2-propanol. This indicated that vapour phase transfer of these light alcohols between vials was occurring even under 15 bar at 4 °C, and it was identified as the cause of significant decrease in TTN values with increasing enzyme concentration for the ethane oxidation. Ethanol is more volatile than 1- and 2-propanol, and lower concentrations of ethanol being produced

compared to propanol products meant that a small loss of ethanol led to a significant change in TTN.

Three reaction mixtures were prepared in the Parr autoclave, with each containing the same enzyme and the same concentration of 0.5 µM, to minimise the effect of phase transfer. TTN values of the E32 mutant thus determined were 6,270 ± 180 for propane oxidation, and 420 ± 40 for ethane oxidation. The KU4/AP mutant gave higher TTNs of 15,240 ± 150 and 1,010 ± 80, for propane and ethane, respectively. The highest activity was achieved by the RL/YF/NMA mutant with PFC11 as shown in Figure 5-10, where the TTN of 26,320 ± 1,010 was observed for propane oxidation. The ethane oxidation by the same mutant with PFC11 gave the TTN of 1,440 ± 70. Ratios of 1- and 2-propanol products remained the same for all three enzymes, and up to 4% (*ca.* 12 µM) acetaldehyde product was observed for the ethane oxidation by the RL/YF/NMA mutant.

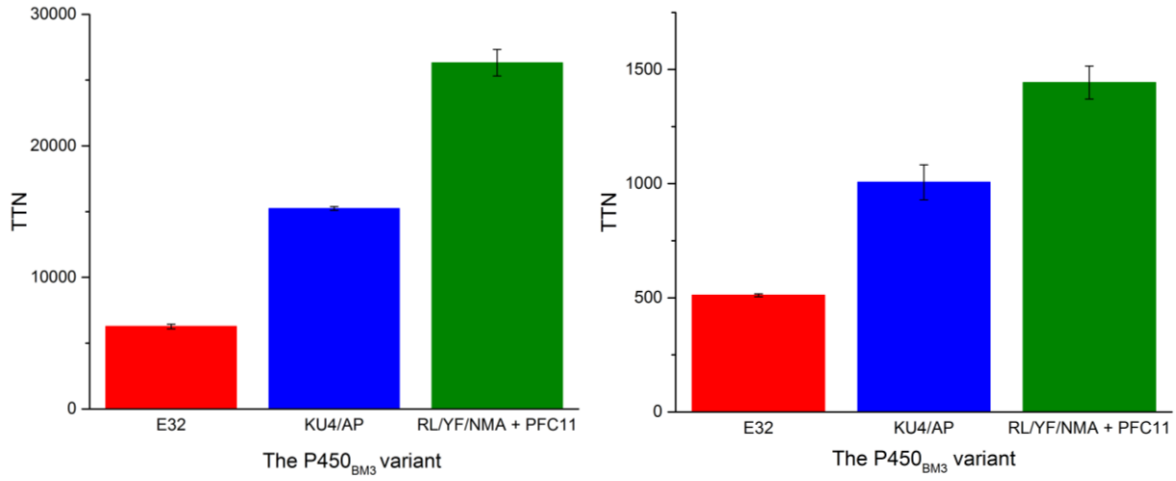

Figure 5-10: Comparison of propane and ethane oxidation TTNs of three different mutants under 2 bar propane (left) and 15 bar ethane (right), both at 4 °C, with [$P450_{BM3}$] = 0.5 µM.

5.7 Methane hydroxylation

Methane oxidations were performed using KU4/AP, and RL/YF/NMA with PFC11, with an enzyme concentration of 5 µM under 40 bar methane pressure at 4 °C. The reaction mixtures

were stirred in the Parr autoclave for 20 hours. No methanol above background was observed for both enzymes.

5.8 Summary

The idea of incorporating decoy substrates was to fill the empty pocket within the active site to constrain both propane and ethane to bind closer to the haem, without competing with substrates and inhibiting alkane oxidation reactions. A range of PFCs (PFC9 – 12) were tested, and the best PFC was selected for each variant to give maximum enzymatic activities.

The addition of PFC to WT significantly benefited the oxidation of both propane and ethane as previously reported by Watanabe and Reetz, and the ethanol peak was observed for the first time by WT in this work when decoy molecules were used under 8 bar ethane pressure. The initial test with the benchmark mutant, RT2/AP, which gave relatively high propane activity, with TTNs of 680 ± 10 and 10,900 ± 420 under atmospheric and 5 bar propane pressure, respectively, did not benefit from the addition of PFC. Indeed the TTN dropped to 5,770 ± 140 with the addition of PFC9 under 5 bar pressure.

Other variants were screened for propane oxidation under 5 bar propane partial pressure, and most mutants without the A330P mutation improved with the addition of PFC. RL/YF gave a four-fold increase when PFC11 was added, and the TTN of KT2 improved from 1,260 ± 280 to 8,650 ± 110. N70S, M237L and A328V mutants were screened with various PFCs, as the 29E12 variant containing these mutations reportedly favoured terminal oxidation of palmitic acid.[260] TTN values of these mutants with PFC decoys were >3,000. H171L is part of the KSK19 mutant, and the addition of PFC11 led to a high TTN of 9,140 ± 440. The KT2 set, and one of N70S, H171L, M237L and A328V mutations were thus combined but no significant increase in activities were observed. N70S, M237L, and A328V mutations were combined, and the resulting NMA mutant gave a TTN of 8,630 ± 340 with PFC11. The

addition of the H171L mutation did not improve the activity. The RL/YF couplet was combined with NMA and H171L, and the RL/YF/NMA mutant showed higher propane oxidation activity with PFC11 (TTN of 13,590 ± 30), whilst the RL/YF/H171L mutant showed a 20% drop in TTN compared to the H171L mutant with PFC11. No significant changes in selectivity were observed, with the exception of variants containing mutations at Ala328, which led to slightly more terminal oxidation with up to 8% 1-propanol product.

KU4/AP and the RL/YF/NMA mutant with PFC11 showed highest activities towards propane and ethane oxidations under mild pressure at ambient temperature, and thus these variants were directly compared with the E32 mutant at 4 °C. Propane oxidation reactions were performed under 2 bar propane pressure, and 15 bar ethane partial pressure was used for ethane oxidations. Vapour phase transfer of products was found to occur in the Parr autoclave, and thus three reactions of the same 0.5 μM enzyme was set up to determine TTN values of each mutants. KU4/AP and RL/YF/NMA with PFC11 both showed higher activities for propane and ethane oxidations than the E32 mutant. The highest TTNs of 26,320 ± 1,010 for propane and 1,440 ± 70 for ethane, were observed by the RL/YF/NMA mutant with PFC11. Methane oxidation was performed under 40 bar methane partial pressure at 4 °C for 20 hours with the enzyme concentration of 5 μM, but no methanol product above background was detected.

Chapter 6

Dihydrogen-driven NADPH regeneration system

6.1 Introduction

Hydrogen as a source of electrons offers a much cleaner system. A robust, oxygen-tolerant hydrogenase from *Ralstonia eutropha* is used to oxidise H_2 and the two electrons are used to reduce $NAD(P)^+$ by a diaphorase-like moiety to give NAD(P)H.[261–263] Most interestingly the two H^+ generated, when H_2-driven NAD(P)H regeneration is coupled to $P450_{BM3}$ monooxygenase activity, are also used by the $P450_{BM3}$ enzyme to activate O_2. In other words the coupled system is 100% atom-efficient for NAD(P)H recycling and the overall reaction is:

$$R–H + H_2 + O_2 \rightarrow R–OH + H_2O$$

The amination of ketones using the hydrogen driven NAD^+ regeneration system has been reported, with *R* and *S*-enantiomer of amines synthesised with up to >99% *ee* and 98% conversion.[264] Oda *et al.* reported that the selective reduction of hydroxyacetone to (*R*)-1,2-propanediol was possible using hydrogen and *R. eutropha* with NAD-dependent alcohol dehydrogenase from *Kluyveromyces lactis*.[265] The hydrogen-driven oxidation of octane to 1-octanol was also possible using P450 monooxygenase (CYP153A) in the recombinant *Pseudomonas putida* KT2440 cells.[266]

Trial H_2-driven reactions were carried out in collaboration with Dr. Holly Reeve. The initial work involved performing octane oxidation by $P450_{BM3}$ under atmospheric pressure at ambient temperature using soluble hydrogenase (SH) cofactor regeneration system. Hydrogen-driven propane oxidation was then performed under mild pressure at ambient temperature. The WT *R. eutropha* hydrogenase is specific to NAD^+/NADH but an engineered variant also accepts $NADP^+$ to regenerate NADPH.[267,268] Rational mutagenesis was performed on the HoxF homologue (see Figure 1-42), by introducing a new set of mutations

to modify the binding pocket size to accommodate the larger and more negatively charged $NADP^+$ cofactors. The E341A/S342R mutant was used for octane, and propane oxidation was performed using the E341A/D467S mutant.[269] The electrochemical analysis of the E341A/D467S mutant indicated that K_M of $NADP^+$ decreased from 8,300 µM to 300 µM compared to the WT,[268] i.e. lower $NADP^+$ concentration was required to reach the maximum activity of the SH enzyme.

6.2 Hydrogen-driven octane oxidation using soluble hydrogenase

Whitehouse *et al.* previously reported that the selectivity of octane oxidation can be changed with the addition of the A330P mutation. The WT gave equal amounts of 3- and 4-octanol, with 15% 2-octanol product. The A330P mutant, however, shifted the selectivity more towards the ω–1 position, with 53% 2-octanol product, and the 3-octanone peak was also observed (Table 6-1).[202]

Table 6-1: The data representing the difference in selectivity with WT and A330P towards octane under standard oxidation conditions reported by Whitehouse.[202]

	3-one (%)	**4-ol (%)**	**3-ol (%)**	**2-ol (%)**
WT	–	42	43	15
A330P	1	16	30	53

Three different reaction conditions were set up for each of the WT and the A330P mutant. The reaction mixture in the positive control contained 0.5 µM $P450_{BM3}$, hydrogen-saturated 100 mM KPi buffer, pH 7.4, 200 mM glucose, 10 U mL^{-1} GDH, 20 mg mL^{-1} catalase, 5 mM octane, and 320 µM $NADP^+$. The negative control contained the same components, except GDH and $NADP^+$. The full reaction mixture contained 100 µL of the NADP-dependent SH, with a $H_2 \rightarrow$ NADH activity of 0.001 µmol min^{-1} $(\mu L\text{-enzyme})^{-1}$, instead of glucose and GDH. Reactions were performed under 2% O_2 for two hours.

The negative control reaction gave a clean background on the GC as observed in Figure 6-1. The positive control reaction gave three expected products, with the same selectivity as reported by Whitehouse.[202] The reaction performed using SH similarly gave the same three products in the same product ratio (Table 6-2).

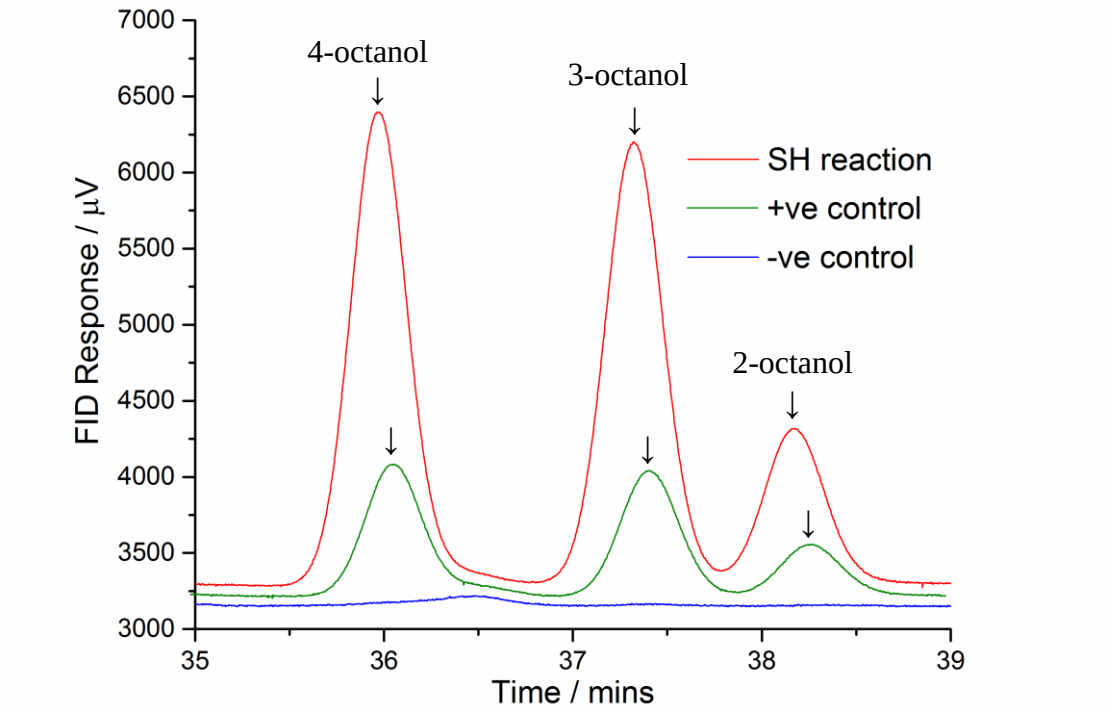

Figure 6-1: Comparison of octane oxidation reactions performed by WT $P450_{BM3}$ using soluble hydrogenase (red), glucose and GDH (green), and the background (blue).

Table 6-2: The data illustrating the similarity in selectivity with WT under hydrogen-driven oxidation and normal conditions. [a]The reaction was performed using glucose and GDH cofactor recycling system in this work. [b]The reaction was performed by Whitehouse using glucose and GDH cofactor recycling system.

	4-one (%)	3-one (%)	2-one (%)	4-ol (%)	3-ol (%)	2-ol (%)
SH reaction	–	–	–	44	41	15
Standard condition[a]	–	–	–	43	40	17
Standard condition[b]	–	–	–	42	43	15

Experiments were repeated with the A330P mutant, and five peaks were observed on the GC in both the SH and positive control reactions. This contradicted with four peaks observed by Whitehouse.[202] An extra product has been identified as 2-octanone, with 3% of the overall products formed (Table 6-3). The octane oxidation performed by Whitehouse was analysed by GC with a 7 m column, whereas octane oxidation performed in this work was analysed using the 60 m column, leading to a better separation of peaks, and thus the separation of 2-octanone product from 4-octanol was possible (Figure 6-2). The negative control again showed clean background.

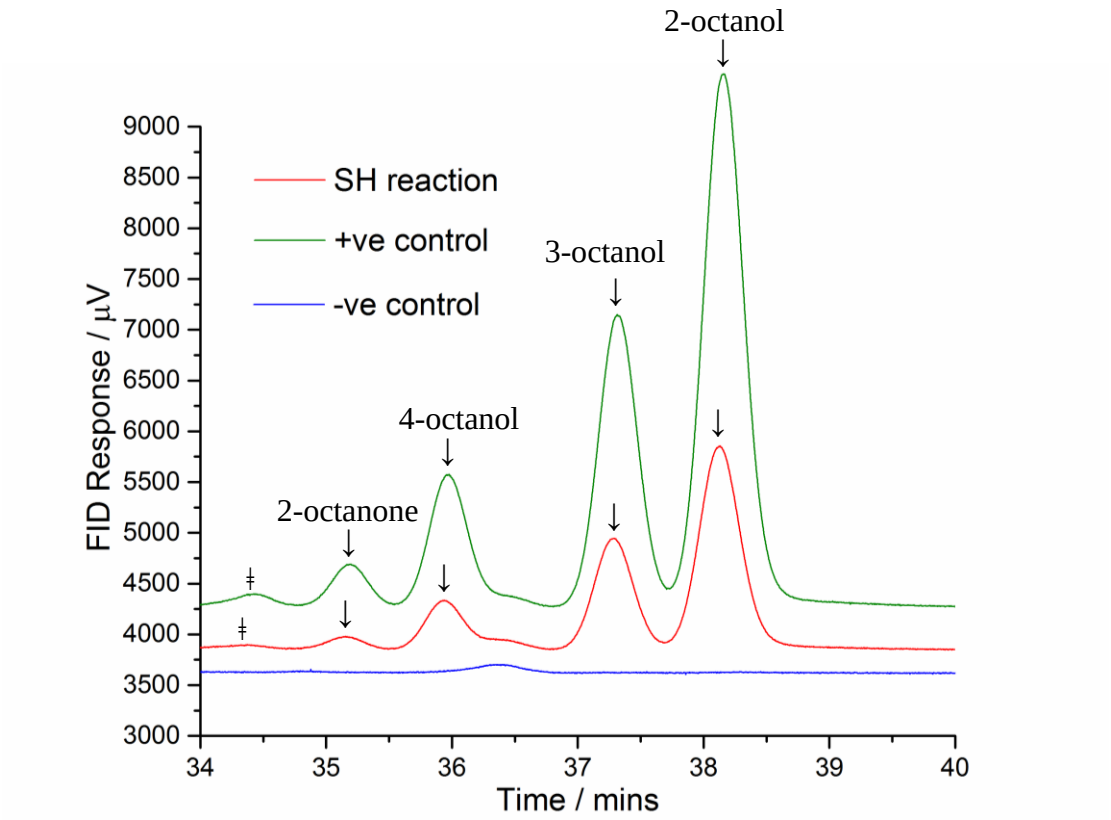

Figure 6-2: The product distribution of octane oxidation reaction performed by A330P $P450_{BM3}$ using soluble hydrogenase (red), glucose and GDH (green), and the background (blue). ǂdenotes the 3-octanone product.

Table 6-3: Product selectivity of the A330P mutant under hydrogen-driven oxidation and normal conditions. [a]The reaction was performed using glucose and GDH cofactor recycling system in this work. [b]The distribution reported by Whitehouse using glucose and GDH cofactor recycling system.

	4-one (%)	3-one (%)	2-one (%)	4-ol (%)	3-ol (%)	2-ol (%)
SH reaction	–	1	3	13	29	54
Standard condition[a]	–	1	3	13	29	54
Standard condition[b]	–	1	–	16	30	53

Hydrogen-driven octane oxidation was performed using WT $P450_{BM3}$ and the A330P mutant, and the same product distributions were observed as the glucose/GDH system for both enzymes. The use of longer column length in GC (from 7 m to 60 m) allowed the 2-octanone product peak to be separated from the 4-octanol product.

6.3 Hydrogen-driven propane oxidation using soluble hydrogenase

Propane oxidation was performed under 2 bar propane, 2 bar hydrogen and 0.5 bar air (2% oxygen). The propane, hydrogen, and oxygen ratio of 49 : 49 : 2 was chosen for safety reasons. Three reaction mixtures (positive control, negative control, SH) were prepared as described in **6.2**, except a different variant of SH, E341A/D467S was used, and no octane substrate was added. The $NADP^+$ concentration was also lowered to 320 µM to allow direct comparisons with other propane TTN values. The activity of E341A/D467S was similar to the E341A/S342R variant used in octane oxidation, with the $H_2 \rightarrow NADH$ activity of *ca.* 0.001 µmol min^{-1} $(\mu L\text{-enzyme})^{-1}$. The KU4/AP mutant, which showed high TTN of 14.250 ± 1,370 under partial propane pressure of 5 bar and 2 bar air at ambient temperature was chosen for this work.

The positive control reaction gave TTN of 6,480 ± 70 under 2 bar propane, 2 bar hydrogen and 0.5 bar air after 20 hours at ambient temperature. The SH reaction gave TTN of 990,

which was 6.5-fold lower than the reaction driven by the glucose/GDH cofactor recycling system. Nevertheless, 1- and 2-propanol concentrations of 20 µM and 480 µM, respectively, were formed using the hydrogen-driven cofactor recycling system for the first time (Figure 6-3).

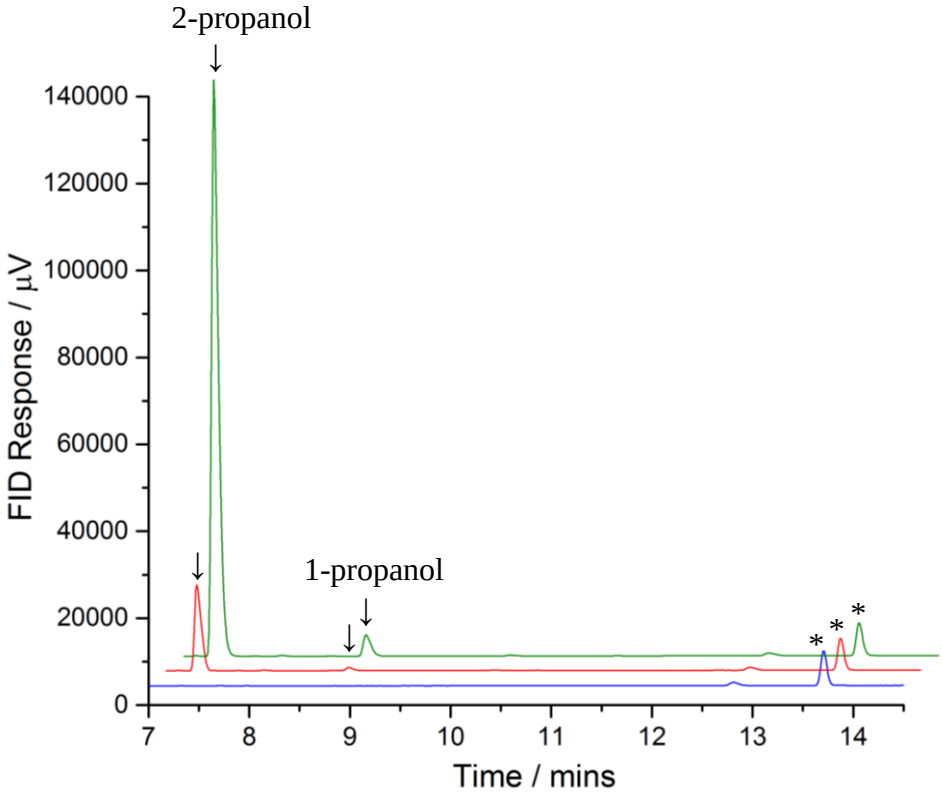

Figure 6-3: Comparison of propane oxidation reactions performed by the KU4/AP mutant $P450_{BM3}$ using soluble hydrogenase (red), glucose and GDH (green), and the background (blue). *denotes the 2-pentanone internal standard.

6.4 Conclusion

Octane and propane oxidations were performed using $P450_{BM3}$ monooxygenases and two different $NADP^+$ recycling SH variants. WT $P450_{BM3}$ and the A330P mutant were chosen for octane oxidation, and the E341A/S342R variant (SH) was used to drive $NADP^+$ recycling with the aid of hydrogen. The reaction was performed for two hours under 2% oxygen at ambient temperature. Both enzymes gave the expected products, with no changes in selectivity observed compared to the standard glucose/GDH cofactor recycling systems. WT gave 2-, 3- and 4-octanol products, and the A330P mutant gave the same three products, as

well as 2- and 3-octanone. Addition of the A330P mutation led to a selectivity shift, with more ω–1 product (from 15% to 53%) and further oxidation products being formed.

The KU4/AP mutant was selected for propane oxidation, as it showed high TTN of >14,000 under 5 bar propane pressure at ambient temperature using the standard glucose/GDH system. TTN of KU4/AP under 2 bar propane, 2 bar hydrogen and 0.5 bar air using the same cofactor recycling system after 20 hours at ambient temperature was 6,480 ± 70. The hydrogen-driven propane oxidation reaction was performed using the E341A/D467S (SH) variant under the same conditions, and the resulting TTN was 15% of the glucose/GDH system. The 1- and 2-propanol peaks, however, were significantly higher than the background (see Figure 6-3).

Further optimisations of reaction conditions are required for the hydrogen-driven system to reach the high TTN value observed in the glucose/GDH system. Work performed in this chapter, however, demonstrated that alkane oxidation reactions are possible without the need of a carbon source such as glucose. The use of higher partial propane and hydrogen pressure may improve the activity of the hydrogen-driven systems. Alternatively, the reaction can be performed at 4 °C to improve the aqueous propane and hydrogen saturation, although the activity of the SH at 4 °C is not yet known.

Chapter 7

Overview of the thesis

Main goals of this thesis were to perform protein engineering on $P450_{BM3}$ and alter reaction conditions to maximise hydrocarbon oxidation activities, and combining these with the hydrogen-driven cofactor regeneration system. The R47L/Y51F, KT2, I401P and A330P mutants previously showed higher activities for various substrates ('generic accelerator variants'), and these templates were used to build a library of mutants for butane, propane and ethane oxidation.

The KT2 set contains five mutations (A191T/N239H/I259V/A276T/L353I), and this was combined with the R47L/Y51F couplet and the A330P mutation. Higher propane oxidation activity was observed with the RT2/AP mutant than the WT, with the total 1- and 2-propanol product concentration increasing from none to 340 ± 5 μM (coupling = 25.7 ± 0.9%) under atmospheric pressure at ambient temperature. The R47L/Y51F, KT2 and RT2 mutants did not produce significant 1- and 2-propanol products above background under the same conditions.

The introduction of I401P to RT2/AP caused protein folding problems, and thus the I401M mutation was added. The resulting RT2/AP/I401M mutant showed low expression levels (6 mg L^{-1}) but high coupling of 62.0 ± 18.0% for propane. The TTN, however, was lower than the RT2/AP mutant, at 570 ± 50 (290 ± 30 μM total product). The yield of the R47L/Y51F/I401P/A330P (RP/AP) mutant was higher than the RT2/AP/I401M mutant with 20 mg L^{-1}, but TTN was 1.5-fold lower, at 350 ± 30.

New sets of mutations were introduced to residues around the active site and the substrate access channel to close down the substrate pocket to improve the substrate binding close to the haem. Mutations at Ala82 and Ala184 residues were introduced to RT2/AP and RP/AP variants, and high turnover rates were generally observed, with the RP/AP/A82M mutant showing 4,480 ± 100 min^{-1} for propane. These bulky amino acid substitutions around the

active site, however, led to non-productive alkane binding and reduced the propane oxidation TTN activity, with the TTN of RT2/AP/A82M being 3.5-fold lower than the RT2/AP mutant. No ethanol peak above background was detected with any of the mutants under atmospheric pressure.

Arnold *et al.* reported high oxidation activities with the application of 30 psi (*ca.* 2 bar) at 4 °C to improve alkane saturation in buffer, with the E32 mutant (A74W/V78I/A82L/A184V/L188W/A328F/A330W) reportedly giving TTN values of 16,800 and 1,200 for propane and ethane, respectively.[222] The application of mild pressure was investigated, and the total 1- and 2-propanol product concentration of 12 ± 5 μM was observed for the WT under 5 bar propane pressure at ambient temperature. The TTN of RT2/AP similarly improved by over 16-fold under the same conditions, reaching 10,900 ± 420. The effect of partial pressure and the total pressure was investigated with the RT2/AP mutant, and the partial pressure of alkanes was found to be more important over the total pressure in the reaction vessel.

Activities of the RT2/AP mutant were directly compared with the E32 mutant under various conditions. Best conditions were found to be under 2 bar propane pressure and 15 bar ethane pressure, both at 4 °C. The E32 mutant gave TTN values of 6,270 ± 180 for propane and 420 ± 40 for ethane under these conditions. The TTN values were lower than reported,[222] but this difference may be due to a calibration effect. The RT2/AP mutant gave higher TTN values of 13,170 ± 580 and 630 ± 50, for propane and ethane, respectively.

Other variants were screened for propane oxidation activities under 5 bar propane and 2 bar air at ambient temperature, and those variants with high TTN values were then tested for ethane oxidation activities under 8 bar ethane and 2 bar air. Further introductions of bulky amino acids at active site residues of the RT2/AP mutant unexpectedly reduced the activity,

with V26M, S72Y, A82M and A184I mutations lowering the TTN by up to 70%. RT2/AP/V26M and RT2/AP/S72Y variants also showed poor haem incorporation. The KT2/AP mutant gave a similar propane TTN to RT2/AP with 12,500 ± 1,980, and ethane TTN was higher than the RT2/AP mutant (600 ± 40 vs. 350 ± 30). The L353I mutation was thus removed from KT2 to see the effect on propane oxidation activity. The KU/AP variant (A191T/N239H/I259V/A276T/A330P) gave a TTN of 13,910 ± 100, indicating not all the KT2 mutations were required for improved propane oxidation. Both I259V and A330P mutations were identified to be crucial in achieving high propane oxidation activity, whilst the A276T mutation and one of A191T or N239H, were important. Introductions of other polar amino acids (e.g. serine and asparagine) and amino acids with positively charged side chains (e.g. histidine) at the Ala276 residue, may be of interest. The R47L/Y51F couplet and the L353I mutations did not improve in the KU/AP series (A191T/N239H/I259V/A276T/A330P) to achieve high propane oxidation activity. Highest propane oxidation TTN was observed by the KU4/AP mutant with 14,250 ± 1,370, and the KU3/AP mutant showed high ethane TTN of 920 ± 50.

The L188Q mutation was added to the A330P template, and propane TTN of 8,550 ± 460 was achieved under 5 bar propane at ambient temperature with just these two mutations. The A191T mutation, which is in the KT2 set, was added to A330P/L188Q, and TTN improved further to 13,590 ± 240 for propane oxidation, and TTN of 740 ± 50 was observed for ethane oxidation. The L188Q mutation was added to KU/AP, but no significant increase in propane oxidation activity was observed.

Watanabe *et al.* and Reetz *et al.* reported improved $C_1 – C_3$ alkane oxidation activities by WT $P450_{BM3}$ with the addition of PFC decoy molecules.[223,226,227,229] Structures of inert PFC decoys resemble those of natural substrates, allowing them to occupy and fill the active site, constraining smaller substrates such as alkane to bind closer to the haem. The addition of

PFC10 under 5 bar propane pressure led to TTN of 6,160 ± 30 by the WT, a greater than 250-fold increase under the same condition. The addition of PFC under 5 bar propane benefited most of the $P450_{BM3}$ variants, with the exception of A330P containing variants. The introduction of A330P shifted the adjacent Pro329 residue into the active site, which led to the access channel being too constricted for medium- to long-chain fatty acids (in this case PFCs) and abolishing their oxidation activities.[231] TTN of KT2 improved by almost seven-fold to 8,650 ± 100 with the addition of PFC11, and TTN of R47L/Y47F mutant increased from 1,130 ± 80 to 4,970 ± 50 with PFC11. Some single-mutation variants, such as N70S, H171L, M237L and A328V, showed significant propane oxidation activities, with TTN >3,000 with PFCs (the H171L mutant with PFC11 gave 9,140 ± 440), mirroring or higher than that of the A330P mutant without decoy systems. The H171L mutation was added to various variants, but higher propane oxidation was not observed with PFC. The N70S, M237L and A328V mutations were combined, and the N70S/M237L/A328V (NMA) mutant gave a TTN of 8,630 ± 340 with PFC11. The R47L/Y51F couplet was then added to NMA, and higher propane oxidation activity was observed, with TTN of 13,590 ± 30 under 5 bar propane at ambient temperature.

KU4/AP and the RL/YF/NMA mutant with PFC11 showed highest activities towards propane and ethane oxidations under mild pressure at ambient temperature, and thus these variants were tested at 4 °C to further improve the aqueous alkane saturation. The E32 mutant was investigated as the benchmark. Three reactions of the same 0.5 μM enzyme was set up in the Parr autoclave to minimise the effect of vapour phase transfer of products. Propane oxidation reactions were performed under 2 bar propane pressure, and 15 bar ethane partial pressure was used for ethane oxidations. KU4/AP, and the RL/YF/NMA with PFC11 both showed higher activities for propane and ethane oxidations than the E32 mutant, and the highest TTNs of 26,320 ± 1,010 for propane and 1,440 ± 70 for ethane were observed by the RL/YF/NMA

mutant with PFC11. Methane oxidation was performed under 40 bar methane partial pressure at 4 °C for 20 hours with the enzyme concentration of 5 μM, but no methanol product above background was observed.

NADPH is required to activate O_2 to insert an oxygen atom into a C–H bond. In biocatalytic applications the NADPH cofactor can be regenerated from $NADP^+$ by glucose and glucose dehydrogenase (GDH), but in this work, variants of oxygen-tolerant hydrogenase from *Ralstonia eutropha* was used to reduce $NADP^+$ to give NADPH. Octane and propane were chosen as test substrates. WT $P450_{BM3}$ and the A330P mutant were chosen for octane oxidation, and the E341A/S342R variant (SH) was used to drive $NADP^+$ recycling with the aid of hydrogen. Both variants gave the expected products, with no changes in selectivity observed compared to the standard glucose/GDH cofactor recycling system. Addition of the A330P mutation led to a selectivity shift, with more ω–1 product and further oxidation products formed compared to the WT. The KU4/AP mutant was selected for propane oxidation, and TTN of KU4/AP under 2 bar propane, 2 bar hydrogen and 0.5 bar air using the glucose/GDH cofactor recycling system after 20 hours at ambient temperature was 6,480 ± 70. The hydrogen-driven propane oxidation reaction was performed using the E341A/D467S (SH) variant under the same conditions, and 1- and 2-propanol products above background were observed (20 μM and 480 μM, respectively), though the resulting TTN was 15% of the glucose/GDH system.

Further engineering of $P450_{BM3}$, and optimising conditions will be required to tackle methane oxidation in future. The approach of adding decoy molecules to variants gave promising TTN values for both propane and ethane oxidation, without the need of introducing too many mutations that may disrupt protein folding. The use of pressure and lowering the temperature to improve aqueous alkane saturation, were effective at reaching higher enzymatic activities towards gaseous alkanes. The introduction of bulky amino acid around the active site was

ineffective at improving propane TTN, and a drastic change in the engineering approach may be necessary. An alternative approach may be to add an insertion mutation in the B′-helix, with V78AV, F87IF and T88IT being the suggestions, as these mutations will cause major changes in conformation around the haem. One or two mutations within the KT2 set (A191T, N239H, I259V, A276T, L353I) could be added to the RL/YF/NMA mutant to see the effect on its activity. Alternatively, different amino acids can be introduced at positions Arg47, Tyr51, Asn70, Met237 and Ala328 to potentially further improve the activity in combination with PFC decoy molecules. The 'second generation decoy molecules' approach by Watanabe may also be of interest.[229]

Appendix 1: Sequencing primers

BM3PF2: CTG CAG CGA GCA AAT CCA GAC GAC

HD647: GTC GAC AGC GCC GCG GAT ATG CCG

The role of T7F primer was to bind with the T7 promoter sequence in the vector. The role of BM3FP2 primer was to bind with the DNA sequence responsible for coding amino acid residues 188 – 195. The role of HD647 primer was to bind with the DNA sequence responsible for coding amino acid residues 647 – 654.

Appendix 2: Mutagenesis primers

V26M

Fwd: CCGTTATTAAACACAGATAAACCGATGCAAGCTTTGATGAAAATTGCG

Rev: GGCAATAATTTGTGTCTATTTGGCTACGTTCGAAACTACTTTTAACGC

R47L/Y51F

Fwd: CGAGGCGCCTGGTTTAGTAACGCGCTTTTTATCAAG

Rev: CGCTGACTTGATAAAAAGCGCGTTACTAAACCAGGCGC

N70S

Fwd: CACGCTTTGATAAAAGCTTAAGTCAAGCGC

Rev: GACTTAAGCTTTTATCAAAGCGTGATTCATCGC

S72A

Fwd: CACGCTTTGATAAAAACTTAGCTCAAGCGCTTAAATTTGTACG

Rev: CGTACAAATTTAAGCGCTTGAGCTAAGTTTTTATCAAAGCGTG

S72L

Fwd: CACGCTTTGATAAAAACTTACTTCAAGCGCTTAAATTTGTACG

Rev: CGTACAAATTTAAGCGCTTGAAGTAAGTTTTTATCAAAGCGTG

S72Y

Fwd: CACGCTTTGATAAAAACTTATATCAAGCGCTTAAATTTGTACG

Rev: CGTACAAATTTAAGCGCTTGATATAAGTTTTTATCAAAGCGTG

A74G

Fwd: GATAAAAACTTAAGTCAAGGGCTTAAATTTGTACG

Rev: CGTACAAATTTAAGCCCTTGACTTAAGTTTTTATC

A74W

Fwd: GATAAAAACTTAAGTCAATGGCTTAAATTTGTACGTG

Rev: CACGTACAAATTTAAGCCATTGACTTAAGTTTTTATC

A74V/V78I/A82L

Fwd: CGTGATTTTCTAGGAGACGGGTTATTTACAAGCTG

Rev: AAAATCACGTATAAATTTAAGCCATTGACTTAAGTTTTTATCAAAGCGTG

L75Q

Fwd: GTCAAGCGCAAAAATTTGTACGTGATTTTGC

Rev: CGTACAAATTTTTGCGCTTGACTTAAGTTTTTATC

V78I

Fwd: CAAGCGCTTAAATTTATACGTGATTTTGC

Rev: GCAAAATCACGTATAAATTTAAGCGCTTG

F81W

Fwd: GTACGTGATTGGGCAGGAGACGGGTTATTTACAAGCTGGACG

Rev: CCCGTCTCCTGCCCAATCACGTACAAATTTAAGCGCTTG

A82G

Fwd: GTACGTGATTTTGGAGGAGACGGGTTATTTACAAGCTGGACG

Rev: CCCGTCTCCTCCAAAATCACGTACAAATTTAAGCGCTTG

A82L

Fwd: GTACGTGATTTTTTAGGAGACGGGTTATTTACAAGCTGGACG

Rev: CCCGTCTCCTAAAAAATCACGTACAAATTTAAGCGCTTG

A82M

Fwd: GTACGTGATTTTATGGGAGACGGGTTATTTACAAGCTGGACG

Rev: CCCGTCTCCCATAAAATCACGTACAAATTTAAGCGCTTG

F87V

Fwd: GAGACGGGTTAGTTACAAGCTGG

Rev: GTCCAGCTTGTAACTAACCCGTC

F87W

Fwd: GAGACGGGTTATGGACAAGCTGG

Rev: GTCCAGCTTGTCCATAACCCGTC

T88H

Fwd: GAGACGGGTTATTTCATAGCTGGACG

Rev: CATGCGTCCAGCTATGAAATAACCCG

H171L

Fwd: CCGAGATCAGCCTCTTCCATTTATTACAAGTATG

Rev: GTAATAAATGGAAGAGGCTGATCTCGGTAAAAGC

A184I

Fwd: CGTGCACTGGATGAAATAATGAACAAGCTGCAGC

Rev: GCTGCAGCTTGTTCATTATTTCATCCAGTGCACG

A184V/L188W

Fwd: ATGAACAAGTGGCAGCGAGCAAATCCAGAC

Rev: CTTGTTCATTACTTCATCCAGTGCACGGACC

M185K

Fwd: GTGCACTGGATGAAGCAAAGAACAAGCTGCAGCGAG

Rev: CAGCTTGTTCTTTGCTTCATCCAGTGCACGGACCATAC

L188Q

Fwd: GAAGCAATGAACAAGCAGCAGCGAGCAAATCCAGACGACCCAG

Rev: CTGGATTTGCTCGCTGCTGCTTGTTCATTGC

L188Q/A191T

Fwd: GAAGCAATGAACAAGCAGCAGCGAACAAATCC

Rev: CTGGATTTGTTCGCTGCTGCTTGTTCATTGC

L188W

Fwd: GAAGCAATGAACAAGTGGCAGCGAGCAAATCCAGACGACCCAG

Rev: CTGGATTTGCTCGCTGCCACTTGTTCATTGC

A191T

Fwd: CAAGCTGCAGCGAACAAATCCAGACGAC

Rev: GCTGGGTCGTCTGGTGTTCGCTG

T191A

Fwd: CTGCAGCGAGCAAATCCAGACGAC

Rev: GATTTGCTCGCTGCAGCTTGTTCATTGC

M237L

Fwd: CGCATCTGCTAAACGGAAAAGATCCAG

Rev: CCGTTTAGCAGATGCGTTAATAAATCATCGC

H239N

Fwd: GCTAAACGGAAAAGATCCAGAAACGGGTG

Rev: GGATCTTTTCCGTTTAGCATATGCGTTAATAAATCATC

N239H

Fwd: ACGCATATGCTACACGGAAAAGATCCAGAAACG

Rev: TGGATCTTTTCCGTGTAGCATATGCGTTAATAAATCATCGC

I259V

Fwd: CGCTATCAAATTGTTACATTCTTAATTGCGGGACACG

Rev: CAATTAAGAATGTAACAATTTGATAGCGAATGTTCTCGTCATCAAG

V259I

Fwd: CGCTATCAAATTATTACATTCTTAATTGCGGGA

Rev: GAATGTAATAATTTGATAGCGAATGTTCTCGTC

I259A

Fwd: CAAATTGCTACATTCTTAGATGCGGGACACG

Rev: CAATTAAGAATGTAGCAATTTGATAGCGAATGTTCTCG

I259V/T260L

Fwd: CGCTATCAAATTGTTCTATTCTTAATTGCGGG

Rev: CAATTAAGAATAGAACAATTTGATAGCGAATGTTCTC

I259V/A264V

Fwd: CAAATTGTTACATTCTTAATTGTGGGACACGAAAC

Rev: CGTGTCCCACAATTAAGAATGTAACAATTTGATAG

A264G

Fwd: CAAATTGTTACATTCTTAATTGGGGGACACGAAAC

Rev: CGTGTCCCCCAATTAAGAATGTAATAATTTGATAG

A264V

Fwd: CAAATTGTTACATTCTTAATTGTGGGACACGAAAC

Rev: CGTGTCCCACAATTAAGAATGTAATAATTTGATAG

E267F

Fwd: CTTAATTGCGGGACACTTTACAACAAGTG

Rev: GATAAAAGACCACTTGTAAAGTGTCCCG

A276T

Fwd: GGTCTTTTATCATTTACGCTGTATTTCTTAGTGAAAAATCCA

Rev: CACTAAGAAATACAGCGTAAATGATAAAAGACCACTTGA

T276A

Fwd: CTTTTATCATTTGCGCTGTATTTCTTAGTGAAAAATCCAC

Rev: CTAAGAAATACAGCGCAAATGATAAAAGACCACTTG

Q307H

Fwd: GTTCCAAGCTACAAACATGTCAAACAGCTTAAATATGTCGGC

Rev: CATATTTAAGCTGTTTGACATGTTTGTAGCTTGGAACAGGATC

N319Y

Fwd: GGCATGGTCTTATACGAAGCGCTGCGCTTATGGC

Rev: CGCAGCGCTTCGTATAAGACCATGCCGACATATTTAAG

A328F

Fwd: CTTATGGCCAACTTTTCCTGCGTTTTCC

Rev: GCATATAGGGAAAACGCAGGAAAAGTTGG

A328F/A330P

Fwd: TGGCCAACTTTTCCTCCGTTTTCCCTATATGCAAAAGAAGATACGG

Rev: ATATAGGGAAAACGGAGGAAAAGTTGGCCATAAGCGCAG

A328F/A330W

Fwd: TGGCCAACTTTTCCTTGGTTTTCCCTATATG

Rev: GGAAAACCAAGGAAAAGTTGGCCATAAGC

A328I

Fwd: CTTATGGCCAACTATTCCTGCGTTTTCC

Rev: GCATATAGGGAAAACGCAGGAATAGTTGG

A328V

Fwd: CTTATGGCCAACTGTTCCTGCGTTTTCC

Rev: GCATATAGGGAAAACGCAGGAACAGTTGG

P329V/A330P

Fwd: CTTATGGCCAACTGCTGTTCCGTTTTCC

Rev: GCATATAGGGAAAACGGAACAGCAGTTGG

P329W

Fwd: CAACTGCTTGGGCGTTTTCCCTATATGC

Rev: GAAAACGCCCAAGCAGTTGGCCATAAG

A330P

Fwd: CTTATGGCCAACTGCTCCTCCGTTTTCC

Rev: GCATATAGGGAAAACGGAGGAGCAGTTGG

A330W

Fwd: CCAACTGCTCCTTGGTTTTCCCTATATGCAAAAGAAGATACG

Rev: GCATATAGGGAAAACCAAGGAGCAGTTGGCCATAAGCGCAGCGCTTCG

I353L

Fwd: GAAAAAGGCGACGAACTAATGGTTCTGATTCCTCAGCTTCACCG

Rev: CAGAACCATTAGTTCGTCGCCTTTTTCTAAAGGATATTCTCCTCCAAGCAC

L353I

Fwd: GAAAAAGGCGACGAAATAATGGTTCTGATTCCTCAGCTTCACCG

Rev: CAGAACCATTATTTCGTCGCCTTTTTCTAAAGGATATTCTCCTCCAAGCAC

K391N

Fwd: GCAGCATGCGTTTAATCCGTTTGGAAAC

Rev: CTGACCGTTTCCAAACGGATTAAACGC

I401M

Fwd: GCGTGTATGGGTCAGCAGTTCGCTCTTC

Rev: CTGACCCATACACGCACGCTGACCGTTTC

I401P

Fwd: GCGTGTCCCGGTCAGCAGTTCGCTCTTC

Rev: CTGACCGGGACACGCACGCTGACCGTTTC

G402P

Fwd: GCGTGTATCCCTCAGCAGTTCG

Rev: CTGCTGAGGGATACACGCACG

Q403P

Fwd: GCGTGTATCGGTCCGCAGTTCGCTCTTCATGAAGCAACG

Rev: CTGACCGATACACGCACGCTGCGGGTTTCCAAACGG

L437LV

Fwd: GGATATTAAAGAAACTTTAGTTACGTTAAAACCTGAAGGC

Rev: GGTTTTAACGTAACTAAAGTTTCTTTAATATCCAGCTCG

L437S

Fwd: GGATATTAAAGAAACTAGTACGTTAAAACCTGAAGGCTTTG

Rev: GGTTTTAACGTACTAGTTTCTTTAATATCCAGCTCGTAG

T438F

Fwd: CTTTATTTTTAAAACCTGAAGGCTTTGTGGTAAAAGC

Rev:GGTTTTAAAAATAAAGTTTCTTTAATATCCAGCTCGTAG

T438L

Fwd: GATATTAAAGAAACTTTATTGTTAAAACCTGAAGG

Rev: CCTTCAGGTTTTAACAATAAAGTTTCTTTAATATC

T438P

Fwd: GAAACTTTACCGTTAAAACCTGAAGGCTTTG

Rev: GGTTTTAACGGTAAAGTTTCTTTAATATCCAGCTC

T438V

Fwd: GAAACTTTAGTGTTAAAACCTGAAGGCTTTGTG

Rev: GGTTTTAACACTAAAGTTTCTTTAATATCCAGCTCG

K440L

Fwd: CTTTAACGTTATTACCTGAAGGCTTTGTGGTAAAAG

Rev: CTTCAGGTAATAACGTTAAAGTTTCTTTAATATCCAGCTC

G443A

Fwd: AAACCTGAAGCCTTTGTGGTAAAAGCAAAATCGAAAAAAA

Rev: TTCAGGTTTTAACGTTAAAGTTTCTTTAATATCCAGCT

Appendix 3: List of amino acids

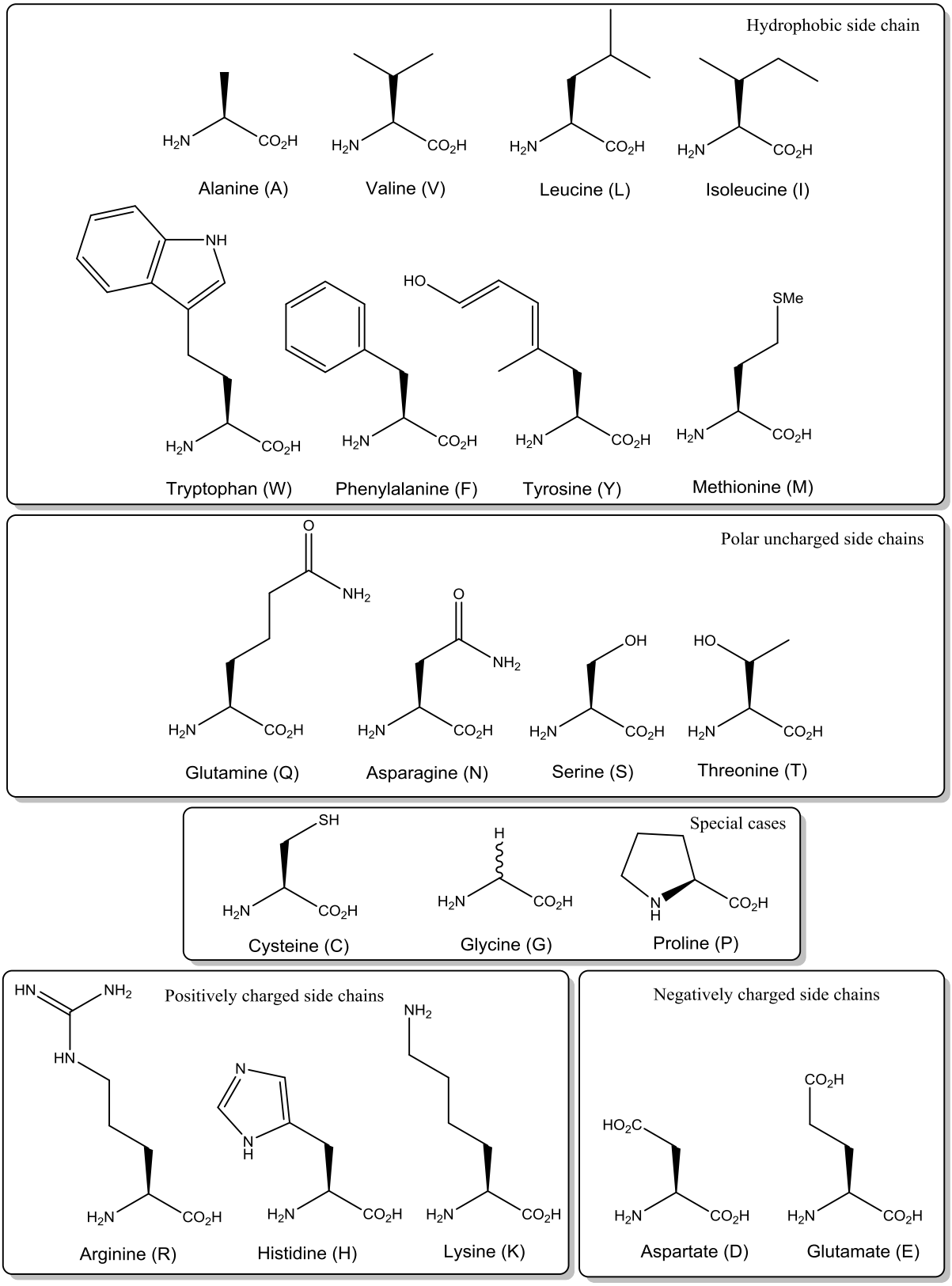

References

1 N. R. C. (US) C. SciencesRoundtable, *Increasing Efficiencies for Hydrocarbon Activation*, National Academies Press (US), 2001.
2 J. Goldemberg, *Biotechnol. Biofuels*, 2008, **1**, 6.
3 C. Schubert, *Nat. Biotechnol.*, 2006, **24**, 777–784.
4 A. Demirbas, *Prog. Energy Combust. Sci.*, 2007, **33**, 1–18.
5 E. C. Petrou and C. P. Pappis, *Energy Fuels*, 2009, **23**, 1055–1066.
6 F. O. Ajibola, M. O. Edema and O. B. Oyewole, *Niger. Food J.*, 2012, **30**, 114–121.
7 H. Shigechi, J. Koh, Y. Fujita, T. Matsumoto, Y. Bito, M. Ueda, E. Satoh, H. Fukuda and A. Kondo, *Appl. Environ. Microbiol.*, 2004, **70**, 5037–5040.
8 A. Melis, M. Seibert and M. L. Ghirardi, *Adv. Exp. Med. Biol.*, 2007, **616**, 110–121.
9 K. Hirose, *Faraday Discuss.*, 2011, **151**, 11–18; discussion 95–115.
10 M. Z. Jacobson, W. G. Colella and D. M. Golden, *Science*, 2005, **308**, 1901–1905.
11 K. Ledjeff, *Int. J. Hydrog. Energy*, 1990, **15**, 629–633.
12 M. Fischer, *Int. J. Hydrog. Energy*, 1986, **11**, 495–501.
13 A. Züttel, *Naturwissenschaften*, 2004, **91**, 157–172.
14 A. Yilanci, I. Dincer and H. K. Ozturk, *Prog. Energy Combust. Sci.*, 2009, **35**, 231–244.
15 Y. Bang, S. Park, S. J. Han, J. Yoo, J. H. Choi, T. H. Kang, J. Lee and I. K. Song, *J. Nanosci. Nanotechnol.*, 2016, **16**, 4605–4611.
16 C. Koroneos, A. Dompros, G. Roumbas and N. Moussiopoulos, *Resour. Conserv. Recycl.*, 2005, **44**, 99–113.
17 R. G. Miller and S. R. Sorrell, *Philos. Transact. A Math. Phys. Eng. Sci.*, 2014, **372**.
18 M. Asadullah, S. Ito, K. Kunimori, M. Yamada and K. Tomishige, *Environ. Sci. Technol.*, 2002, **36**, 4476–4481.
19 M. H. Park, B. K. Choi, Y. H. Park, D. J. Moon, N. C. Park and Y. C. Kim, *J. Nanosci. Nanotechnol.*, 2015, **15**, 5255–5258.
20 P. Jaramillo, W. M. Griffin and H. S. Matthews, *Environ. Sci. Technol.*, 2008, **42**, 7559–7565.
21 C. D. Chang, *Catal. Rev.*, 1983, **25**, 1–118.
22 G. A. Ferguson, L. Cheng, L. Bu, S. Kim, D. J. Robichaud, M. R. Nimlos, L. A. Curtiss and G. T. Beckham, *J. Phys. Chem. A*, 2015, **119**, 11397–11405.
23 Y. Takamitsu, K. Yamamoto, S. Yoshida, H. Ogawa and T. Sano, *J. Porous Mater.*, 2014, **21**, 433–440.
24 M. M. Forde, R. D. Armstrong, R. McVicker, P. P. Wells, N. Dimitratos, Q. He, L. Lu, R. L. Jenkins, C. Hammond, J. A. Lopez-Sanchez, C. J. Kiely and G. J. Hutchings, *Chem. Sci.*, 2014, **5**, 3603–3616.
25 J. A. Labinger and J. E. Bercaw, *Nature*, 2002, **417**, 507–514.
26 C.-T. Wu, K. M. K. Yu, F. Liao, N. Young, P. Nellist, A. Dent, A. Kroner and S. C. E. Tsang, *Nat. Commun.*, 2012, **3**, 1050.
27 A. Conde, L. Vilella, D. Balcells, M. M. Díaz-Requejo, A. Lledós and P. J. Pérez, *J. Am. Chem. Soc.*, 2013, **135**, 3887–3896.
28 F.-Y. Liang, M. Ryvak, S. Sayeed and N. Zhao, *Chem. Cent. J.*, 2012, **6**, S4.
29 R. W. Howarth, *Energy Sci. Eng.*, 2014, **2**, 47–60.
30 R. S. Hanson and T. E. Hanson, *Microbiol. Rev.*, 1996, **60**, 439–471.
31 M. J. Prather, *Geophys. Res. Lett.*, 1994, **21**, 801–804.
32 J. Lelieveld, F. J. Dentener, W. Peters and M. C. Krol, *Atmos Chem Phys*, 2004, **4**, 2337–2344.
33 J. Lelieveld, P. J. Crutzen and C. Brühl, *Chemosphere*, 1993, **26**, 739–768.

34 S. Prasad, A. Singh and H. C. Joshi, *Resour. Conserv. Recycl.*, 2007, **50**, 1–39.
35 L. Soobramoney, M. D. Bala and H. B. Friedrich, *Dalton Trans. Camb. Engl. 2003*, 2014, **43**, 15968–15978.
36 J. M. Thomas, R. Raja, G. Sankar and R. G. Bell, *Nature*, 1999, **398**, 227–230.
37 M. K. Akhtar, H. Dandapani, K. Thiel and P. R. Jones, *Metab. Eng. Commun.*, 2015, **2**, 1–5.
38 D. Haubenberger, F. Nahab, C. Toro, L. Wittevrongel, C. Lungu, M. Hallett and J. A. McLane, *Neurotherapeutics*, 2009, **6**, 605.
39 Z. Gu, B. A. Glatz and C. E. Glatz, *Biotechnol. Bioeng.*, 1998, **57**, 454–461.
40 T. A. Heming and D. J. Randall, *J. Exp. Zool.*, 1982, **219**, 125–128.
41 H. J. H. Fenton, *J. Chem. Soc. Trans.*, 1894, **65**, 899–910.
42 J. Kiwi, A. Lopez and V. Nadtochenko, *Environ. Sci. Technol.*, 2000, **34**, 2162–2168.
43 M. Strlic, J. Kolar, V. S. Selih, D. Kocar and B. Pihlar, *ACTA CHIM SLOV*, 2003, **50**, 619–632.
44 H. Hansson, F. Kaczala, M. Marques, W. Hogland, H. Hansson, F. Kaczala, M. Marques and W. Hogland, *Int. J. Photoenergy Int. J. Photoenergy*, 2012, **2012, 2012**, e531076.
45 G. J. P. Britovsek, J. England and A. J. P. White, *Inorg. Chem.*, 2005, **44**, 8125–8134.
46 C. Espro, S. Marini, F. Mendolia, F. Frusteri and A. Parmaliana, *Catal. Today*, 2009, **141**, 306–310.
47 G. Centi and F. Trifiró, *New Developments in Selective Oxidation*, Elsevier, 1990.
48 J. W. Morzycki and A. Sobkowiak, *Beilstein J. Org. Chem.*, 2015, **11**, 392–402.
49 G. Balavoine, D. H. R. Barton, J. Boivin, A. Gref, N. Ozbalik and H. Rivière, *Tetrahedron Lett.*, 1986, **27**, 2849–2852.
50 L. I. Simándi, *Catalytic Activation of Dioxygen by Metal Complexes*, Springer Science & Business Media, 2012.
51 D. H. Barton, E. Csuhai, D. Doller, N. Ozbalik and G. Balavoine, *Proc. Natl. Acad. Sci. U. S. A.*, 1990, **87**, 3401–3404.
52 N. F. Gol'dshleger and A. A. Shteinman, *React. Kinet. Catal. Lett.*, **6**, 43–50.
53 M. Lersch and M. Tilset, *Chem. Rev.*, 2005, **105**, 2471–2526.
54 C. I. Herrerías, X. Yao, Z. Li and C.-J. Li, *Chem. Rev.*, 2007, **107**, 2546–2562.
55 A. E. Shilov and G. B. Shul'pin, *Chem. Rev.*, 1997, **97**, 2879–2932.
56 L. Que and W. B. Tolman, *Nature*, 2008, **455**, 333–340.
57 T. Mouri, J. Michizoe, H. Ichinose, N. Kamiya and M. Goto, *Appl. Microbiol. Biotechnol.*, 2006, **72**, 514–520.
58 M. Kok, R. Oldenhuis, M. P. van der Linden, P. Raatjes, J. Kingma, P. H. van Lelyveld and B. Witholt, *J. Biol. Chem.*, 1989, **264**, 5435–5441.
59 J. A. Peterson, D. Basu and M. J. Coon, *J. Biol. Chem.*, 1966, **241**, 5162–5164.
60 G. Eggink, H. Engel, W. G. Meijer, J. Otten, J. Kingma and B. Witholt, *J. Biol. Chem.*, 1988, **263**, 13400–13405.
61 M. Suzuki, T. Hayakawa, J. P. Shaw, M. Rekik and S. Harayama, *J. Bacteriol.*, 1991, **173**, 1690–1695.
62 R. T. Ruettinger, S. T. Olson, R. F. Boyer and M. J. Coon, *Biochem. Biophys. Res. Commun.*, 1974, **57**, 1011–1017.
63 Q. Chen, D. B. Janssen and B. Witholt, *J. Bacteriol.*, 1996, **178**, 5508–5512.
64 I. E. Staijen, J. B. van Beilen and B. Witholt, *Eur. J. Biochem.*, 2000, **267**, 1957–1965.
65 M. Nieder and J. Shapiro, *J. Bacteriol.*, 1975, **122**, 93–98.
66 J. B. van Beilen, T. H. M. Smits, F. F. Roos, T. Brunner, S. B. Balada, M. Röthlisberger and B. Witholt, *J. Bacteriol.*, 2005, **187**, 85–91.
67 J. B. van Beilen, D. Penninga and B. Witholt, *J. Biol. Chem.*, 1992, **267**, 9194–9201.

68 H. Kataoka and M. Sekiguchi, *Mol. Gen. Genet. MGG*, 1985, **198**, 263–269.
69 S. S. Boddupalli, B. C. Pramanik, C. A. Slaughter, R. W. Estabrook and J. A. Peterson, *Arch. Biochem. Biophys.*, 1992, **292**, 20–28.
70 J. B. van Beilen, J. Kingma and B. Witholt, *Enzyme Microb. Technol.*, 1994, **16**, 904–911.
71 A. Glieder, E. T. Farinas and F. H. Arnold, *Nat. Biotechnol.*, 2002, **20**, 1135–1139.
72 J. Shanklin, C. Achim, H. Schmidt, B. G. Fox and E. Münck, *Proc. Natl. Acad. Sci. U. S. A.*, 1997, **94**, 2981–2986.
73 E. L. Johnson and M. R. Hyman, *Appl. Environ. Microbiol.*, 2006, **72**, 950–952.
74 H. Dalton, *Philos. Trans. R. Soc. Lond. B. Biol. Sci.*, 2005, **360**, 1207–1222.
75 J. G. Leahy, P. J. Batchelor and S. M. Morcomb, *FEMS Microbiol. Rev.*, 2003, **27**, 449–479.
76 A. Miuran and H. Dalton, *Biosci. Biotechnol. Biochem.*, 1995, **59**, 853–859.
77 J. Lund, M. P. Woodland and H. Dalton, *Eur. J. Biochem.*, 1985, **147**, 297–305.
78 J. Colby and H. Dalton, *Biochem. J.*, 1978, **171**, 461–468.
79 B. G. Fox, W. A. Froland, J. E. Dege and J. D. Lipscomb, *J. Biol. Chem.*, 1989, **264**, 10023–10033.
80 T. J. Smith and J. C. Murrell, *Methods Enzymol.*, 2011, **495**, 135–147.
81 B. Wilkinson, M. Zhu, N. D. Priestley, H.-H. T. Nguyen, H. Morimoto, P. G. Williams, S. I. Chan and H. G. Floss, *J. Am. Chem. Soc.*, 1996, **118**, 921–922.
82 S.-P. Huang, Y. Shiota and K. Yoshizawa, *Dalton Trans. Camb. Engl. 2003*, 2013, **42**, 1011–1023.
83 S. D. PRIOR and H. DALTON, *Microbiology*, 1985, **131**, 155–163.
84 R. L. Lieberman and A. C. Rosenzweig, *Nature*, 2005, **434**, 177–182.
85 S. Stolyar, A. M. Costello, T. L. Peeples and M. E. Lidstrom, *Microbiol. Read. Engl.*, 1999, **145 (Pt 5)**, 1235–1244.
86 J. D. Semrau, A. Chistoserdov, J. Lebron, A. Costello, J. Davagnino, E. Kenna, A. J. Holmes, R. Finch, J. C. Murrell and M. E. Lidstrom, *J. Bacteriol.*, 1995, **177**, 3071–3079.
87 T. J. Lawton, J. Ham, T. Sun and A. C. Rosenzweig, *Proteins*, 2014, **82**, 2263–2267.
88 M. Takeguchi and I. Okura, *Catal. Surv. Jpn.*, **4**, 51–63.
89 M. A. Correia, P. R. Sinclair and F. De Matteis, *Drug Metab. Rev.*, 2011, **43**, 1–26.
90 V. B. Urlacher and M. Girhard, *Trends Biotechnol.*, 2012, **30**, 26–36.
91 T. Omura and R. Sato, *J. Biol. Chem.*, 1962, **237**, PC1375–PC1376.
92 R. H. Wickramasinghe and C. A. Villee, *Nature*, 1975, **256**, 509–511.
93 P. B. Danielson, *Curr. Drug Metab.*, 2002, **3**, 561–597.
94 F. P. Guengerich and Q. Cheng, *Pharmacol. Rev.*, 2011, **63**, 684–699.
95 I. C. Gunsalus and G. C. Wagner, *Methods Enzymol.*, 1978, **52**, 166–188.
96 B. P. Unger, I. C. Gunsalus and S. G. Sligar, *J. Biol. Chem.*, 1986, **261**, 1158–1163.
97 I. Sevrioukova, G. Truan and J. A. Peterson, *Biochemistry (Mosc.)*, 1996, **35**, 7528–7535.
98 D. Werck-Reichhart and R. Feyereisen, *Genome Biol.*, 2000, **1**, reviews3003.1–reviews3003.9.
99 S. Sarapusit, S. Pethuan and P. Rongnoparut, *Arch. Insect Biochem. Physiol.*, 2010, **73**, 232–244.
100 H.-B. Jiang, J.-J. Wang, G.-Y. Liu and W. Dou, *J. Insect Sci.*, 2008, **8**.
101 D. R. Nelson, L. Koymans, T. Kamataki, J. J. Stegeman, R. Feyereisen, D. J. Waxman, M. R. Waterman, O. Gotoh, M. J. Coon, R. W. Estabrook, I. C. Gunsalus and D. W. Nebert, *Pharmacogenetics*, 1996, **6**, 1–42.

102 D. W. Nebert, M. Adesnik, M. J. Coon, R. W. Estabrook, F. J. Gonzalez, F. P. Guengerich, I. C. Gunsalus, E. F. Johnson, B. Kemper, W. Levin, I. R. Phillips, R. Sato and M. R. Waterman, *DNA*, 1987, **6**, 1–11.
103 R. Feyereisen, *Annu. Rev. Entomol.*, 1999, **44**, 507–533.
104 J. L. Raucy and S. W. Allen, *Pharmacogenomics J.*, 2001, **1**, 178–186.
105 F. Yu, M. Li, C. Xu, Z. Wang, H. Zhou, M. Yang, Y. Chen, L. Tang and J. He, *PLOS ONE*, 2013, **8**, e81526.
106 P. A. Williams, J. Cosme, V. Sridhar, E. F. Johnson and D. E. McRee, *Mol. Cell*, 2000, **5**, 121–131.
107 B. Zhao and M. R. Waterman, *IUBMB Life*, 2011, **63**, 473–477.
108 S. Yoshioka, T. Tosha, S. Takahashi, K. Ishimori, H. Hori and I. Morishima, *J. Am. Chem. Soc.*, 2002, **124**, 14571–14579.
109 B. Kemper, *Toxicol. Appl. Pharmacol.*, 2004, **199**, 305–315.
110 R. Bernhardt, *J. Biotechnol.*, 2006, **124**, 128–145.
111 D. R. Davydov, N. Y. Davydova, E. V. Sineva and J. R. Halpert, *J. Biol. Chem.*, 2015, **290**, 3850–3864.
112 K. Monostory and Z. Dvorak, *Curr. Drug Metab.*, 2011, **12**, 154–172.
113 A. P. Klein, G. Anarat-Cappillino and E. S. Sattely, *Angew. Chem. Int. Ed Engl.*, 2013, **52**, 13625–13628.
114 F. P. Guengerich and A. W. Munro, *J. Biol. Chem.*, 2013, **288**, 17065–17073.
115 S. Prasad, S. Mazumdar and S. Mitra, *FEBS Lett.*, 2000, **477**, 157–160.
116 T. Ericsson, J. Sundell, A. Torkelsson, K.-J. Hoffmann and M. Ashton, *Xenobiotica Fate Foreign Compd. Biol. Syst.*, 2014, **44**, 615–626.
117 G. R. Wilkinson, *J. Pharmacokinet. Biopharm.*, 1996, **24**, 475–490.
118 R. A. B. van Waterschoot and A. H. Schinkel, *Pharmacol. Rev.*, 2011, **63**, 390–410.
119 J. A. Williams, B. J. Ring, V. E. Cantrell, D. R. Jones, J. Eckstein, K. Ruterbories, M. A. Hamman, S. D. Hall and S. A. Wrighton, *Drug Metab. Dispos. Biol. Fate Chem.*, 2002, **30**, 883–891.
120 S. A. Wrighton, W. R. Brian, M. A. Sari, M. Iwasaki, F. P. Guengerich, J. L. Raucy, D. T. Molowa and M. Vandenbranden, *Mol. Pharmacol.*, 1990, **38**, 207–213.
121 M. Morant, K. Jørgensen, H. Schaller, F. Pinot, B. L. Møller, D. Werck-Reichhart and S. Bak, *Plant Cell*, 2007, **19**, 1473–1487.
122 G. Jones, D. E. Prosser and M. Kaufmann, *J. Lipid Res.*, 2014, **55**, 13–31.
123 I. A. Pikuleva, *Drug Metab. Dispos. Biol. Fate Chem.*, 2006, **34**, 513–520.
124 J. C. McGiff, *Annu. Rev. Pharmacol. Toxicol.*, 1991, **31**, 339–369.
125 S.-F. Zhou, J.-P. Liu and B. Chowbay, *Drug Metab. Rev.*, 2009, **41**, 89–295.
126 F. P. Guengerich, M. V. Martin, C. D. Sohl and Q. Cheng, *Nat. Protoc.*, 2009, **4**, 1245–1251.
127 L. C. Wienkers and T. G. Heath, *Nat. Rev. Drug Discov.*, 2005, **4**, 825–833.
128 J. T. Groves, *Proc. Natl. Acad. Sci.*, 2003, **100**, 3569–3574.
129 X. He and P. R. O. de Montellano, *J. Biol. Chem.*, 2004, **279**, 39479–39484.
130 J. Rittle and M. T. Green, *Science*, 2010, **330**, 933–937.
131 C. J. C. Whitehouse, S. G. Bell and L.-L. Wong, *Chem. Soc. Rev.*, 2012, **41**, 1218–1260.
132 B. Meunier, S. P. de Visser and S. Shaik, *Chem. Rev.*, 2004, **104**, 3947–3980.
133 P. J. Loida and S. G. Sligar, *Biochemistry (Mosc.)*, 1993, **32**, 11530–11538.
134 K. Buchholz, V. Kasche and U. T. Bornscheuer, *Biocatalysts and Enzyme Technology*, John Wiley & Sons, 2012.
135 S. G. Bell, A. Dale, N. H. Rees and L.-L. Wong, *Appl. Microbiol. Biotechnol.*, 2009, **86**, 163–175.

136 K. J. McLean, M. Sabri, K. R. Marshall, R. J. Lawson, D. G. Lewis, D. Clift, P. R. Balding, A. J. Dunford, A. J. Warman, J. P. McVey, A.-M. Quinn, M. J. Sutcliffe, N. S. Scrutton and A. W. Munro, *Biochem. Soc. Trans.*, 2005, **33**, 796–801.
137 W. Yang, S. G. Bell, H. Wang, W. Zhou, N. Hoskins, A. Dale, M. Bartlam, L.-L. Wong and Z. Rao, *J. Biol. Chem.*, 2010, **285**, 27372–27384.
138 S. L. Kelly and D. E. Kelly, *Phil Trans R Soc B*, 2013, **368**, 20120476.
139 C.-W. Chiang, H.-C. Yeh, L.-H. Wang and N.-L. Chan, *J. Mol. Biol.*, 2006, **364**, 266–274.
140 G. A. Roberts, G. Grogan, A. Greter, S. L. Flitsch and N. J. Turner, *J. Bacteriol.*, 2002, **184**, 3898–3908.
141 O. Pylypenko and I. Schlichting, *Annu. Rev. Biochem.*, 2004, **73**, 991–1018.
142 S. Y. Park, K. Yamane, S. Adachi, Y. Shiro, K. E. Weiss and S. G. Sligar, *Acta Crystallogr. D Biol. Crystallogr.*, 2000, **56**, 1173–1175.
143 S. Modi, W. U. Primrose, L. Y. Lian and G. C. Roberts, *Biochem. J.*, 1995, **310 (Pt 3)**, 939–943.
144 S. Rupasinghe, M. A. Schuler, N. Kagawa, H. Yuan, L. Lei, B. Zhao, S. L. Kelly, M. R. Waterman and D. C. Lamb, *FEBS Lett.*, 2006, **580**, 6338–6342.
145 L. O. Narhi and A. J. Fulco, *J. Biol. Chem.*, 1987, **262**, 6683–6690.
146 X. Wang, S. Peter, M. Kinne, M. Hofrichter and J. T. Groves, *J. Am. Chem. Soc.*, 2012, **134**, 12897–12900.
147 Y. Ni, E. Fernández-Fueyo, A. G. Baraibar, R. Ullrich, M. Hofrichter, H. Yanase, M. Alcalde, W. J. H. van Berkel and F. Hollmann, *Angew. Chem. Int. Ed.*, 2016, **55**, 798–801.
148 D. Holtmann, M. W. Fraaije, I. W. C. E. Arends, D. J. Opperman and F. Hollmann, *Chem. Commun.*, 2014, **50**, 13180–13200.
149 S. Peter, M. Kinne, X. Wang, R. Ullrich, G. Kayser, J. T. Groves and M. Hofrichter, *FEBS J.*, 2011, **278**, 3667–3675.
150 P. Molina-Espeja, E. Garcia-Ruiz, D. Gonzalez-Perez, R. Ullrich, M. Hofrichter and M. Alcalde, *Appl. Environ. Microbiol.*, 2014, **80**, 3496–3507.
151 A. Karich, M. Kluge, R. Ullrich and M. Hofrichter, *AMB Express*, 2013, **3**, 5.
152 M. Kluge, R. Ullrich, K. Scheibner and M. Hofrichter, *Green Chem.*, 2012, **14**, 440–446.
153 E. Aranda, R. Ullrich and M. Hofrichter, *Biodegradation*, 2009, **21**, 267–281.
154 S. Bormann, A. G. Baraibar, Y. Ni, D. Holtmann and F. Hollmann, *Catal. Sci. Technol.*, 2015, **5**, 2038–2052.
155 F. Hollmann, A. Taglieber, F. Schulz and M. T. Reetz, *Angew. Chem. Int. Ed.*, 2007, **46**, 2903–2906.
156 M. M. Grau, J. C. van der Toorn, L. G. Otten, P. Macheroux, A. Taglieber, F. E. Zilly, I. W. C. E. Arends and F. Hollmann, *Adv. Synth. Catal.*, 2009, **351**, 3279–3286.
157 M. E. Ener, Y.-T. Lee, J. R. Winkler, H. B. Gray and L. Cheruzel, *Proc. Natl. Acad. Sci. U. S. A.*, 2010, **107**, 18783–18786.
158 N.-H. Tran, D. Nguyen, S. Dwaraknath, S. Mahadevan, G. Chavez, A. Nguyen, T. Dao, S. Mullen, T.-A. Nguyen and L. E. Cheruzel, *J. Am. Chem. Soc.*, 2013, **135**, 14484–14487.
159 E. Churakova, M. Kluge, R. Ullrich, I. Arends, M. Hofrichter and F. Hollmann, *Angew. Chem. Int. Ed.*, 2011, **50**, 10716–10719.
160 A. J. Fulco, *Annu. Rev. Pharmacol. Toxicol.*, 1991, **31**, 177–203.
161 A. Kariakin, D. Davydov, J. A. Peterson and C. Jung, *Biochemistry (Mosc.)*, 2002, **41**, 13514–13525.

162 A. W. Munro, J. G. Lindsay, J. R. Coggins, S. M. Kelly and N. C. Price, *FEBS Lett.*, 1994, **343**, 70–74.
163 R. Neeli, H. M. Girvan, A. Lawrence, M. J. Warren, D. Leys, N. S. Scrutton and A. W. Munro, *FEBS Lett.*, 2005, **579**, 5582–5588.
164 M. Wang, D. L. Roberts, R. Paschke, T. M. Shea, B. S. Masters and J. J. Kim, *Proc. Natl. Acad. Sci. U. S. A.*, 1997, **94**, 8411–8416.
165 T. L. Poulos, *Chem. Rev.*, 2014, **114**, 3919–3962.
166 S. D. Black and S. T. Martin, *Biochemistry (Mosc.)*, 1994, **33**, 12056–12062.
167 D. Roccatano, *J. Phys. Condens. Matter*, 2015, **27**, 273102.
168 M. G. Joyce, I. S. Ekanem, O. Roitel, A. J. Dunford, R. Neeli, H. M. Girvan, G. J. Baker, R. A. Curtis, A. W. Munro and D. Leys, *FEBS J.*, 2012, **279**, 1694–1706.
169 J. Hudeèek, V. Baumruk, P. Anzenbacher and A. W. Munro, *Biochem. Biophys. Res. Commun.*, 1998, **243**, 811–815.
170 S.-H. Park, J.-Y. Kang, D.-H. Kim, T. Ahn and C.-H. Yun, *Biomol. Ther.*, 2012, **20**, 562–568.
171 L. O. Narhi and A. J. Fulco, *J. Biol. Chem.*, 1986, **261**, 7160–7169.
172 B. Rowlatt, J. A. Yorke, A. J. Strong, C. J. C. Whitehouse, S. G. Bell and L.-L. Wong, *Protein Cell*, 2011, **2**, 656–671.
173 M. A. Noble, C. S. Miles, S. K. Chapman, D. A. Lysek, A. C. MacKay, G. A. Reid, R. P. Hanzlik and A. W. Munro, *Biochem. J.*, 1999, **339**, 371–379.
174 B. Rowlatt, Oxford University, 2010.
175 A. K. Udit, F. H. Arnold and H. B. Gray, *J. Inorg. Biochem.*, 2004, **98**, 1547–1550.
176 S. Pflug, S. M. Richter and V. B. Urlacher, *J. Biotechnol.*, 2007, **129**, 481–488.
177 G. Grogan, *Curr. Opin. Chem. Biol.*, 2011, **15**, 241–248.
178 S. Kumar, *Expert Opin. Drug Metab. Toxicol.*, 2010, **6**, 115–131.
179 D. C. Haines, I. F. Sevrioukova and J. A. Peterson, *Biochemistry (Mosc.)*, 2000, **39**, 9419–9429.
180 S. E. Graham and J. A. Peterson, *Arch. Biochem. Biophys.*, 1999, **369**, 24–29.
181 K. G. Ravichandran, S. S. Boddupalli, C. A. Hasermann, J. A. Peterson and J. Deisenhofer, *Science*, 1993, **261**, 731–736.
182 W. K. Alderton, C. E. Cooper and R. G. Knowles, *Biochem. J.*, 2001, **357**, 593–615.
183 A. W. Munro, D. G. Leys, K. J. McLean, K. R. Marshall, T. W. B. Ost, S. Daff, C. S. Miles, S. K. Chapman, D. A. Lysek, C. C. Moser, C. C. Page and P. L. Dutton, *Trends Biochem. Sci.*, 2002, **27**, 250–257.
184 D. N. Muller, C. Schmidt, E. Barbosa-Sicard, M. Wellner, V. Gross, H. Hercule, M. Markovic, H. Honeck, F. C. Luft and W.-H. Schunck, *Biochem. J.*, 2007, **403**, 109–118.
185 A. W. Munro, J. G. Lindsay and J. R. Coggins, *Biochem. Soc. Trans.*, 1993, **21**, 412S–412S.
186 C. F. Oliver, S. Modi, W. U. Primrose, L. Y. Lian and G. C. Roberts, *Biochem. J.*, 1997, **327**, 537–544.
187 S. Graham-Lorence, G. Truan, J. A. Peterson, J. R. Falck, S. Wei, C. Helvig and J. H. Capdevila, *J. Biol. Chem.*, 1997, **272**, 1127–1135.
188 C. F. Oliver, S. Modi, M. J. Sutcliffe, W. U. Primrose, L.-Y. Lian and G. C. K. Roberts, *Biochemistry (Mosc.)*, 1997, **36**, 1567–1572.
189 U. Schwaneberg, C. Schmidt-Dannert, J. Schmitt and R. D. Schmid, *Anal. Biochem.*, 1999, **269**, 359–366.
190 E. M. J. Gillam, A. M. A. Aguinaldo, L. M. Notley, D. Kim, R. G. Mundkowski, A. A. Volkov, F. H. Arnold, P. Souček, J. J. DeVoss and F. P. Guengerich, *Biochem. Biophys. Res. Commun.*, 1999, **265**, 469–472.

191 Q. S. Li, U. Schwaneberg, P. Fischer and R. D. Schmid, *Chem. Weinh. Bergstr. Ger.*, 2000, **6**, 1531–1536.
192 I. D. Macdonald, A. W. Munro and W. E. Smith, *Biophys. J.*, 1998, **74**, 3241–3249.
193 H. Li and T. L. Poulos, *Nat. Struct. Biol.*, 1997, **4**, 140–146.
194 A. B. Carmichael and L.-L. Wong, *Eur. J. Biochem.*, 2001, **268**, 3117–3125.
195 E. T. Farinas, U. Schwaneberg, A. Glieder and F. H. Arnold, *Adv. Synth. Catal.*, 2001, **343**, 601–606.
196 R. J. Sowden, S. Yasmin, N. H. Rees, S. G. Bell and L.-L. Wong, *Org. Biomol. Chem.*, 2005, **3**, 57–64.
197 A. Dhawan, D. Parmar, M. Dayal and P. K. Seth, *Mol. Cell. Biochem.*, 1999, **200**, 169–176.
198 B. M. A. Lussenburg, L. C. Babel, N. P. E. Vermeulen and J. N. M. Commandeur, *Anal. Biochem.*, 2005, **341**, 148–155.
199 B. M. A. van Vugt-Lussenburg, E. Stjernschantz, J. Lastdrager, C. Oostenbrink, P. E. Vermeulen and J. N. M. Commandeur, *J. Med. Chem.*, 2007, **50**, 455–461.
200 M. C. Damsten, B. M. A. van Vugt-Lussenburg, T. Zeldenthuis, J. S. B. de Vlieger, J. N. M. Commandeur and N. P. E. Vermeulen, *Chem. Biol. Interact.*, 2008, **171**, 96–107.
201 W.-C. Huang, A. C. G. Westlake, J.-D. Maréchal, M. G. Joyce, P. C. E. Moody and G. C. K. Roberts, *J. Mol. Biol.*, 2007, **373**, 633–651.
202 C. J. C. Whitehouse, S. G. Bell, H. G. Tufton, R. J. P. Kenny, L. C. I. Ogilvie and L.-L. Wong, *Chem. Commun. Camb. Engl.*, 2008, 966–968.
203 X. Ren, J. A. Yorke, E. Taylor, T. Zhang, W. Zhou and L. L. Wong, *Chem. – Eur. J.*, 2015, **21**, 15039–15047.
204 R. J. F. Branco, A. Seifert, M. Budde, V. B. Urlacher, M. J. Ramos and J. Pleiss, *Proteins*, 2008, **73**, 597–607.
205 A. Seifert, S. Vomund, K. Grohmann, S. Kriening, V. B. Urlacher, S. Laschat and J. Pleiss, *Chembiochem Eur. J. Chem. Biol.*, 2009, **10**, 853–861.
206 E. Weber, A. Seifert, M. Antonovici, C. Geinitz, J. Pleiss and V. B. Urlacher, *Chem. Commun. Camb. Engl.*, 2011, **47**, 944–946.
207 A. M. Sawayama, M. M. Y. Chen, P. Kulanthaivel, M.-S. Kuo, H. Hemmerle and F. H. Arnold, *Chem. Weinh. Bergstr. Ger.*, 2009, **15**, 11723–11729.
208 E. Vottero, V. Rea, J. Lastdrager, M. Honing, N. P. E. Vermeulen and J. N. M. Commandeur, *J. Biol. Inorg. Chem.*, 2011, **16**, 899–912.
209 M. T. Reetz, M. Bocola, J. D. Carballeira, D. Zha and A. Vogel, *Angew. Chem. Int. Ed.*, 2005, **44**, 4192–4196.
210 S. Kille, F. E. Zilly, J. P. Acevedo and M. T. Reetz, *Nat Chem*, 2011, **3**, 738–743.
211 P. Meinhold, M. W. Peters, M. M. Y. Chen, K. Takahashi and F. H. Arnold, *Chembiochem Eur. J. Chem. Biol.*, 2005, **6**, 1765–1768.
212 R. Fasan, Y. T. Meharenna, C. D. Snow, T. L. Poulos and F. H. Arnold, *J. Mol. Biol.*, 2008, **383**, 1069–1080.
213 P. S. Coelho, E. M. Brustad, A. Kannan and F. H. Arnold, *Science*, 2013, **339**, 307–310.
214 M. W. Peters, P. Meinhold, A. Glieder and F. H. Arnold, *J. Am. Chem. Soc.*, 2003, **125**, 13442–13450.
215 P. Meinhold, M. W. Peters, A. Hartwick, A. R. Hernandez and F. H. Arnold, *Adv. Synth. Catal.*, 2006, **348**, 763–772.
216 M. S. Quesenberry and Y. C. Lee, *Anal. Biochem.*, 1996, **234**, 50–55.
217 O. Salazar, P. C. Cirino and F. H. Arnold, *Chembiochem Eur. J. Chem. Biol.*, 2003, **4**, 891–893.

218 T. Omura and R. Sato, *J. Biol. Chem.*, 1964, **239**, 2370–2378.
219 M. L. Geddie and I. Matsumura, *J. Biol. Chem.*, 2004, **279**, 26462–26468.
220 J. Damborsky and J. Brezovsky, *Curr. Opin. Chem. Biol.*, 2009, **13**, 26–34.
221 T. P. Treynor, C. L. Vizcarra, D. Nedelcu and S. L. Mayo, *Proc. Natl. Acad. Sci.*, 2007, **104**, 48–53.
222 M. M. Y. Chen, C. D. Snow, C. L. Vizcarra, S. L. Mayo and F. H. Arnold, *Protein Eng. Des. Sel. PEDS*, 2012, **25**, 171–178.
223 F. E. Zilly, J. P. Acevedo, W. Augustyniak, A. Deege, U. W. Häusig and M. T. Reetz, *Angew. Chem. Int. Ed Engl.*, 2011, **50**, 2720–2724.
224 W. R. LaCourse, D. C. Johnson, M. A. Rey and R. W. Slingsby, *Anal. Chem.*, 1991, **63**, 134–139.
225 S. Staudt, C. A. Müller, J. Marienhagen, C. Böing, S. Buchholz, U. Schwaneberg and H. Gröger, *Beilstein J. Org. Chem.*, 2012, **8**, 186–191.
226 N. Kawakami, O. Shoji and Y. Watanabe, *Angew. Chem. Int. Ed Engl.*, 2011, **50**, 5315–5318.
227 N. Kawakami, O. Shoji and Y. Watanabe, *Chem. Sci.*, 2013, **4**, 2344–2348.
228 D. C. Haines, D. R. Tomchick, M. Machius and J. A. Peterson, *Biochemistry (Mosc.)*, 2001, **40**, 13456–13465.
229 Z. Cong, O. Shoji, C. Kasai, N. Kawakami, H. Sugimoto, Y. Shiro and Y. Watanabe, *ACS Catal.*, 2015, **5**, 150–156.
230 R.Kenny, Oxford University, 2004.
231 C. J. C. Whitehouse, W. Yang, J. A. Yorke, B. C. Rowlatt, A. J. F. Strong, C. F. Blanford, S. G. Bell, M. Bartlam, L.-L. Wong and Z. Rao, *ChemBioChem*, 2010, **11**, 2549–2556.
232 N.-H. Tran, N. Huynh, G. Chavez, A. Nguyen, S. Dwaraknath, T.-A. Nguyen, M. Nguyen and L. Cheruzel, *J. Inorg. Biochem.*, 2012, **115**, 50–56.
233 C. J. C. Whitehouse, W. Yang, J. A. Yorke, H. G. Tufton, L. C. I. Ogilvie, S. G. Bell, W. Zhou, M. Bartlam, Z. Rao and L.-L. Wong, *Dalton Trans.*, 2011, **40**, 10383–10396.
234 S. K. Spaans, R. A. Weusthuis, J. van der Oost and S. W. M. Kengen, *Front. Microbiol.*, 2015, **6**.
235 W. Liu and P. Wang, *Biotechnol. Adv.*, 2007, **25**, 369–384.
236 K. Schneider and H. G. Schlegel, *Biochem. J.*, 1981, **193**, 99–107.
237 T. Burgdorf, E. van der Linden, M. Bernhard, Q. Yuan Yin, J. W. Back, A. F. Hartog, A. O. Muijsers, C. G. de Koster, S. P. J. Albracht and B. Friedrich, *J. Bacteriol.*, 2005, **187**, 3122–3132.
238 L. Lauterbach, H. Wang, M. Horch, L. B. Gee, Y. Yoda, Y. Tanaka, I. Zebger, O. Lenz and S. P. Cramer, *Chem. Sci. R. Soc. Chem. 2010*, 2015, **6**, 1055–1060.
239 E. van der Linden, B. W. Faber, B. Bleijlevens, T. Burgdorf, M. Bernhard, B. Friedrich and S. P. J. Albracht, *Eur. J. Biochem.*, 2004, **271**, 801–808.
240 W. Lubitz, H. Ogata, O. Rüdiger and E. Reijerse, *Chem. Rev.*, 2014, **114**, 4081–4148.
241 I. Ali and S. Omanovic, *ResearchGate*, 2013, **8**, 4283.
242 L. Lauterbach, O. Lenz and K. A. Vincent, *FEBS J.*, 2013, **280**, 3058–3068.
243 L. Lauterbach, J. Liu, M. Horch, P. Hummel, A. Schwarze, M. Haumann, K. A. Vincent, O. Lenz and I. Zebger, *Eur. J. Inorg. Chem.*, 2011, **2011**, 1067–1079.
244 T. Thum and J. Borlak, *FASEB J.*, 2002, **16**, 1537–1549.
245 V. B. Urlacher and R. D. Schmid, ed. B.-M. in Enzymology, Academic Press, 2004, vol. 388, pp. 208–224.
246 H. Liu and J. H. Naismith, *BMC Biotechnol.*, 2008, **8**, 91.

247 M. J. Cryle, R. D. Espinoza, S. J. Smith, N. J. Matovic and J. J. D. Voss, *Chem. Commun.*, 2006, 2353–2355.
248 A. B. Carmichael, *The oxidations of hydrocarbons by variants of cytochrome P450BM3*, Oxford University, 2002.
249 R. Fasan, M. M. Chen, N. C. Crook and F. H. Arnold, *Angew. Chem. Int. Ed.*, 2007, **46**, 8414–8418.
250 C.J.C. Whitehouse, Oxford University, 2009.
251 L. Barreto, *Towards a one-pot synthesis of δ-lactones via fatty acid oxidation*, Oxford University, 2015.
252 H. Yeom and S. G. Sligar, *Arch. Biochem. Biophys.*, 1997, **337**, 209–216.
253 H. T.-H. Nguyen, N. Takenaka, H. Bandow and Y. Maeda, *Anal. Sci.*, 2001, **17**, 639–643.
254 O. Shoji and Y. Watanabe, *Isr. J. Chem.*, 2015, **55**, 32–39.
255 S.H. Yalkowsky, P. Jain, *CRC Press*, 2010.
256 V. B. Urlacher, A. Makhsumkhanov and R. D. Schmid, *Appl. Microbiol. Biotechnol.*, 2006, **70**, 53–59.
257 L. Knight, Oxford University, 2011.
258 A. Weckbecker and W. Hummel, in *Microbial Enzymes and Biotransformations*, ed. J. Barredo, Humana Press, 2005, pp. 225–238.
259 S. D. Munday, O. Shoji, Y. Watanabe, L.-L. Wong and S. G. Bell, *Chem. Commun.*, 2016, **52**, 1036–1039.
260 F. Brühlmann, L. Fourage, C. Ullmann, O. P. Haefliger, N. Jeckelmann, C. Dubois and D. Wahler, *J. Biotechnol.*, 2014, **184**, 17–26.
261 E. van der Linden, T. Burgdorf, A. L. de Lacey, T. Buhrke, M. Scholte, V. M. Fernandez, B. Friedrich and S. P. J. Albracht, *JBIC J. Biol. Inorg. Chem.*, 2006, **11**, 247–260.
262 T. Burgdorf, E. van der Linden, M. Bernhard, Q. Y. Yin, J. W. Back, A. F. Hartog, A. O. Muijsers, C. G. de Koster, S. P. J. Albracht and B. Friedrich, *J. Bacteriol.*, 2005, **187**, 3122–3132.
263 T. Burgdorf, S. Löscher, P. Liebisch, E. Van der Linden, M. Galander, F. Lendzian, W. Meyer-Klaucke, S. P. J. Albracht, B. Friedrich, H. Dau and M. Haumann, *J. Am. Chem. Soc.*, 2005, **127**, 576–592.
264 A. K. Holzer, K. Hiebler, F. G. Mutti, R. C. Simon, L. Lauterbach, O. Lenz and W. Kroutil, *Org. Lett.*, 2015, **17**, 2431–2433.
265 T. Oda, K. Oda, H. Yamamoto, A. Matsuyama, M. Ishii, Y. Igarashi and H. Nishihara, *Microb. Cell Factories*, 2013, **12**, 2.
266 T. H. Lonsdale, L. Lauterbach, S. Honda Malca, B. M. Nestl, B. Hauer and O. Lenz, *Chem. Commun. Camb. Engl.*, 2015, **51**, 16173–16175.
267 Z. Idris, Oxford University, 2012.
268 H. Reeve, Oxford University, 2014.
269 L. Lauterbach, Z. Idris, K. A. Vincent and O. Lenz, *PloS One*, 2011, **6**, e25939.